2014-07-21

Analysis of the Interactions between Graphene Oxide and Biomolecules and Protein Fibrillation Using Surface Chemistry and Spectroscopy

Shanghao Li
University of Miami, shanghao_li@hotmail.com

Recommended Citation

Li, Shanghao, "Analysis of the Interactions between Graphene Oxide and Biomolecules and Protein Fibrillation Using Surface Chemistry and Spectroscopy" (2014). *Open Access Dissertations*. 1253.
https://scholarlyrepository.miami.edu/oa_dissertations/1253

UNIVERSITY OF MIAMI

ANALYSIS OF THE INTERACTIONS BETWEEN GRAPHENE OXIDE AND BIOMOLECULES AND PROTEIN FIBRILLATION USING SURFACE CHEMISTRY AND SPECTROSCOPY

By

Shanghao Li

A DISSERTATION

Submitted to the Faculty
of the University of Miami
in partial fulfillment of the requirements for
the degree of Doctor of Philosophy

Coral Gables, Florida

August 2014

UNIVERSITY OF MIAMI

A dissertation submitted in partial fulfillment of
the requirements for the degree of
Doctor of Philosophy

ANALYSIS OF THE INTERACTIONS BETWEEN GRAPHENE OXIDE AND BIOMOLECULES AND PROTEIN FIBRILLATION USING SURFACE CHEMISTRY AND SPECTROSCOPY

Shanghao Li

Approved:

Roger M. Leblanc, Ph.D.
Professor of Chemistry

Thomas K. Harris, Ph.D.
Associate Professor of Chemistry

Jamie D. Walls, Ph.D.
Assistant Professor of Chemistry

M. Brian Blake, Ph.D.
Dean of the Graduate School

Fotios Andreopoulos, Ph.D.
Associate Professor of Biomedical Engineering

LI, SHANGHAO (Ph.D., Chemistry)
Analysis of the Interactions between Graphene Oxide and Biomolecules
and Protein Fibrillation Using Surface Chemistry and Spectroscopy (August 2014)

Abstract of a dissertation at the University of Miami.

Dissertation supervised by Professor Roger M. Leblanc.
No. of pages in text. (144)

Graphene oxide (GO), a novel 2−dimensional carbon based nanomaterial, has shown potential applications in biomedical and biological field, including drug and gene delivery, sensing, and bioimaging. However, one critical question needs to be addressed before any actual application: how does GO interact with biological molecules, such as amino acids, peptides, proteins, and biomembranes? In this study, spectroscopy, microscopy, and surface chemistry were applied to fundamentally understand the nature of interactions between these molecules and GO.

GO was found to interact with amino acids, peptides, and proteins by fluorescence quenching. The main quenching mechanism between GO and Trp or Tyr was determined as static quenching, slightly combined with dynamic quenching. Both electrostatic interaction and hydrophobic interaction contributed to the interactions between GO and Trp or Tyr. Particularly, strong electrostatic interaction between GO and lysozyme was demonstrated and confirmed using fluorescence quenching, zeta potential, dynamic light scattering, and atomic force microscopy. This interaction was so strong that one was able to subsequently eliminate and separate lysozyme using GO. The strong electrostatic interaction also rendered the selective adsorption of lysozyme on GO from a mixture of proteins. As polymer Pluronic F127 (PF127) was used to disperse GO and block the

hydrophobic interaction between GO and Trp or Tyr, the interaction and behavior between GO and PF127 were also characterized using Langmuir monolayer technique at the air–water interface.

To study the nature and orientation of interaction between GO and lipid models, Langmuir monolayer technique was applied at the air−water/aqueous interface. Five lipids with the same 18−carbon alkyl chain but different head groups of charges were chosen to rationalize the possible interactions. Experimental results showed that the interaction was governed by electrostatic interaction between the polar head groups and GO. GO could incorporate into the monolayer of positively charged lipids DODAB and DSEPC, but not the neutrally or negatively charged lipids (DSPC, DSPA and SA). When GO was injected to the subphase underneath the monolayer of positively charged lipid DODAB and DSEPC, different behaviors of surface pressure were observed. An orientation model of GO was proposed to explain the different adsorption of GO.

Another topic of this thesis is on protein fibrillation. Pathological conditions of human neurodegenerative diseases are now believed to be commonly associated with protein misfolding processes. Human insulin and human islet amyloid polypeptide (hIAPP) are two major hormones involved in diabetes. Fibrillation of insulin at various interfaces was summarized. The conformation and self−assembly of the hIAPP were studied at the air−aqueous interface using the Langmuir monolayer technique. Experimental results showed that hIAPP Langmuir monolayer was relatively stable and did not form aggregates when compressed. However, ongoing experiments showed there existed interaction between hIAPP and insulin, favoring the fibrillation between the two.

ACKNOWLEDGEMENTS

Most importantly, I would like to sincerely thank my advisor and mentor, Dr. Roger M. Leblanc, for supporting and guiding me during my graduate studies at the University of Miami. He has provided me with insightful guidance and invaluable discussions concerning my research. Through Dr. Leblanc's philosophy "ALWAYS HELP STUDENTS TO SUCCEED", he has consistently put students and their academic careers first. His dedication as a role model has been the paradigm which I will follow in my future career. He always teaches me to be positive throughout life by telling me, "Be happy because nature will take care of its people". Graduate studies can be a challenging, difficult and stressful experience, but I am proud to say that my experience under Dr. Leblanc's guidance was happy and exciting. I always feel so grateful and lucky to have Dr. Leblanc as my advisor and mentor in my academic career.

I would like to sincerely thank my graduate committee members Dr. Jamie D. Walls and Dr. Thomas K. Harris for their many insightful discussions, scientific advice, and invaluable suggestions on my career through all my graduate studies. Also, I would like to extend my thanks to Dr. Fotios Andreopoulos for his advice, discussions, and help with my thesis and defense.

I would like to give my appreciation to every faculty member and staff in the Department of Chemistry for their help during the past five years, especially Dr. Francisco M. Raymo, Dr. Rajeev Prabhakar, Dr. Burjor Captain, Dr. Tegan Eve, Lydia Gonzalez, Juanita Hernandez, Raul Hernandez, Susana Gadanyi, Sara Sucklal, Marlene Triana, Edward Torres, and Dr. David Hudson.

I would like to thank all the current and past group members in Dr. Leblanc's research group: Nicholas Crawford, Sheba Johnson, Lorenzo Sansalone, Eric Waidely, Jerome Mulloor, Ari Stein, Wei Liu, Kristen Sessions, Stuart Sacks, Aaron Kruger, Jingru Guo, Ravi Patel, Anup Dadlani, Yiwen Ji, Andrew Garcia, Dr. Miodrag Micic, and Dr. Jhony Orbulescu. Among them, I would like to give special thanks to Nicholas Crawford and Sheba Johnson for the great support, sharing, and encouragement during my graduate studies. I have learned a lot from both of them, not just skills, but also personality. As we said, we three should reunite in California in future!

I am also grateful to Prof. Chengshan Wang (Middle Tennessee State University), Prof. Treen Huo (University of Central Florida), and Prof. Elsa Yan (Yale University) for their collaboration in research. I also appreciate the help with experimental techniques from Lingyu Wang and Nicholas Merrill. I sincerely thank my friends and classmates at Miami, to name a few, Dr. Zhenghua Tang, Zhili Peng, Jiaojiao Li, Tingting Zhang, Xiaowen Yu, Xiaoxia Zhu, Barnali Mondal, Mehmet Ozbil, and Anjaneyulu Koppaka.

Furthermore, I want to extend my thanks to the College of Arts and Sciences at University of Miami for the financial support in the past five years. Without this, it would not be possible for me to pursue my studies at the University of Miami.

Last, but certainly not least, I would like to thank my parents for all the love and support that they have provided throughout my graduate career at the University of Miami. Particularly, I want to give my most heartfelt thanks to my wife Jiajia Lei for her great love, understanding, encouragement, support, and consideration. Without the support from my family, it would be impossible for me to complete my graduate study.

TABLE OF CONTENTS

LIST OF FIGURES

Chapter 2

Chapter 3

Chapter 4

Chapter 5

Chapter 6

Chapter 7

Chapter 8

LIST OF TABLES

Chapter 3

LIST OF ABBREVIATIONS

2-D	two-dimensional
AFM	atomic force microscopy
$A\beta_{40}$	amyloid beta 1-40
BAM	Brewster angle microscopy
BSA	bovine serum albumin
DODAB	dioctadecyldimethylammonium bromide
DSEPC	1,2–distearoyl–sn–glycero–3–ethylphosphocholine
DSPA	1,2–distearoyl–sn–glycero–3–phosphate
DSPC	1,2–distearoyl–sn–glycero–3–phosphocholine
FRET	Förster resonance energy transfer
GO	graphene oxide
HSA	human serum albumin
hIAPP	human islet amyloid polypeptide
IRRAS	infrared absorption-reflection spectroscopy
LB	Langmuir–Blodgett
LYZ	lysozyme
NMR	nuclear magnetic resonance
OVA	ovalbumin
PEG	polyethylene glycol
PEO	poly(ethylene oxide)
PF127	Pluronic F127
pI	isoelectric point

PM-IRRAS	polarization modulation infrared reflection-absorption spectroscopy
PPO	poly(propylene oxide)
SA	stearic acid
SDS-PAGE	sodium dodecyl sulfate polyacrylamide gel electrophoresis
SFG	sum frequency generation
Trp	tryptophan
Tyr	tyrosine

Chapter 1 Introduction

Part I: Interaction between Graphene Oxide and Biomolecules

Graphene, a one−atom−thick planar sheet of sp^2 hybridized carbon atoms, has recently attracted tremendous attention in various studies and applications due to its novel optical, mechanical, electronic, thermal and biological properties.[1-3] Graphene oxide (GO), an oxidized form of graphene, holds a similar atomically thin structure to graphene, but it possesses plenty of oxygen−containing functional groups, such as carboxyls on the edges and hydroxyls and epoxies on the basal plane.[1] Compared with graphene, GO has demonstrated advantageous applications in biosensing and biomedical field owing to its special physical and chemical properties, such as low−cost manufacturing process, rich colloidal property, high adsorbility and fluorescence quenching.[4-6]

Since the first drug delivery research in 2008 of using GO to efficiently load hydrophobic drug,[7] much progress has been achieved for explorations of GO in the biological and biomedical field, including drug and gene delivery, biosensing, cellular imaging, etc.[6] The surface of GO allows electrostatic, hydrophobic, hydrogen bonding and π–π stacking interactions, which are generally favored for molecules with poor water solubility. Covalent functionalization of GO with chitosan,[8] folic acid,[9] and poly(*N*−isopropylacrylamide),[10] has recently been developed for drug delivery with pH−controlled or thermal−responsive drug release. GO was also recently studied for gene delivery.[11] The single−stranded DNA was found to be preferentially adsorbed onto the GO surface over the double−stranded form, as the later prevented the binding of GO surface to the DNA base inside the double helix.[12] Besides drug and gene delivery, GO has been exploited for near−infrared photothermal treatment for cancers and Alzheimer's disease.[13,14]

As mentioned above, GO has shown potential applications in biological and biomedical fields; however, one critical question needs to be addressed before any actual application: how does GO interact with biomolecules, such as amino acids, peptides, and proteins? There is very limited information on such an important question. In Chapter 2, we will discuss the possible interaction between GO and amino acids (tryptophan and tyrosine), peptides (Alzheimer's disease related amyloid beta 1-40 and type 2 diabetes related human islet amyloid polypeptide), and proteins (drug-related bovine and human serum albumin). The quenching mechanism between GO and tryptophan (Trp) or tyrosine (Tyr) will be determined using Stern–Volmer plot and fluorescence lifetime.

Biosensing methods and devices using graphene oxide (GO) have recently been explored for detection and quantification of specific biomolecules from body fluid samples, such as saliva, milk, urine, and serum.[15-17] For a practical diagnostics application, any sensing system must show an absence of nonselective detection of abundant proteins in the fluid matrix. Because lysozyme is an abundant protein in these body fluids,[18,19] it may interfere with detections and quantification due to the charge difference between lysozyme and GO. Therefore, one fundamental question that needs to be addressed is how GO interacts with lysozyme. In Chapter 3, strong and selective adsorption of lysozyme on GO will be demonstrated in details.[20]

Another challenge of GO in biomedical application is its agglomeration or precipitation in electrolyte solutions. Recently, non−covalently suspending GO in electrolyte solutions has been explored using triblock copolymer Pluronic F127 (PF127, PEO_{100}–PPO_{65}–PEO_{100}).[21] However, the nature of the interaction and the behavior between GO and PF127 are not well understood and characterized. In Chapter 4, we will try to answer these questions using a 2-dimensional Langmuir monolayer methodology at the air–water interface.

Previous studies have reported that GO could be applied for cellular imaging, drug and gene delivery, indicating it could possibly enter cells.[22-24] But inconsistent results are obtained on the cytotoxicity of GO and how it enters cell membranes.[25,26] Moreover, compared with spherical or tubular nanomaterials, GO is an extremely thin layer (~1 nm) with large surface area and irregular shape. It is still unknown how GO orientates itself when interacting with the cell membrane. Therefore, it is necessary to understand the interaction and orientation between GO and various lipid models. In Chapter 5, Langmuir monolayer technique will be applied at the air–water interface to study the nature and orientation of interaction between GO and lipid models. Five lipids with the same 18-carbon alkyl chain but different head groups of charges are purposely chosen to rationalize the possible interactions.

To summarize, the objectives of Part I are: 1) To investigate the interaction and fluorescence quenching between GO and fluorescent assay of amino acids, peptides, and proteins; 2) To examine the interaction between GO and lysozyme and the possible applications in separation and selective adsorption; 3) To understand and characterize the interaction and the behavior between GO and nonionic surfactant Pluronic F127; 4) To study and define the nature and orientation of interaction between GO and lipid model with different head groups.

Part II. Protein Fibrillation at the Interface and Interaction between Human Insulin and Human Islet Amyloid Polypeptide

Protein fibrillation involves formation of intermolecular hydrogen bonding of extended polypeptide strands (also called "cross-β" architecture) as a consequence of protein misfolding. It is widely accepted that misfolding of some specific peptides or proteins is involved in a wide variety of human diseases,[27,28] such as islet amyloid polypeptide (IAPP) in type 2 diabetes, amyloid−β peptide (Aβ) in Alzheimer's disease (AD), α−synuclein in Parkinson's disease (PD), and prion protein in the spongiform encephalopathies.[29,30]

It is widely recognized that surfaces and interfaces are ubiquitous environments and play key roles in a wide variety of physical and chemical processes, including biomedical engineering, drug delivery, catalysis, and energy production.[31,32] As a specific example, great attention has been paid to investigate properties of insulin at various interfaces, a peptide used to regulate blood glucose levels for diabetes patients. This is because insulin has been long observed to be vulnerable to change conformation and develop aggregates at the surface of storage vials, infusion pumps, controlled release devices, etc.[33-36] However, a molecule−level understanding of the detailed structure and property of insulin at the interfaces remains a great challenge. In Chapter 6, a summary of insulin aggregation at different interfaces will be studied and discussed.[37]

Human insulin and human islet amyloid polypeptide (hIAPP, also known as amylin) are two major hormones involved in diabetes. They are innately related, as both possess common promoter sequences and are co−synthesized in an approximately 1:100 molar ratio (hIAPP: insulin) from secretory granules of pancreatic β−cells.[38] The monomeric hIAPP is involved in the glycemic down−regulation and the monomeric insulin regulates blood glucose levels. Similar to the Alzheimer−related beta amyloid, hIAPP is also a highly amyloidogenic peptide, and its amyloid deposits are observed in the islets of Langerhans of around 95% type 2 diabetic patients,[39,40] as well as in pancreatic cancer.[41] In order to understand the fibrillation of hIAPP and its interaction with human insulin *in vivo*, we will first investigate the properties of hIAPP at the air−water interface in Chapter 7 and explore the interaction between hIAPP and human insulin in Chapter 8.

To summarize, the objectives of Part II are: 1) To provide an overview on the current state of our understanding of insulin aggregation at interfaces; 2) To obtain the conformation and self−assembly properties of hIAPP at the air−water interface; and 3) To study the interaction between hIAPP and human insulin.

Chapter 2 Graphene Oxide as a Quencher for Fluorescent Assay of Amino Acids, Peptides and Proteins

2.1 Background

Graphene oxide (GO) is a two−dimensional, atomically thin carbon nanomaterial with functional groups, such as carboxylic acid at the edges, phenol hydroxyl and epoxide groups mainly at the basal plane, and some C=C sp^2 domains.[2] The advantages of GO over other nanomaterials lie in its unique properties, such as extremely large surface area, good physisorption, high water dispersibility and excellent biocompatibility.[7]

Since the groundbreaking research of PEGylated−GO (PEG = polyethylene glycol) used to efficiently load hydrophobic drug,[7] much progress has been achieved for explorations of graphene oxide in the biological and biomedical field, including drug and gene delivery, biological sensing, and cellular imaging.[6] The surface of GO allows electrostatic, hydrophobic, hydrogen bonding and π–π stacking interactions, which are generally favored for molecules with poor water solubility. Covalent functionalization of GO with chitosan,[8] folic acid,[9] and poly(*N*−isopropylacrylamide),[10] has recently been developed for drug delivery with pH−controlled or thermal−responsive drug release. GO was also recently studied for gene delivery.[11] The single−stranded DNA was found to be preferentially adsorbed onto the GO surface over the double−stranded form, as the later prevents the binding of GO surface to the DNA base inside the double helix.[12] GO has also been exploited for near−infrared photothermal treatment for cancers and Alzheimer's disease.[13,14,42] Moreover, GO based materials are applied to biosensing, cellular probing and real−time monitoring based on fluorescence.[43,44]

Although GO has shown potential promising applications, one critical question needs to be addressed before any actual application: How does GO interact with biomolecules, such as amino acids, peptides and proteins? However, there is very limited information on such question. It was found that GO could adsorb amino acids via electrostatic interaction and/or π–π stacking interaction, such as arginine, histidine, lysine, tryptophan, tyrosine and phenylalanine.[44] GO could quench the fluorescence of several dye−labeled peptides for biosensing,[44-46] but the quenching mechanism of GO has not been studied. Furthermore, there is no fluorescence study based on the interaction between GO and amino acids, peptides, and proteins without fluorescent dye−labeled probe. Understanding the interaction between GO and biomolecules is fundamentally essential, especially for disease− and drug−related peptides and proteins. The present study is intended to investigate the interaction between GO and fluorescent assay of amino acids (tryptophan and tyrosine), peptides (Alzheimer's disease related amyloid beta 1−40 and type II diabetes related human islet amyloid polypeptide), and proteins (drug related bovine and human serum albumin) using fluorescence spectroscopy.

2.2 Experimental Section

2.2.1 Materials

Single layer GO was purchased from ACS Material LLC (Medford, MA). L−tyrosine (Tyr), L−tryptophan (Trp) and Pluronic F127 were bought from Sigma (St. Louis, MO). Amyloid beta 1−40 ($A\beta_{40}$), human islet amyloid polypeptide (hIAPP), human serum albumin (HSA) and bovine serum albumin (BSA) and 1,1,1,3,3,3−hexafluoroisopropanol (HFIP) were obtained from MP Biomedicals (Solon, OH). All these chemicals were used without any further purification. The deionized water used in the experiments was obtained from a Modulab 2020 Water purification system. The resistivity, surface tension and pH of deionized water were 18 MΩ·cm, 72.6 mN/m and 5.6 at 20.0 ± 0.5 ^{o}C, respectively.

2.2.2 Methods and Characterization

1 mg/mL GO aqueous solution was obtained by dispersing 5 mg GO into 5 mL pure water, followed by 1 h of sonication in a cold water bath (Branson, model 1510, Danbury, CT). Then, the as−prepared GO solution was diluted to 100 μg/mL. The concentrations of the fluorescent assay of amino acid (Tyr and Trp), and protein (HSA and BSA) were prepared individually as 2.5×10^{-6} M, if not specifically mentioned. The concentration of both $A\beta_{40}$ and hIAPP for the fluorescence emission was prepared as 2.5×10^{-5} M as the fluorescence intensity of 2.5×10^{-6} M solution was too weak. Due to the propensity of aggregation, peptide $A\beta_{40}$ or hIAPP was first dissolved into HFIP to render the monomeric form, and then was put in a vacuum desiccator for 2 h to remove the solvent HFIP. In order to fix the final concentration of fluorescent assay as 10^{-6} M (10^{-5} M for $A\beta_{40}$ and hIAPP) with gradually increased concentration of GO in the range of 0 ~ 30 μg/mL, a total volume of 400 μL mixture was obtained by mixing 160 μL 2.5×10^{-6} M (2.5×10^{-5} M for $A\beta_{40}$ and hIAPP) fluorescent assay, a certain volume of 100 μg/mL GO (from 0 to 120 μL, 20 μL as each increment) and pure water (from 240 to 120 μL, 20 μL as each decrement). In the fluorescence lifetime study of Trp or Tyr mixed with different amounts of GO, the concentrations of Trp and Tyr were fixed at 2.5×10^{-5} and 5×10^{-5} M, respectively.

Atomic force microscopy (AFM) images were taken with tapping mode using Agilent 5420 AFM instrument (Agilent, Santa Clara, CA). The cantilever had a resonance frequency of 342 kHz with typical force constant 42 N/m, a silicon probe at the tip. The fluorescence spectra were measured by Fluorolog−3 spectrofluorimeter (Horiba Scientific, Edison, NJ) using a 1 cm × 0.2 cm quartz cell. The slit widths in spectrofluorimeter for both excitation and emission were set at 5 nm. The excitation wavelength for Tyr, $A\beta_{40}$ and hIAPP was set as 270 nm, Trp, BSA and HSA as 290 nm, and GO as 425 nm. The excitation wavelengths were selected to assure that the Raman scattering peak did not interfere with the emission wavelength. Frequency−domain fluorescence lifetime measurements were performed using a ChronosFD spectrofluorometer (ISS, Champaign, IL). Samples were excited with a 280 nm modulated diode and emission was collected using 305 nm long−pass filters (Andover, Salem, NH). 2,5−Diphenyoxazole (DPO) in ethanol (lifetime = 1.4 ns) was used as a lifetime reference and polarizers were set at a magic angle configuration (54.7 °). All measurements were conducted at room temperature in 0.5 × 1 cm quartz cells. Modulation−phase data were analyzed using GlobalsWE software and the χ^2 parameter was used as criterion for goodness of fit. The average intensity decay lifetime was obtained by fitting the data with a multiple−exponential decay model. UV−vis absorption was performed by a Lambda 900 UV/Vis/NIR spectrophotometer (Perkin−Elmer, Norwalk, CT) using a 1 cm × 1 cm quartz cell.

2.3 Results and Discussions

2.3.1 The characterization of GO by UV−vis and AFM

To confirm that the commercial available GO used in this study had similar properties as previously reported, UV−vis absorption and AFM were applied to characterize it. The sample of diluted GO aqueous dispersion (15 μg/mL) was examined by UV−vis absorption spectrum, as shown in Figure 2.1(A). It displayed a maximum absorption at 229 nm due to the $\pi-\pi^*$ transition of aromatic C=C bonds and a shoulder around 300 nm due to the $n-\pi^*$ transition of C=O bonds. Both were consistent with previous reports.[47,48] To further verify the single−layer morphology of GO by AFM, 5 μL of 15 μg/mL GO aqueous dispersion was spread onto a freshly cleaved mica surface and left dry in the air. The AFM image showed that all heights of GO sheets were around 0.9 nm (Figure 2.1(B)), which were also similar to previous reported single layer GO.[42,45,47,48] All these results confirmed that the GO used in this study was truly single layer sheet.

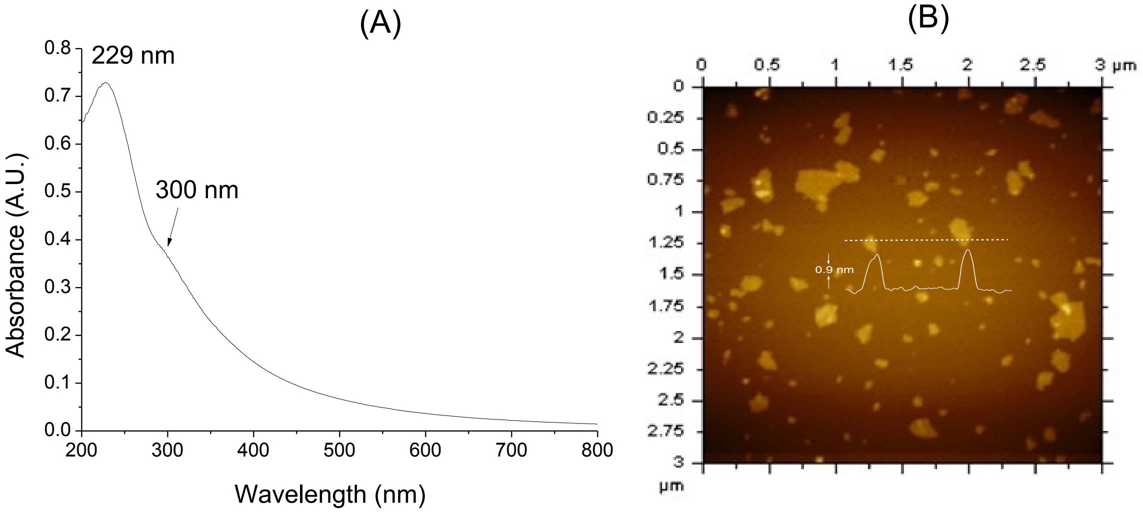

Figure 2.1 Characterization of GO by UV−vis absorption and AFM. The UV−vis absorption spectrum of 15 μg/mL GO aqueous dispersion (A); Tapping mode AFM image of GO deposited on freshly cleaved mica surface with height of ~ 0.9 nm (B).

2.3.2 Fluorescence quenching of Trp or Tyr by GO

It has been known that GO can quench the emission of fluorescent molecules or particles, such as organic dye molecules,[49-51] fluorescent labels,[43,45,46,52-54] and quantum dots (QD),[48,55] through the process of Förster resonance energy transfer (FRET) from the fluorescent moiety to GO. The fluorescent dyes or labels usually contain aromatic rings and the quenching is via non−covalent interactions, such as electrostatic interaction, hydrogen bonding, hydrophobic and π−π interactions between GO and the dye molecules or fluorescent labels.[45,46,53,54] Based on the structure and component of fluorescent amino acids, peptides and proteins, there should be a non−covalent interaction between them and GO, affecting the fluorescent intensity of fluorescent assay. Indeed, the experiments in the present study showed the strong quenching effect of GO.

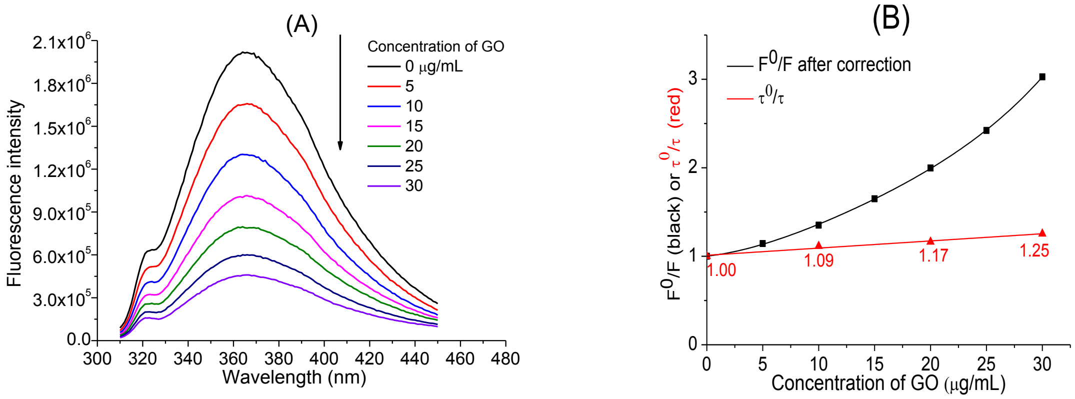

Figure 2.2 Fluorescence quenching of Trp by GO. (A) The fluorescence quenching of Trp (10^{-6} M) by mixing with different concentrations of GO. (B) The quenching of Trp (F^0/F after inner filter effect correction, black) and fluorescence lifetime ratio (τ^0/τ, red) as a function of GO concentrations.

When mixed with GO aqueous dispersion, the fluorescence intensity of 10^{-6} M Trp assay was strongly reduced without any shift of the emission maximum, as shown in Figure 2.2 (A). Very similar phenomenon of reduced fluorescence intensity was also found for 10^{-6} M tyrosine (Tyr) assay. Due to the fact that GO had strong absorption in the range of 270~360 nm, which overlaps with the excitation and emission of Trp or Tyr, the change of fluorescence after the addition of GO could be caused by the so–called "inner filter effect". This effect refers to the absorbance of light at the excitation or emission wavelength by the molecules present in the solution.[56] Therefore, it must be properly considered before any discussion of interaction or binding between the fluorescent molecules and GO. As the fluorescence intensity was collected from the center of a cuvette, the inner filter effect could be estimated from the following equation:[56,57]

$$F_{obs} = F_{corr} * 10^{-\frac{A_{ex} * d_{ex}}{2} - \frac{A_{em} * d_{em}}{2}}$$

where F_{obs} is the measured fluorescence, F_{corr} the correct fluorescence intensity that would be measured in the absence of inner filter effect, d_{ex} and d_{em} are the cuvette pathlength in the excitation and emission direction (in cm), respectively, and A_{ex} and A_{em} represent the measured absorption value at the excitation and emission wavelength with the addition of compound, respectively. Due to the fact that the UV−vis absorption of 10^{-6} M Trp or Tyr in the range of 270~360 nm was negligible compared with the high absorption of GO dispersion, A_{ex} and A_{em} used for correction were the absorption of GO alone at room temperature as an approximation. After this correction, Stern−Volmer plot of F^0/F against the concentration of GO showed that there did exist quenching when GO was added to the solution of Trp (Figure 2.2 (B), black color), where F^0 and F were the fluorescence intensity at the maxima in the absence and in the presence of GO, respectively. Values of F^0/F discussed below had been corrected by the inner filter effect.

The decrement of fluorescence intensity after removing the inner filter effect meant that there was strong quenching effect between GO and Trp. A previous theoretical investigation had shown that Trp could be strongly adsorbed on the surface of graphene via $\pi-\pi$ interactions with a preferring parallel orientation with respect to the plane of graphene.[58] Although GO was the oxidized form of graphene with carboxylic acid group at the edge and hydroxyl and epoxy groups on the basal plane, it still had plenty of small aromatic areas with sp^2 carbons.[59,60] Therefore, GO could still have $\pi-\pi$ interaction or hydrophobic interaction with Trp or Tyr.

2.3.3 The Quenching Mechanism of Trp by GO

After the correction of inner filter effect, the possible quenching mechanisms of Trp by GO were: 1) Collisional quenching due to random collision; 2) Static quenching through the ground−state complex formation; 3) Dynamic quenching; 4) Static and dynamic combined quenching.[56,57] These possibilities are discussed below.

The observed reduction of fluorescence intensity could be possibly due to collisional quenching, which could be described by the classical Stern−Volmer equation:

$$\frac{F^0}{F} = 1 + K_D[Q]$$

where F^0 and F are the fluorescence intensity at the maxima in the absence and in the presence of the quencher, respectively; [Q] is the concentration of the quencher; K_D is the collisional quenching constant.[57] One good way to discriminate collisional quenching from binding−related quenching was to study how temperature affected the quenching efficiency. For collisional quenching, higher temperature increased the probability of collision and resulted in higher quenching efficiency, while less quenching was observed at lower temperature. The fluorescence emission data of Trp mixed with GO were collected at three different temperatures, namely 5, 20 and 45 °C. The Stern−Volmer plot in Figure 2.3 showed that temperature did affect the quenching efficiency. However, a higher quenching efficiency was observed at lower temperature, indicating that the collisional quenching was not the main mechanism of quenching by GO. Similar observation was also found for Tyr.

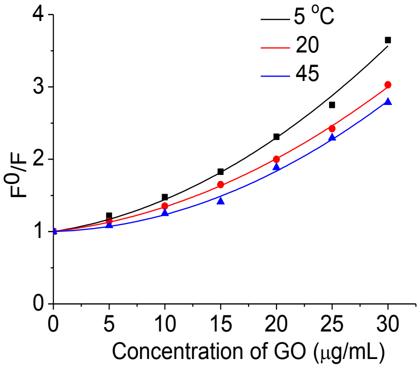

Figure 2.3 The Stern-Volmer plot at different temperatures. F^0/F of 10^{-6} M Trp against the concentration of GO as the quencher at 5, 20 and 45 °C.

In static quenching alone mechanism, the non−fluorescence complex is formed between the ground state of chromophore and the quencher, decreasing the population of fluorophore and thus resulting in the reduction of fluorescence intensity. The fluorescence lifetime remains the same during quenching, as this process does not affect the excitation state of the fluorophore.[57] Also, neither the concentrations of chromophore nor the inner filter effect affects fluorescence lifetime. Due to observation that there was a slightly linear decrement of the fluorescence lifetime of Trp when GO was added (Figure 2.2 (B)), the quenching mechanism could not be only attributed to the static quenching. Dynamic quenching also slightly contributes to the quenching mechanism.

2.3.4 UV−vis Absorption of Trp and GO

To further verify the quenching mechanism, it was necessary to study the UV−vis absorption spectrum. In static quenching, the UV−vis absorption spectrum of the fluorophore will be changed due to the formation of complex between the ground state of the fluorophore and the quencher. However, the spectrum of fluorophore should keep the same in the dynamic quenching.[61] As the quenching of Trp by GO was static and dynamic combined, one would expect that the absorption peak of Trp was shifted after mixing with GO. The UV−vis spectrum of Trp in the presence of 30 μg/mL GO did show some small differences compared with the one without GO (Figure 2.4 (A)). The absorption peaks of GO did not seem to be shifted, as shown in Figure 2.4 (B). On one hand, it was possible that one may not be able to observe clear differences of absorption due to the nature of the complex formed. On the other hand, one may not exclude the possibility that these small differences of UV−vis absorption of Trp were due to the experimental error. Similar observation was found for Tyr. Therefore, UV–vis absorption did not clearly distinguish the quenching mechanism.

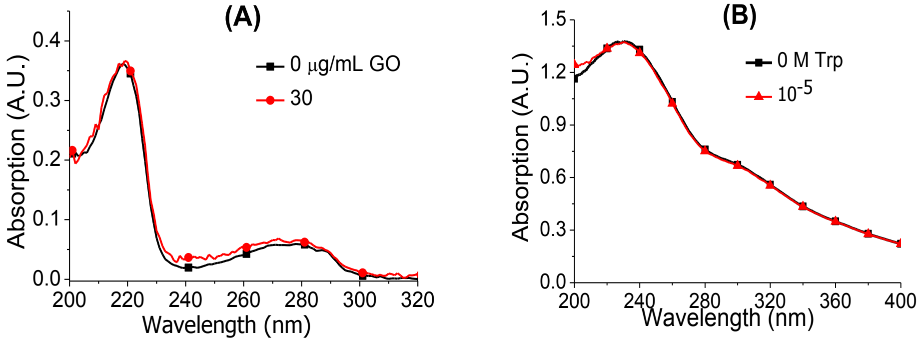

Figure 2.4 UV–vis absorption spectra of (A) 10^{-5} M Trp with and without the presence of 30 μg/mL of GO. Water or 30 μg/mL GO aqueous dispersion were used as the background. (B) 30 μg/mL of GO aqueous dispersion without and with the presence of 10^{-5} M Trp. Water or 10^{-5} M Trp were used as the background solutions.

2.3.5 Hydrophobic Interaction Study between Trp and GO using Pluoronic F127 as a Screening

Based on the discussion above, there was a strong interaction between GO and Trp or Tyr. Both Trp and Tyr had a hydrophobic moiety, indicating that the hydrophobic interaction with GO might play a critical role during quenching. To verify this assumption, Pluronic F127 (PF127) was utilized to block the interaction between GO and Trp or Tyr, as PF127 was previously shown to have strong hydrophobic interaction with GO[21] and graphene.[62] PF127 was a triblock copolymer consisting of a central hydrophobic block of polypropylene glycol flanked by two hydrophilic blocks of polyethylene glycol. The hydrophobic segments had previously been shown to interact with the hydrophobic part of GO while the hydrophilic chains extended to the aqueous solution.[21] When mixed GO with PF127, the hydrophobic moiety of GO would be expected to be covered by the hydrophobic part of PF127, therefore screening the hydrophobic interaction between GO and Trp. As PF127 had no effect on the fluorescence emission of 10^{-6} M Trp in experiments, one would expect to observe a lower quenching efficiency for the mixture of GO and PF127. Indeed, as shown in Figure 2.5 (A), the mixture of GO:PF127 (1:1, w/w) did have a lower quenching efficiency than the corresponding GO concentration in the absence of PF127. This observation supported the assumption that the added PF127 blocked the hydrophobic interaction between GO and Trp. Lower quenching effect of the mixture of GO and PF127 was also observed for Tyr. In Chapter 4, the interaction between PF127 and GO will be investigated at the air–water interface using Langmuir monolayer technique.

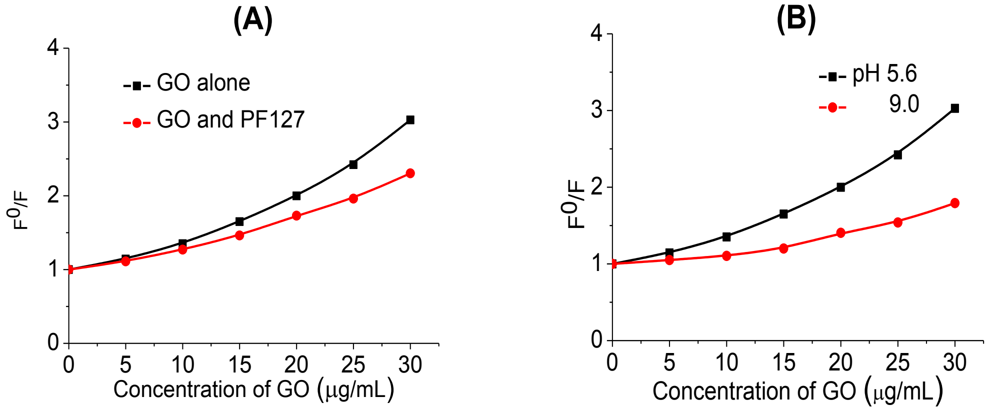

Figure 2.5 Sterm–Volmer plot of Trp under different conditions. (A) 10^{-6} M Trp against the concentration of GO alone, and the mixture of GO:PF127 (1:1, w/w). (B) 10^{-6} M Trp against the concentration of GO at pH 5.6 and 9.

2.3.6 Electrostatic Interaction Study between Trp and GO

Another possible interaction between GO and Trp during quenching could be electrostatic interaction. The carboxylic groups of GO were readily deprotonated when dispersed in water, making it negatively charged. If electrostatic interaction was important for the quenching, decreased quenching efficiency between GO and Trp at basic pH was expected, as GO and Trp were both negatively charged (the isoelectric point for Trp was 5.9). To eliminate any change of pH during mixing, all solutions were prepared at pH 9. The experimental results were shown in Figure 2.5 (B). As expected, the value of F^0/F was lower at pH 9 compared with that at pH 5.6, suggesting that electrostatic interaction did participate in the quenching process. Similar to Trp, the quenching efficiency between GO and Tyr at pH 9 was also lower than that at pH 5.6.

2.3.7 Fluorescence Quenching of Peptides and Proteins by GO

As GO has recently been exploited for drug delivery, and near−infrared photothermal treatment for cancers and Alzheimer's disease,[13,14,42] the understanding of the biophysicochemical interaction between GO and peptides or proteins is fundamentally essential, especially for those drug− or disease−related peptides or proteins, such as amyloid peptides (Aβ) and human islet amyloid polypeptide (hIAPP). $A\beta_{40}$ is the most abundant form of Aβ peptides, associated with Alzheimer's disease. hIAPP, a 37 amino acid residues peptide, is the major source of the amyloid deposits found in the islets of Langerhans of around 95 % type 2 diabetic patients.[39] Both had only one fluorophore, the Tyr residue at position 10 for $A\beta_{40}$ and position 37 for hIAPP in the amino acid sequence, respectively. Serum albumin is the most abundant protein in the circulatory system in mammals, contributing to the osmotic blood pressure and aid in the transport, distribution and metabolism of many endogenous and exogenous ligands.[63] Bovine serum albumin (BSA) and human serum albumin (HSA) have similar structures and are among the most widely used and characterized proteins in the pharmaceutical field.

When mixed with GO, the fluorescence of Tyr in peptides $A\beta_{40}$ or hIAPP was quenched, as shown in Figure 2.6 (A). The emission maximums of both peptides were not shifted. The quenching meant that there was non−covalent interaction between GO and peptide $A\beta_{40}$ or hIAPP, changing the chemical environment of Tyr residue. The difference of quenching efficiency should not be due to the charge differences of $A\beta_{40}$ and hIAPP (The isoelectric point for $A\beta_{40}$ and hIAPP are 5.4 and 8.8, respectively). Instead, the structure differences between $A\beta_{40}$ and hIAPP were probably responsible for the quenching efficiency. The only Tyr reside in $A\beta_{40}$ was located at the hydrophilic N−terminal domain, which had six aromatic amino acid residues (three phenylalanine and three histidine). It was possible that there existed strong π−π interaction or hydrophobic interaction between these residues and GO. While the Tyr residue in hIAPP was located at the hydrophilic domain of the C−terminus, there was no aromatic residues in this domain for the interaction with GO.

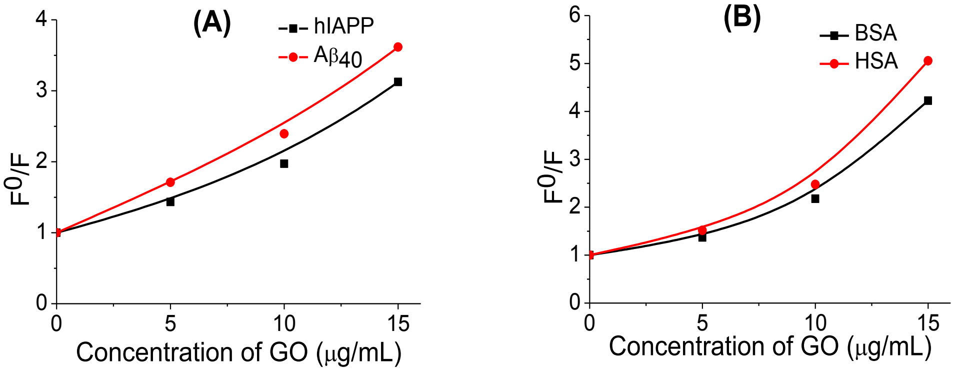

Figure 2.6 The Stern-Volmer plot of different proteins quenched by GO. (A) 10^{-5} M hIAPP and 10^{-5} M $A\beta_{40}$ against the concentration of GO; (B) 10^{-6} M BSA and 10^{-6} M HSA against GO.

GO could also strongly quench the fluorescence of BSA and HSA, with a higher quenching efficiency for HSA, as shown in Figure 2.6 (B). From the view of fluorescent spectroscopy, the main difference between these two proteins was the number of Trp residues. BSA had two Trp (Trp^{135} and Trp^{214}) and HSA only one (Trp^{214}).[64] As the Trp^{214} in both proteins were located in a similar environment, the lower quenching efficiency of GO for BSA was considered to be due to the additional presence of the Trp^{135} in its sequence. Another possibility could be due to conformational changes of protein due to the interaction between GO and these proteins, decreasing the fluorescence intensity.

Based on the observation of the quenching of fluorescent assay of amino acids, peptides, and proteins, it is possible that GO is a universal quencher for tryptophan or tyrosine containing peptides and proteins.

2.4 Summary

In summary, GO was found to interact with amino acids (Trp and Tyr), peptides (Alzheimer's disease related Aβ_{40} and type 2 diabetes related hIAPP), and proteins (drug−related BSA and HSA) by fluorescence quenching. Based on the Stern−Volmer plot and fluorescence lifetime study between Trp or Tyr and GO, the main quenching mechanism was determined as static quenching, slightly combined with dynamic quenching (Förster resonance energy transfer). Both electrostatic interaction and hydrophobic interaction contribute to the interactions between Trp or Tyr and GO. The electrostatic interaction was confirmed by pH effect, while the hydrophobic interaction was proved by the presence of nonionic amphiphilic copolymer PF127. The strong hydrophobic interaction between GO and PF127 efficiently blocked the hydrophobic interaction between GO and Trp or Tyr, lowering the quenching efficiency. Based on the present study, it is possible that GO could be a universal fluorescent quencher for tryptophan or tyrosine containing peptides and proteins.

Chapter 3 Strong and Selective Adsorption of Lysozyme on Graphene Oxide

3.1 Background

An area of significant interest in the biomedical field is application of graphene and graphene oxide (GO) for diagnostics and therapeutic purposes. This is due to their unique chemical and physical properties, such as one−atom−thick two−dimensional nanostructure, high surface to volume ratio, good biocompatibility, and special electronic and mechanical properties.[65-67] The past few years have witnessed great research progress of graphene and GO in diagnostics applications, such as biosensing,[4,68-70] controlled drug delivery (including peptides, proteins, nucleic acids and anticancer drugs),[7,12,23] cellular microscopic imaging,[22,24,71] and photothermal treatment for cancers and Alzheimer's disease.[13,14,42] For such applications, graphene and GO have been explored since 2012 to create a system for analyte detection and quantification *in situ* or in collected biological fluid sample environment, such as milk, saliva, serum, and urine. Liu et al. were able to use GO as a platform to enrich and detect tetracyclines from milk samples by MALDI−TOF mass spectroscopy.[15] To analyze crotonaldehyde rapidly and selectively in saliva samples, Sha et al. developed a magnetic graphene composite as an adsorbent and a matrix.[16] Mannoor et al. recently reported a direct integration of graphene nanosensors with biomaterials for biochemical detection and wireless monitoring in human saliva.[17] To detect and monitor glucose level in human serum and urine samples, Murugan et al. designed a graphene oxide−based electrochemical biosensor with high sensitivity and good stability.[72]

For any biosensor to be considered for diagnostics applications, it needs to show selectivity, sensitivity and specificity in regards to the analyte being tested, either in situ or in collected biological fluids. In other words, the sensor or diagnostic method must be robust to the interference of most abundant proteins and other components in the complex matrix of biological fluid. It is worth noticing that human fluid samples of tears, milk, saliva, serum, and urine contain fairly high amounts of lysozyme (also called 1,4−β−N−acetylmuramidase). In this chapter, interactions between lysozyme and graphene oxide (GO) will be studied to further explore the diagnostics and biosensing applications of GO in biological fluid.

Lysozyme is a small monomeric globular enzymatic protein with 129 amino acids cross−linked by four disulfide bridges. It is part of the innate immune system, hydrolyzing the peptidoglycan present in the bacterial cell walls. It is extremely abundant in human tears, with an average level of 1 568 μg/mL (numbers may vary depending on different samples and methods).[73] Milk and saliva also contain high levels of lysozyme (around 21.4 and 7 μg/mL, respectively).[18,19] The concentrations of lysozyme are lower in serum and urine samples (about 1.7 and 0.18 μg/mL, respectively) from normal human adults.[74,75] However, serum and urine lysozyme levels can be significantly elevated to more than 15 or even 100 μg/mL in patients suffering from leukemia, renal disease, and sarcoidosis.[76-78] Because of the abundance of lysozyme and the detection of specific biomolecules using GO from biological fluid samples as mentioned above, it is extremely important and necessary to investigate the possible adsorption and the interaction between lysozyme and GO. Besides the detection of specific biomolecules, GO has also been used to adhere to and sense leukemia K562 cells.[79] Recently, Yan et al. studied both *in vitro* and *in vivo* biocompatibility and cytotoxicity of GO when it was intravitreally injected into eyes.[80] Their preliminary results suggested that GO had good intraocular biocompatibility with little influence on cell morphology, cell viability, membrane integrity, and apoptosis. Again, due to the presence of extremely high concentration of lysozyme in leukemia cell media and eye tears, one has to concern the possible interaction and adsorption between lysozyme and GO in the process.

Compared with other common nanomaterials, the extremely large surface area on both sides, one−atom thickness (~1 nm), abundant functional groups, and good dispersion in water render GO as an ideal solid substrate to load external species through both covalent and non−covalent binding.[65,81] Studies have shown that some protein molecules can be directly adsorbed on the surface of GO by non−covalent binding without any additional cross−linking reagent.[81-83] However, the nature of the interaction has not been clearly defined. Another issue is that in some practical applications, it is necessary to release and separate the adsorbed species from the substrate. Unfortunately, presently there is no such study showing the separation of immobilized protein from the surface of GO. Moreover, it is important to investigate the selectivity of adsorption on the surface of GO from a mixture of proteins.

In this study, we examined the interaction between GO and lysozyme and the possible applications of this interaction in separation and selective adsorption. Compared with other proteins, such as bovine serum albumin and human serum albumin, the huge fluorescence quenching of lysozyme by GO lysozyme indicates the presence of a much stronger interaction between GO and lysozyme. This interaction and the assembled structure between GO and lysozyme were further characterized using fluorescence quenching, zeta potential, dynamic light scattering, and atomic force microscopy. The nature of the interaction was determined to be mainly an electrostatic interaction. This interaction was so strong that one was able to subsequently eliminate and separate lysozyme from aqueous solution onto the surface of GO. After that, the adsorbed lysozyme could be released from the surface of GO by adding pH 11.5 NaOH solution and then precipitating GO with $CaCl_2$. Furthermore, the strong electrostatic interaction also rendered the selective adsorption of lysozyme on GO from binary and ternary proteins mixtures. This selectivity was confirmed by sodium dodecyl sulfate polyacrylamide gel electrophoresis (SDS−PAGE), fluorescence spectroscopy, and UV−vis absorption spectroscopy.

3.2 Experimental Section

3.2.1 Materials

Single layer graphene oxide (GO) was bought from ACS Material LLC (Medford, MA). Hen egg white lysozyme (LYZ), bovine serum albumin (BSA), and human serum albumin (HSA) were obtained from MP Biomedicals (Solon, OH). Ovalbumin (OVA) and other inorganic salts used in experiments were purchased from Sigma (St. Louis, MO). In gel electrophoresis experiment, Precision Plus Protein™ All Blue Standards were used as the standard protein marker (Bio−Rad, CA). All chemicals were used without any further purification. The deionized water used in the experiments was obtained from a Modulab 2020 Water purification system. The resistivity of the deionized water was 18 MΩ·cm with pH about 5.6 at room temperature.

3.2.2 Methods and Characterization

GO Dispersion. 1 mg/mL GO aqueous dispersion was obtained by adding 10 mL pure water to 10 mg GO, followed by sonication for 1 h in a cold water bath (Branson, model 1510, Danbury, CT). The as−prepared GO dispersion was diluted to certain concentrations either with water or 0.1 M phosphate buffer (pH 7) according to the needs of experiment.

Fluorescence Quenching. For each individual protein (i.e. lysozyme, BSA, HSA, and ovalbumin), 1 mL of 2×10^{-6} M aqueous protein solution was mixed with a certain volume of water (from 1 to 0 mL, in 0.25 mL decrements) and 20 μg/mL GO (from 0 to 1 mL, in 0.25 mL increments). The total volume of mixture solution (GO/protein) was fixed at 2 mL in each case. Therefore, the concentration of protein was fixed at 10^{-6} M, with increment of 2.5 μg/mL GO from 0 to 10 μg/mL. All fluorescence spectra were recorded on a Fluorolog−3 spectrofluorimeter (Horiba Scientific, Edison, NJ) using a 1 cm × 0.2 cm quartz cell. The excitation wavelength was carried out at 290 nm with excitation slit width at 5 nm. The emission was set between 305 to 550 nm with emission slit width at 5 nm. The same experiments were carried out using NaOH aqueous solution at pH 10 and 12 throughout the procedures. Due to the fact that GO had absorption in the range of 270~350 nm, which overlapped with the excitation and emission of the proteins, the fluorescence intensity after the addition of GO was corrected with previous methods to remove “inner filter effect”.[56,57,84] After this correction, F_0/F against the concentration of GO was plotted, where F_0 and F were the maximum fluorescence intensity in the absence and in the presence of GO, respectively.

Zeta Potential and Dynamic Light Scattering (DLS). Solution−based zeta potential and DLS analyses were characterized using a Zetasizer Nano ZS System (Malvern Inc., UK) with irradiation from a standard 633 nm laser. The zeta potentials of 14.3 μg/mL (i.e. 10^{-6} M) lysozyme, 5 μg/mL GO, and the mixture GO/LYZ (5 μg/mL GO and 14.3

μg/mL LYZ) were recorded under pH 5.6, 10, and 12. In order to study the zeta potential changes of the mixture GO/LYZ at pH 5.6, GO was fixed at 5 μg/mL while the concentration of LYZ was varied from 0 to 100 μg/mL. The hydrodynamic diameters of lysozyme, GO, and GO/LYZ at pH 5.6, 10, and 12 were carried out by DLS using the same concentrations as the fluorescence quenching study.

Atomic Force Microscopy (AFM). AFM images were obtained using tapping mode with an Agilent 5420 AFM instrument (Agilent, Santa Clara, CA). The cantilever used in experiments had a resonance frequency of 300 ~ 400 kHz with a typical force constant of 40 N/m. 6 μL of 10 μg/mL GO, 10^{-6} M lysozyme, or GO/LYZ was deposited on a freshly cleaved mica surface and dried for 2 h in air before scanning. All images were taken at a resolution of 512 × 512 pixels.

Adsorption and Desorption. In the adsorption experiment (flow chart **a** to **d** in Figure 3.1), 1 mL of 0.4 mg/mL GO was added to 2 mL of 2×10^{-5} M (i.e. 0.286 mg/mL) lysozyme water solution in a test tube. As a result, the final concentration of lysozyme in the mixture was 0.143 mg/mL, and 0.1 mg/mL for GO (this concentration ratio was chosen based on the fluorescence quenching study). After mixing well on a vortex mixer, 1 mL of 1 M NaCl solution was added and then mixed throughout. Centrifugation at 2500 rpm for 10 min yielded a clear supernatant in the upper layer and dark brown precipitate at the bottom. Control experiments were done under the same procedures by replacing 2 mL of GO with 2 mL of water. The supernatant was pipetted to a 1 cm × 1 cm quartz cell and scanned by a UV−2600 spectrophotometer (Shimadzu Inc., Japan). Fluorescence spectra were obtained using the same methods as fluorescence quenching above.

To desorb lysozyme from the surface of GO, we removed 3 mL of supernatant, added 2.5 mL of pH 11.5 NaOH, and then sonicated for 30 seconds. After that, 0.5 mL of 0.1 M $CaCl_2$ was added to precipitate GO from the solution. The precipitates were removed by centrifugation, while lysozyme was left in the supernatant (flowchart **d**, **f**, **g**, and **h** in Figure 3.1).

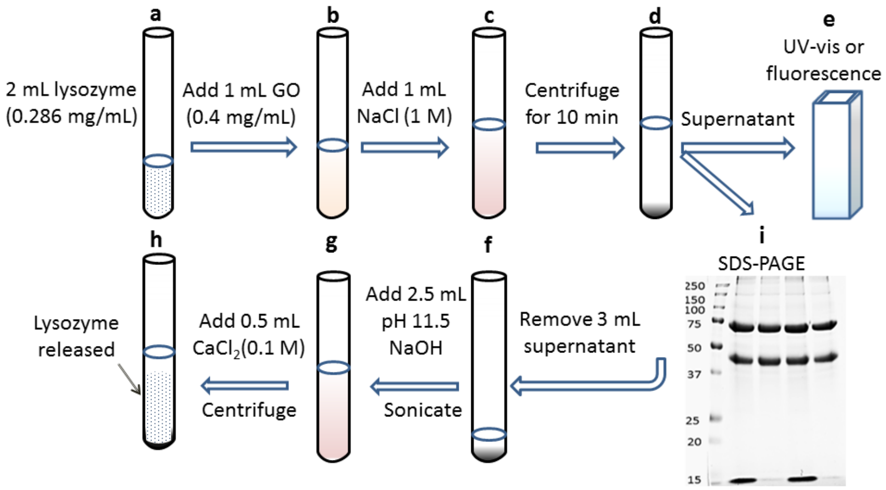

Figure 3.1 Flowchart of adsorption and desorption study of lysozyme on GO.

Selective Adsorption of Lysozyme. The selective adsorption of lysozyme from a mixture of binary proteins (i.e. LYZ/BSA, LYZ/HSA, and LYZ/OVA) and ternary proteins (i.e., LYZ/OVA/BSA and LYZ/OVA/HSA) was carried out using the same procedures as the adsorption experiment above (flowchart **a** to **e** in Figure 3.1). 0.1 M phosphate buffer (pH 7) was used as solvent throughout the experiment instead of water. Each protein had a final concentration of 0.143 mg/mL in the mixture after GO and NaCl were added. The final concentration of GO was 0.1 mg/mL in the mixture. Control experiments were carried out without adding GO. To test the selective adsorption, the supernatant in each case was characterized by SDS−PAGE, fluorescence emission and

UV−vis absorption. 12 % SDS−PAGE gels were used in the experiment. 40 μL of each sample was loaded in each well. The gels were run under 200 V for 40 min, followed by staining with Imperial Protein Stain (Thermo Fisher Scientific Inc., Rockford, IL) according to the manufacturer's protocol.

3.3 Results and Discussions

3.3.1 Fluorescence Quenching of Lysozyme by GO

Characterizations of the commercially available GO used in this study by UV−vis absorption and atomic force microscopy (AFM) were consistent with other studies and our previous results, confirming that GO was indeed a single layer nanosheet.[42,45,48,84,85] In our previous study, we have demonstrated that GO can be a universal fluorescent quencher for peptides and proteins containing tryptophan or tyrosine.[84] Fluorescence quenching studies of GO on proteins supported this assumption, such as human serum albumin (HSA), bovine serum albumin (BSA), amyloid beta−40, and human islet amyloid polypeptide (hIAPP).[84] The Stern−Volmer plot of 10^{-6} M BSA and HSA quenched by GO at pH 5.6 is shown in Figure 3.2 (A). The values of F_0/F of BSA and HSA are both around 1.5 when the concentration of GO is 10 μg/mL, where F_0 and F are the fluorescence intensity at the maxima in the absence and in the presence of GO, respectively. The quenching of 10^{-6} M BSA or HSA by GO is also comparable with that of 10^{-6} M tryptophan (~ 1.4).[84] Surprisingly, compared with the quenching of 10^{-6} M BSA, HSA, and tryptophan by GO, the emission intensity of 10^{-6} M lysozyme dropped much more dramatically as the concentration of GO increased. F_0/F of lysozyme increased to 26.5 in the presence of 10 μg/mL GO, as shown in red color in Figure 3.2

(B). The fast reduction of fluorescence intensity reveals the existence of a strong interaction between GO and lysozyme.

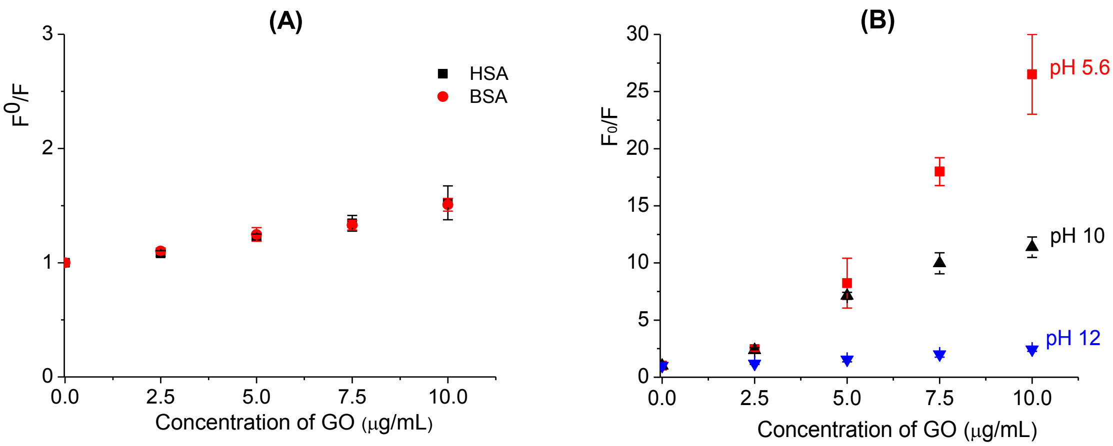

Figure 3.2 Stern−Volmer plot of F_0/F against concentration of GO as quencher. (A) F_0/F of 10^{-6} M HSA and BSA at pH 5.6; (B) F_0/F of 10^{-6} M lysozyme at pH 5.6, 10, and 12. F_0 and F are the fluorescence intensity at the maxima in the absence and in the presence of GO, respectively.

In order to determine the nature of interaction between GO and lysozyme, three pH values were used in the experiment (i.e. pH 5.6, 10, and 12). The pH value is extremely important for determining the charge of lysozyme. If the pH is lower than its isoelectric point (about 11),[86] lysozyme possesses more positive charges. Thus lysozyme is more positively charged at pH 5.6 than at pH 10. Higher pH (i.e. pH 12 in this study) than the isoelectric point renders lysozyme to have more negative charges. Due to the deprotonation of carboxyl and hydroxyl groups on its surface, GO is always negatively charged under pH 5.6, 10 and 12.[87] If the interaction between GO and lysozyme is mainly an electrostatic interaction, pH will play a central role on the quenching effect. Indeed, as pH increases from 5.6 to 12, the quenching effect reduces quickly, as shown in Figure 3.2 (B). At 10 μg/mL of GO, F_0/F drops from 26.5 at pH 5.6 to 11.4 at pH 10. When pH reaches 12, only a slight fluorescence quenching is observed, with the value of F_0/F about 1.6. This small quenching at pH 12 is probably due to the hydrophobic interaction between them.[44] From these observations, it can be stated that the strong quenching of GO on lysozyme is predominantly due to the electrostatic attraction between lysozyme and GO. Further evidence for this assumption will be presented and discussed below. On the contrary, BSA and HSA are both negatively charged in aqueous solution at pH 5.6 as both isoelectric points are below 5.6. As a result, neither BSA nor HSA favors electrostatic interaction with GO at pH 5.6. This explains why the quenching of BSA or HSA by GO is more reduced than that of lysozyme (Figure 3.2).

3.3.2 Zeta Potential Study

Zeta potential was used to further characterize the nature of the interaction between lysozyme and GO (Table 3.1). Due to the protonation of its surface functional groups, 5 μg/mL GO is negatively charged with −38.85 mV at pH 5.6. As pH increases, its zeta potential slightly shifts to −40 mV at pH 10 and −41.25 mV at pH 12. These results are consistent with other reported studies.[87,88] 10^{-6} M lysozyme is slightly positively charged at pH 5.6 and 10. The values of zeta potential of lysozyme may not be the true values probably due to the low concentration. Usually, the concentration of protein used for zeta potential measurement is required to be larger than 0.1 mg/mL. Therefore, the following discussion will be based on the zeta potential changes of GO at 5 μg/mL and the mixture GO/LYZ (5 μg/mL GO and 14.3 μg/mL LYZ). At pH 5.6, the zeta potential of GO is −38.85 mV, while it is changed greatly to −9.05 mV in the mixture GO/LYZ (Table 3.1). However, at pH 10 and 12, the zeta potentials of the mixtures are −35.67 and −39.10 mV, respectively. Both are comparable to the zeta potential values of GO alone at the corresponding pHs. These changes indicate that at pH 5.6 there is a strong electrostatic interaction between GO and lysozyme, neutralizing the surface charge of GO. To further verify this interaction, a titration experiment of zeta potential with GO concentration fixed at 5 μg/mL was performed (Figure 3.3). The zeta potential value of GO/LYZ mixture shifts toward positive as the concentration of lysozyme increases. The value reaches about 0 mV when lysozyme is 20 μg/mL, corresponding to the maximum coverage of lysozyme on the surface of GO.

Table 3.1 Zeta potential data of GO (5 μg/mL), lysozyme (10^{-6} M, i.e. 14.3 μg/mL), and GO/LYZ mixture (5 μg/mL GO, 10^{-6} M lysozyme) at pH 5.6, 10, and 12.

	Zeta potential (mV)		
	pH 5.6	pH 10	pH 12
GO	−38.85	−40.00	−41.25
Lysozyme	4.02	0.06	−8.02
GO/LYZ	−9.05	−35.67	−39.10

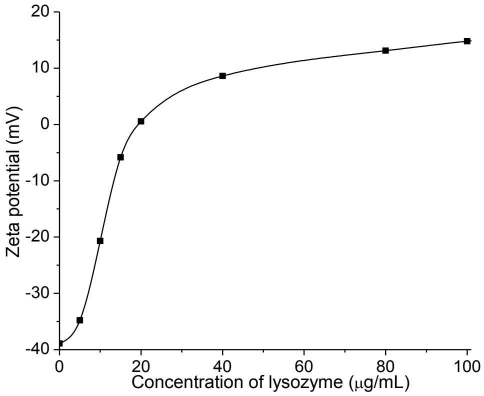

Figure 3.3 Zeta potential of GO/LYZ aqueous solution against LYZ concentration. The concentration of GO was fixed at 5 μg/mL.

3.3.3 Dynamic Light Scattering (DLS) Study

Due to the strong electrostatic interaction and unique large surface area of both sides of GO, lysozyme can be adsorbed onto its surfaces, increasing the size of the assemblies. Dynamic light scattering (DLS) is an analytical technique widely used to characterize the size in terms of hydrodynamic diameter of nanoparticles or colloids in aqueous solution.[89,90] The exact size of GO may vary depending on the method and procedure of processing. As shown in Figure 3.4 (A), the peak distributions (≥ 92%) of the hydrodynamic diameters of GO are around 200 (± 50) nm with limited influence from the pHs studied (i.e. pH 5.6, 10, and 12) and the concentrations (from 0 to 10 μg/mL). This indicates that GO does not flocculate or aggregate under these pHs and concentrations. These observations are consistent with other previous studies of GO by DLS.[21,91] In our experiments, the size distribution of 10^{-6} M lysozyme at pH 5.6, 10, and 12 are below the limitation of the DLS system.

However, in the mixture of GO/LYZ (lysozyme was always fixed at 10^{-6} M in DLS experiments), the size distribution dramatically depends on the pH and the concentration of GO, as illustrated in Figure 3.4 (B). First, the hydrodynamic diameter of the mixture decreases as the pH increases from 5.6 to 12 at each corresponding concentration of GO. The reduction in size at higher pH indicates that the interaction between GO and lysozyme is weaker at higher pH. Second, the size of GO/LYZ mixture at pH 12 is about the same as the pure GO, indicating that no assembly is formed between GO and lysozyme at pH 12. This should be due to the electrostatic repulsion between the negatively charged lysozyme and negatively charged GO at pH 12. These observations also provide further support to the nature of the interaction as we discussed above. Third, it is worth noticing that the hydrodynamic diameter of the mixture decreases as the concentration of GO increases in both cases of pH 5.6 and 10, as shown in Figure 3.4 (B). This trend of decrease in diameter could be due to the diminishing thickness of protein “corona” formed on the surface of GO as a “core” when the concentration of GO increases.[92,93] At lower concentrations of GO at pH 5.6, i.e. 2.5 μg/mL, as the total amount of lysozyme is fixed at a constant in all cases, the amount of lysozyme absorbed per unit surface area of GO will be larger than that at higher concentrations of GO. This means that the thickness of the adsorbed lysozyme “corona” will be larger at lower concentrations of GO. On the contrary, when more GO is present in the solution, fewer amounts of lysozyme are adsorbed on each piece of GO, decreasing the hydrodynamic diameter.

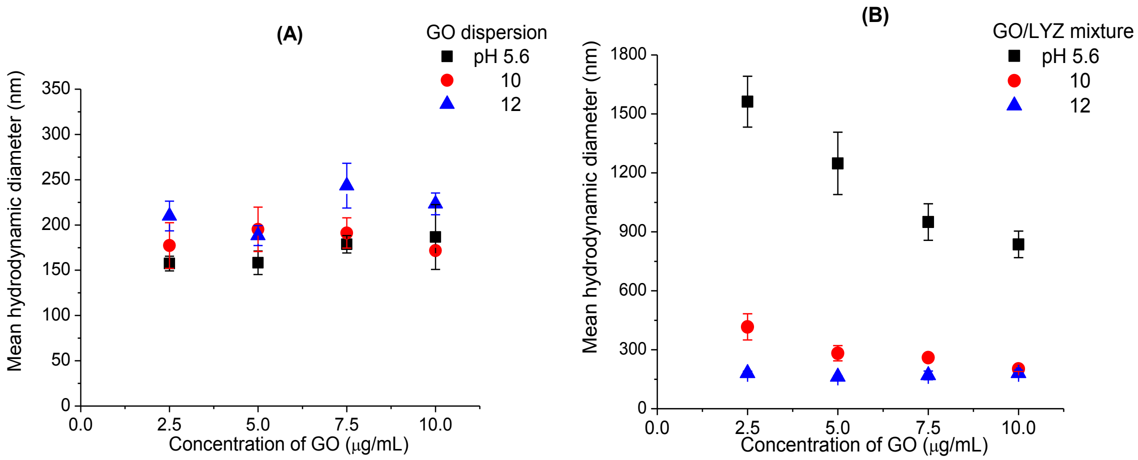

Figure 3.4 Hydrodynamic diameter at pH 5.6, 10, and 12. (A) GO dispersion; (B) GO/LYZ mixture.

3.3.4 Atomic Force Microscopy (AFM) Study

AFM was used to directly visualize morphologies on a freshly cleaved mica surface after the solvent was evaporated. We only obtained AFM images at pH 5.6, since hydroxyl ions at pH 10 and 12 would be neutralized by carbon dioxide from the air while drying. As shown in Figure 3.5 (A), the height of GO nanosheets is around 1 nm after 6 μL of 10 μg/mL GO was deposited and dried on mica surface. The uniform height demonstrates that GO nanosheets do not flocculate or aggregate while drying. The AFM image of 10^{-6} M lysozyme after drying shows very tiny spots with height about 1 nm (Figure 3.5 (B)). The observations here are similar to previous AFM studies of lysozyme adsorption on mica.[94,95] However, the AFM image of GO/LYZ mixture (10 μg/mL GO and 10^{-6} M lysozyme) shows totally different images compared with GO or lysozyme alone (Figure 3.5 (C)). No single nanosheet of GO is observed. Pieces of GO seem to be packed together tightly on each other with uneven height from 3.5 nm to more than 20 nm. These observations provide direct proof that lysozyme is adsorbed on the surface of GO.

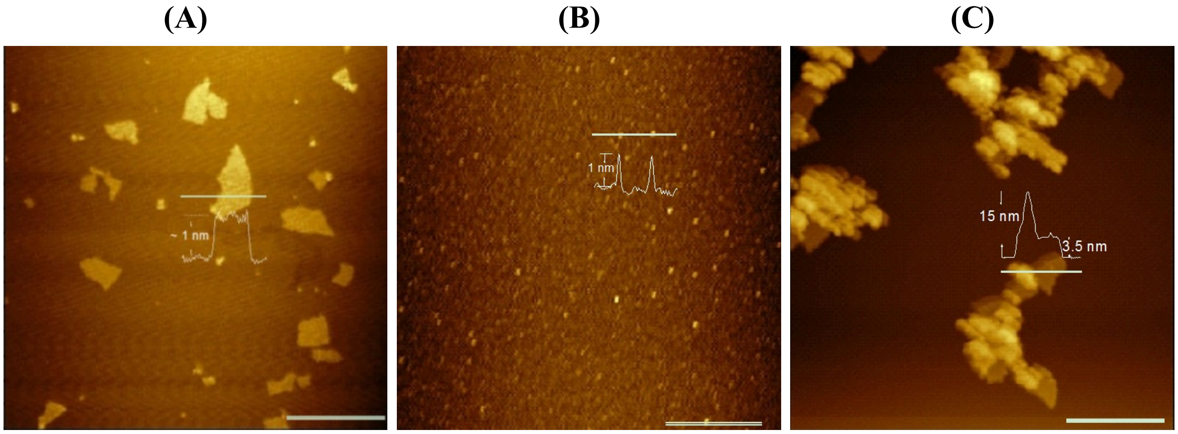

Figure 3.5 AFM images of (A) GO; (B) lysozyme; and (C) GO/LYZ mixture. About 6 μL of corresponding solution was deposited and dried on the surface of mica. The profiles are shown in white curves. The scale bar at the bottom right in each figure is 1 μm.

We have so far demonstrated that the strong interaction between GO and lysozyme is electrostatic interaction using the methods above, but it is worth noticing that some weak interactions may also exist, such as π-π interaction, hydrophobic interaction, and hydrogen bonding. The π-π interaction can exist between the aromatic rings of GO and the indole structure of tryptophan residues. These weak interactions explain the slight fluorescence quenching of lysozyme by GO at pH 12 in Figure 3.2 (B).

3.3.5 Adsorption and Desorption of Lysozyme on GO

We have demonstrated that the interaction between GO and lysozyme is mainly an electrostatic interaction. Indeed, this interaction was so strong that we were able to subsequently remove and separate lysozyme from aqueous solution by GO experimentally. As discussed above, more than 96% of the fluorescent emission of 10^{-6} M (14.3 μg/mL) lysozyme was quenched by 10 μg/mL GO. In order to clearly observe the adsorption effect of lysozyme on GO in experiments, 10−fold concentrations (i.e. 0.143 mg/mL lysozyme and 0.1 mg/mL GO) were used. The procedures were shown in Figure 3.1 (Step **a** to **e**). Once GO was added into lysozyme solutions, larger assemblies between lysozyme and GO were formed as suspension. To precipitate the assemblies, 1 M NaCl was added into the mixture of GO/LYZ. Immediately, one could observe precipitate formation. The ionic strength of NaCl further neutralized the surface charge and promoted the precipitate formation. After agglomeration for 5 min, the mixture was centrifuged at 2500 rpm for 10 min. At the bottom of centrifuge tube, dark brown precipitate was formed, while the upper layer solution was totally clear. The supernatant solution was used for fluorescence spectroscopy, UV−vis absorption, and SDS−PAGE (sodium dodecyl sulfate polyacrylamide gel electrophoresis). With the same excitation conditions, the supernatant solution was slightly fluorescent at 358 nm, about 2.8 % of the fluorescence intensity of 0.143 mg/mL under the same condition without GO, as shown in Figure 3.6 (A). This result suggested that GO adsorbed almost all lysozyme on its surface. To further support this assumption, UV−vis absorption of the supernatant solution was compared with the control experiments. It also confirmed this assumption; because the absorption around 280 nm was almost completely disappeared after the adsorption of GO (Figure 3.6 (B)). SDS−PAGE also showed that the band of lysozyme was completely removed after the adsorption of GO (Figure 3.7 (A), Lane 1 as control and Lane 2 after the adsorption of GO). Therefore, GO could be an excellent adsorbent material to remove lysozyme from its aqueous solution.

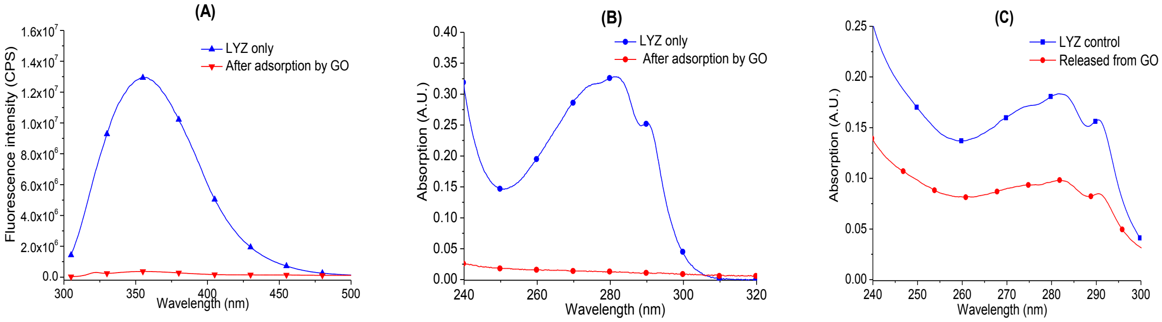

Figure 3.6 Spectra of fluorescence and UV−vis absorption before and after adsorption by GO. (A) Fluorescence spectra of lysozyme before and after adsorption by GO; (B) UV−vis absorption spectra of lysozyme before and after adsorption by GO; (C) UV−vis absorption of lysozyme of original solution and after being released from GO. It is worth noticing that $CaCl_2$ changes the molar absorptivity of lysozyme. This explains the absorption difference of lysozyme in (B) and (C).

It is sometimes necessary in practice to separate the adsorbed protein from the substrate. In the case of lysozyme, we were able to release lysozyme from the surface of GO by chemical approach, as shown in Figure 3.1 (Step **d**, **f**, **g**, and **h**). After centrifugation, remove 3 mL of the supernatant solution and add 2.5 mL pH 11.5 NaOH to disperse the precipitates again. As we discussed above, the interaction between GO and lysozyme at basic pH should be very weak, disassembling lysozyme from the GO surface. Indeed, after sonication, a golden color solution was obtained again. To further separate lysozyme and GO, 0.5 mL of 0.1 M $CaCl_2$ solution was added to precipitate GO. As Ca^{2+} formed precipitates with GO with very large solubility product constant, lysozyme was left in the supernatant. Based on the UV−vis absorption spectrum of the supernatant, about 54 % lysozyme was released (Figure 3.6 (C)).

3.3.6 Selective Adsorption of Lysozyme

If the interaction between lysozyme and GO is strong enough, one will expect to use this interaction to selectively adsorb lysozyme by GO from a mixture of proteins. It is worth noticing that this selectivity is based on electrostatic interaction. If two proteins are positively charged and have similar isoelectric points (pI), both can be adsorbed on the surface of GO without much selectivity. Herein, we studied this application in 0.1 M phosphate buffer at pH 7 in the mixture of lysozyme (LYZ, pI 11, 14.3 kDa), bovine serum albumin (BSA, pI 5.3, 68 kDa), human serum albumin (HSA, pI 4.7, 66.5 kDa), and ovalbumin (OVA, pI 4.9, 43 kDa), following the same procedures of adsorption as shown in Figure 3.1 (Step **a** to **e**). In a binary protein mixture (i.e. LYZ/BSA, LYZ/HSA, or LYZ/OVA), GO and NaCl solutions were added to form precipitates. After centrifugation, the supernatant was characterized by SDS−PAGE (Figure 3.7), fluorescence emission, and UV−vis absorption spectra.

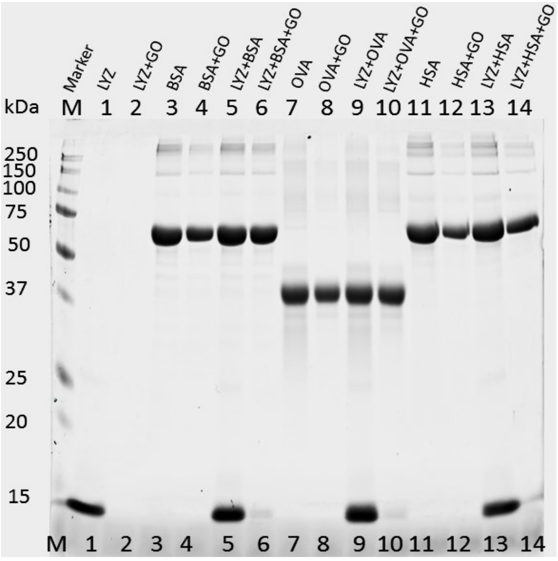

Figure 3.7 Image of electrophoresis on 12 % SDS−PAGE. Protein marker (Lane M), LYZ control (Lane 1), LYZ adsorbed by GO (Lane 2), BSA control (Lane 3), BSA adsorbed by GO (Lane 4), LYZ/BSA control (Lane 5), LYZ/BSA adsorbed by GO (Lane 6), OVA control (Lane 7), OVA adsorbed by GO (Lane 8), LYZ/OVA control (Lane 9), LYZ/OVA adsorbed by GO (Lane 10), HSA control (Lane 11), HSA adsorbed by GO (Lane 12), LYZ/HSA control (Lane 13), and LYZ/HSA adsorbed by GO (Lane 14). The concentration of each protein (i.e. LYZ, BSA, OVA and HSA) was 0.143 mg/mL, while the final concentration of GO was 0.1 mg/mL, if present.

Proteins with different molecular weights could be easily separated by SDS−PAGE, therefore this technique was able to provide visual evidence of selective adsorption of GO. Compared with its band at 14.3 kDa as a control experiment (Lane 1 in Figure 3.7), lysozyme was completely adsorbed when GO was present (Lane 2 in Figure 3.7). On the contrary, BSA (Lane 4) was slightly adsorbed by GO in comparison with its control experiment without GO (Lane 3). In the binary protein mixture of LYZ/BSA, bands of both proteins were clearly seen (Lane 5). After the adsorption by GO (Lane 6), the band of LYZ was barely seen while the band of BSA was as clear as before adsorption. The disappearance of lysozyme band suggested that it was adsorbed and co−precipitated by

GO. Similar observations were also found for LYZ/OVA and LYZ/HSA systems in experiments, as shown in Figure 3.7.

To further support the assumption that GO was able to selectively adsorb lysozyme from a mixture of binary proteins system, fluorescence emission and UV−vis absorption were used to characterize the supernatant after centrifugation, as shown in Figure 3.8. The obtained fluorescence (Figure 3.8 (A), (C) and (E)) and UV−vis absorption (Figure 3.8 (B), (D) and (F)) spectra of the mixture after adsorption by GO (the green curves) were very similar to those of the control experiments using a single protein of BSA, HSA, and OVA (the black curves). These observations again confirmed that lysozyme was selectively adsorbed and co−precipitated by GO, leaving other proteins (i.e. BSA, HSA, and OVA) in the solution.

In a ternary mixture of proteins, i.e. LYZ/OVA/HSA and LYZ/OVA/BSA (each protein was 0.143 mg/mL), a final concentration of GO at 0.1 mg/mL was also able to selectively adsorb lysozyme from the mixture, as shown by the results of SDS−PAGE (Figure 3.9). Compared with the corresponding control experiment, lysozyme in the ternary mixture of proteins was clearly adsorbed by GO, since the band of lysozyme was barely seen.

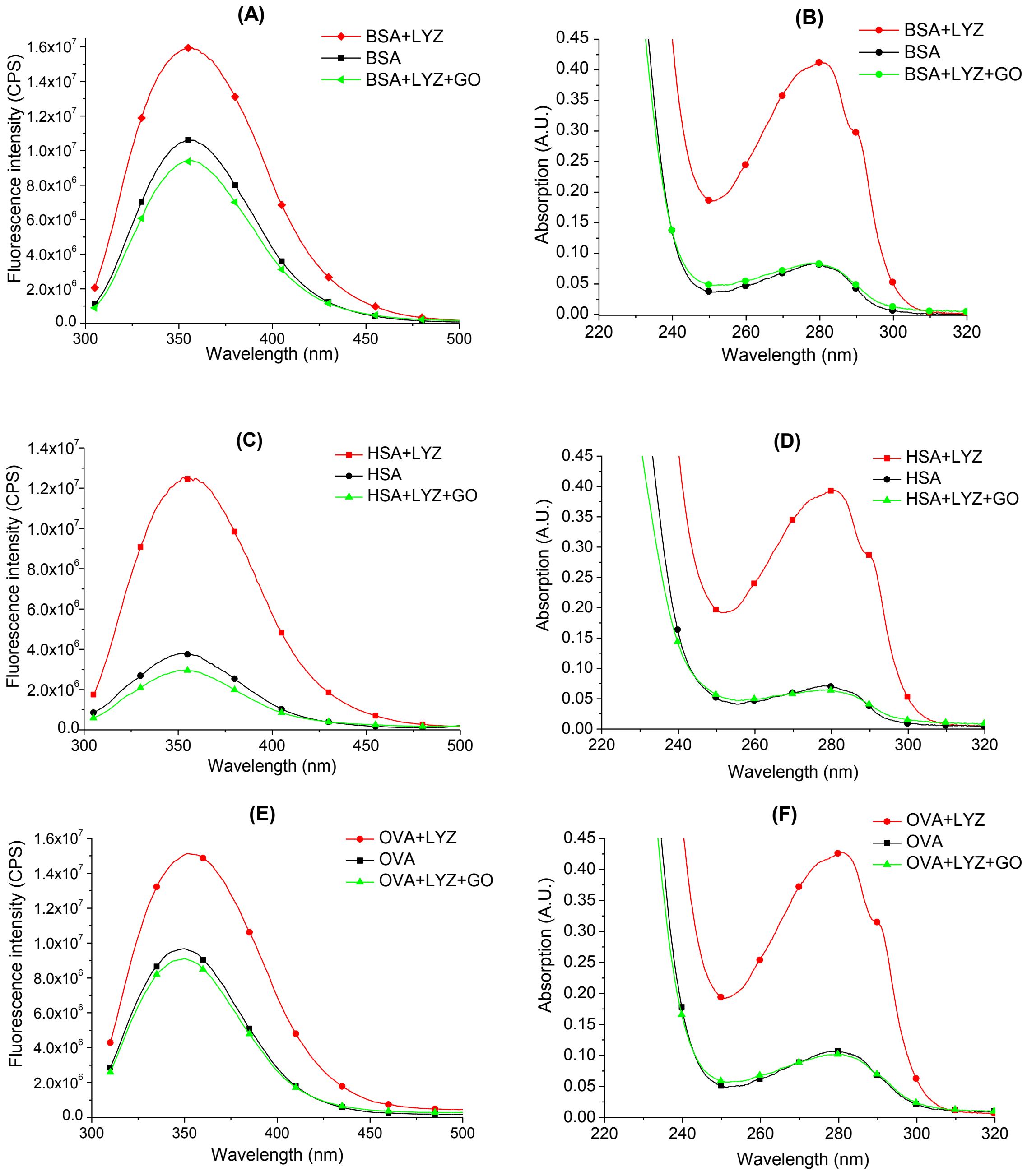

Figure 3.8 Fluorescence (the first column, i.e. A, C and E) and UV−vis (the second column, i.e. B, D and F) absorption spectra of binary protein mixtures before and after adsorption by GO: BSA/LYZ (A, B); HSA/LYZ (C, D); OVA/LYZ (E, F).

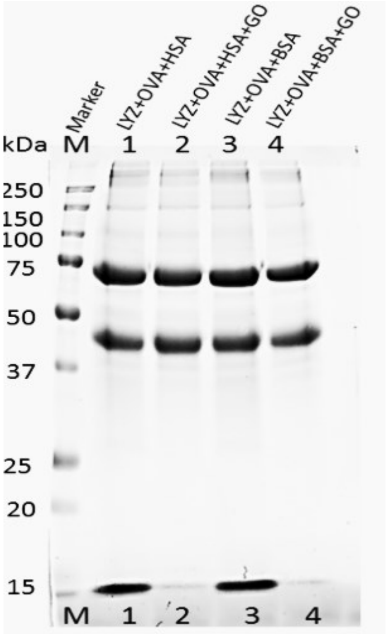

Figure 3.9 Image of electrophoresis of ternary mixture on 12 % SDS−PAGE. Protein marker (Lane M), LYZ/OVA/HSA control (Lane 1), LYZ/OVA/HSA adsorbed by GO (Lane 2), LYZ/OVA/BSA control (Lane 3), LYZ/OVA/BSA adsorbed by GO (Lane 4). The concentration of each protein (i.e. LYZ, BSA, OVA and HSA) was 0.143 mg/mL. The final concentration of GO was 0.1 mg/mL, if present.

3.4 Summary

Graphene oxide (GO) is recently emerging as a promising nanomaterial with potential applications to detect analytes from biological fluid samples, such as milk, saliva, serum, and urine.[15-17,72] Due to the abundance of lysozyme present in such biological fluid samples, it is extremely important and necessary to investigate the possible interaction and adsorption between lysozyme and GO. In this study, we investigated the strong interaction between GO and lysozyme by fluorescence quenching, zeta potential, dynamic light scattering, and atomic force microscopy. The nature of the interaction was determined to be predominantly an electrostatic interaction. This interaction was so strong that we were able to subsequently eliminate and separate lysozyme from aqueous solution by simply mixing with GO. The adsorbed lysozyme could be released from the surface of GO by adding NaOH solution and then precipitating GO with $CaCl_2$. More importantly, the strong electrostatic interaction also rendered the selective adsorption of lysozyme on GO from mixtures of binary proteins and ternary proteins, which was confirmed by fluorescence spectroscopy, UV−vis absorption spectroscopy, and sodium dodecyl sulfate polyacrylamide gel electrophoresis.

As we demonstrate in this study, lysozyme interacts strongly with the surfaces of GO and can be selectively adsorbed and separated via an electrostatic interaction. When the material of GO is explored to detect or sense a specific biomolecule from biological fluid samples, one has to consider the presence of lysozyme and the strong interaction between it and GO.

Chapter 4 Interaction between Graphene Oxide and Pluronic F127 at the Air−Water Interface

4.1 Background

In the past two decades, biocompatible polymers have attracted great attention in the field of medical applications, such as drug delivery, gene therapy, surface coatings, and tissue engineering.[96,97] Amphiphilic and biodegradable polymers are attractive candidates for drug delivery systems with potential to improve drug circulation time, increase drug solubility and reduce toxicity and side effect.[98,99] Among a large family of these polymers, nonionic triblock copolymers composed of poly(propylene oxide) (PPO) hydrophobic midblock and two poly(ethylene oxide) (PEO) hydrophilic end blocks (PEO−PPO−PEO, commercially known as Pluronic or Poloxamer), are of particular interest for properties of adsorption, self−assembly and micellization.[100-105] More recently, PEO−PPO−PEO has been found to be able to seal damaged cell membrane with low toxicity, which is probably due to its surface activity and adsorption capacity into the bilayer of the damaged cell.[106,107]

Graphene oxide (GO), an oxidized form of graphene, has been gaining significant momentum over the last few years for its application in the biomedical field due to the unique properties, such as good water dispersibility, excellent biocompatibility, and strong adsorption capacity.[5] Since GO based material was first used to deliver water insoluble drugs, much progress has been achieved for drug delivery.[7,108] Recently, efforts have been made on GO functionalization to enhance special cellular uptake of anti−tumor drugs with intelligent controlled release, such as conjugation of GO with targeting ligands like folic acid and magnetic Fe_3O_4.[5] GO is also investigated for biosensing,[43,44] and photothermal treatment for cancers and Alzheimer's disease.[13,14,42]

One challenge of GO in biomedical application is its agglomeration or precipitation in electrolyte solutions. Since electrolytes (e.g. sodium, potassium, calcium, chloride, and bicarbonate) are essential components of body fluids, they must be maintained at a specific concentration for the cells to function properly. One strategy to enhance the stability of GO in electrolyte solutions is to covalently modify GO with further oxidization to lower C/O ratio or to functionalize GO with a hydrophilic moiety.[7,21] However, this strategy increases the complexity of the chemical preparation, and covalently modifies the structures and properties of GO. Recently, non−covalently suspending GO in electrolyte solutions has been explored using biocompatible polymers.[21] Pluronic F127 (PF127, PEO_{100}−PPO_{65}−PEO_{100}), approved by FDA (Food and Drug Administration) for drug delivery, has been previously demonstrated to efficiently disperse graphene and GO in cell medium in the presence of electrolytes.[21,62,109] We also have reported in Chapter 2 that PF127 can be applied to block the hydrophobic interaction between GO and L−tryptophan or L−tyrosine. In principle, the hydrophobic segment of PPO in PF127 can interact with the hydrophobic part of GO, while the hydrophilic section of PEO should form hydrogen bonds with the surrounding water molecules, thus stabilizing the suspension.[21,62,110] However, the nature of the interaction and the behavior between GO and PF127 has still not been understood and characterized.

Langmuir monolayer technique at air−water interface is a typical two−dimensional (2D) surface chemistry approach, widely applied for the structure and property studies of amphiphilic molecules at the interface, such as surfactants, polymer, proteins and lipids.[105,106,111,112] The conformation and molecular interactions at the interface can be controlled and tuned by adjusting the interfacial area or by altering the components of the subphase solution. GO has both hydrophobic and hydrophilic parts in its structure, with carboxylic groups at the edge, phenol hydroxyl and epoxide groups mainly at the basal plane, and some intact carbon−carbon sp^2 domains.[2] GO Langmuir monolayer has previously been studied by spreading GO solution at the air−water interface.[113,114] However, compared with a usual spreading volume of less than 100 μL at the air−water interface, the deposited volumes of GO in those studies were so large (from a few mL to 12 mL.[16,17]) that one has to be concerned whether it forms a Langmuir monolayer at the interface without losing GO particles into the subphase solution.

In the present study, we aimed to characterize and understand the interaction between GO and PF127 using a 2D Langmuir monolayer approach at the air−water interface by surface pressure−area isotherm measurements, stability, adsorption, and atomic force microscopy (AFM) imaging. Based on the experimental observations, a hypothesis of the interaction of PF127 and GO at the air−water interface is proposed.

4.2 Experimental Section

4.2.1 Materials

Single layer graphene oxide (GO) was purchased from ACS Material LLC (Medford, MA). Triblock copolymer Pluronic F127 (PF127, PEO_{100}−PPO_{65}−PEO_{100}, mean molecular weight 12,600 g/mol) was obtained from Sigma Aldrich (St. Louis, MO). These chemicals were used without further purification. Throughout the experiments, deionized water was purified with a Modulab 2020 water purification system from Continental Water Systems Corp (San Antonio, TX). The resistivity, surface tension and pH of deionized water were 18 MΩ·cm, 72.6 mN/m and 5.6 at 20.0 ± 0.5 ºC, respectively. V−1 grade mica (Electron Microscopy Sciences, Hatfield, PA) was used as a substrate for atomic force microscopy (AFM) imaging.

All surface pressure−area isotherm measurements and atomic force microscopy (AFM) images were performed in a clean room (class 1000) with constant temperature of 20.0 ± 0.5 ºC and humidity of 50 ± 1%.

4.2.2 Methods and characterization

Langmuir Monolayer Preparation of PF127/GO on Pure Water. 1 mg/mL of GO aqueous solution was obtained by adding 5 mL pure water to 5 mg GO, and followed by sonication for 1 h in a cold water bath (Branson, model 1510, Danbury, CT). The as−prepared GO solution was diluted to 0.1 to 0.5 mg/mL to make the mixture of PF127/GO. We have previously demonstrated using UV−vis absorption and AFM that single layer graphene oxide was yielded using the same material and procedure. 0.1 mg/mL PF127 aqueous solution was obtained by dissolving 10 mg PF127 in a 100 mL flask. As this concentration was much lower than its critical micelle concentration (CMC) of around 50 mg/mL at 20 ºC,[115] no micelle of PF127 was formed during the experiments. For mixtures of PF127/GO, the concentrations of PF127 were kept at 0.05 mg/mL in all cases to compare with the behaviors of 0.05 mg/mL PF127 alone at the air−water interface, while the weight ratios between PF127 and GO were 1:0, 1:2, 1:3, and 1:5 (w/w). A Kibron μ−trough S (Kibron Inc., Helsinki, Finland) with an area of 5.9 cm × 21.1 cm was used for the surface pressure−area isotherms, adsorption and stability studies. The surface pressure was monitored by an alloy wire probe with a sensitivity of ±

0.01 mN/m. Typically, 35 μL of PF127/GO mixture was spread dropwise on the air−water interface of pure water using a 100 μL syringe (Hamilton Co., Reno, NV). A waiting time period of 15 min was taken for the Langmuir monolayer to reach equilibrium. The surface pressure−area isotherms were then recorded at a compression rate of 1200 $Å^2$/molecule per min.

Langmuir Monolayer Study of PF127 at the Air−GO Aqueous Interface. To study the adsorption of GO from the subphase to the Langmuir monolayer of PF127, 35 μL of 0.05 mg/mL PF127 was deposited dropwise at the interface of GO aqueous dispersion with different GO concentrations (0, 0.02 and 0.04 mg/mL). After 15 min, the monolayer was compressed at a rate of 1200 $Å^2$/molecule per min.

Stability study of Langmuir Monolayer. The Langmuir monolayer of PF127 alone or mixed PF127/GO (1:1, w/w) were compressed to 7 mN/m with a rate of 800 $Å^2$/molecule per min. After 5 min for relaxation, the Langmuir monolayer was compressed to 7 mN/m again, and then the stability of surface pressure versus time was monitored at a fixed area.

AFM Imaging. All AFM images were taken with tapping mode using an Agilent 5420 AFM instrument (Agilent, Santa Clara, CA). The cantilever had a resonance frequency of 300 ~ 400 kHz with typical force constant of 40 N/m, and an uncoated silicon probe from Applied NanoStructures Inc. (Santa Clara, CA). To verify whether GO drags PF127 from the Langmuir monolayer at the air−water interface to the subphase, 6 μL solution was taken from the subphase outside the barriers when the Langmuir monolayer of PF127 or PF127/GO mixture (PF127/GO=1:0, 1:1 and 1:5, w/w) was compressed to 4 500 Å^2 per molecule of PF127. Then, spread it on a freshly cleaved mica surface and let it dry for 2 h. All images were taken at a resolution of 512 × 512 points.

4.3 Results and Discussion

4.3.1 Surface Pressure−Area Isotherm of PF127 on Pure Water Subphase

The surface pressure−area isotherm of Langmuir monolayer of PF127 on pure water subphase is shown in Figure 4.1 (red curve, PF127/GO=1:0, w/w). It is worth noting that the surface pressure−area isotherm could not be compressed to area/molecule below 2300 Å^2 in all cases due to the limitation of movable barriers. The obtained isotherm of PF127 at the air−water interface is consistent with other reported results of PF127 at this interface.[116,117] The surface pressure rises slowly at the beginning of compression during the phase transition from gas phase (>12 000 Å^2/molecule) to liquid expanded phase (12 000 to 6 500 Å^2/molecule). The surface pressure increases quickly when the Langmuir monolayer of PF127 is compressed to area/molecule below 6 500 Å^2, which corresponds to the liquid condensed phase. The highest surface pressure of PF127 Langmuir monolayer can only reach around 10.5 mN/m when it is compressed to the minimum area of the trough. Similar to another water insoluble triblock copolymer $(PEO)_6-(PPO)_{39}-(PEO)_6$ at the air−water interface,[103] this copolymer of PF127 can also form Langmuir monolayer.

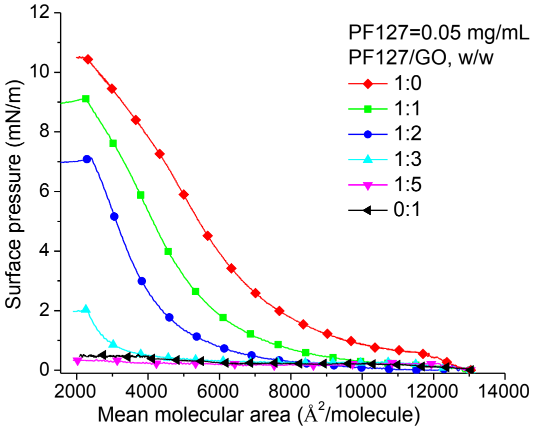

Figure 4.1 The surface pressure–area isotherms of PF127, GO dispersion and PF/GO mixture. In all cases, the concentration of PF127 is 0.05 mg/mL. Mixture PF127/GO=1:1, 1:2, 1:3 and 1:5 (w/w) at the air–water interface. Please notice that the barriers could not compress further when the area/molecule went below 2300 $Å^2$.

The process of compression of PF127 Langmuir monolayer at the air–water interface accompanies its conformation changes. In the structure of triblock copolymer of PF127, the water solubility of the central PPO moiety is dependent on the temperature, while the two end PEO segments are hydrophilic. At 20 ºC, the PPO part is hydrophobic and acting as an anchor at the air–water interface, resulting in the formation of Langmuir monolayer of PF127 at the interface.[116] The large size, different solubility nature and flexibility of PF127 facilitate this polymer a large degree of conformational freedom at the air–water interface, which can be controlled and studied over a large range of compression in molecular area. At large molecular area, the molecules are loosely packed with each other. All hydrophobic PPO and hydrophilic PEO groups stay flat at the air–water interface. The suggested conformation is like a pancake, as shown in Figure 4.2A (top).[118] When the monolayer is further compressed, the two end hydrophilic PEO groups tend to merge into the water subphase, leaving the hydrophobic PPO moiety as an anchor at the air–water interface, as shown in Figure 4.2A (bottom). When both end moieties of PEO are merged into the subphase solution, the conformation is called mushroom state. During the process of compression, the conformation of PF127 changes from pancake to mushroom. This kind of conformational change has been reported for other triblock copolymers at the air–water interface.[118-120]

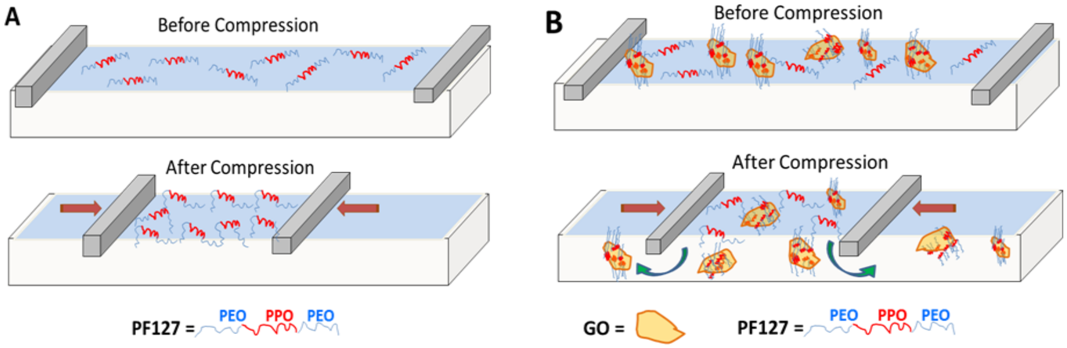

Figure 4.2 The schemed conformation at the air–water interface before and after compression. (A) PF127 alone; and (B) PF127/GO.

4.3.2 Surface Pressure–Area Isotherm of GO on Pure Water Subphase

The structure of GO has both hydrophobic and hydrophilic parts. The hydrophilicity of GO is attributed to the carboxylic groups at the edge, phenol hydroxyl and epoxide groups mainly at the basal plane. The hydrophobicity of GO stems from its intact carbon–carbon sp^2 domains.[2] As its structure strongly depends on the process of chemical oxidation and size distribution, GO is not a molecule with specific structure and molecular weight. Due to the existence of amphiphilic groups, GO might form Langmuir monolayer at the air–water interface. We had tried to deposit 100 uL to 500 uL of GO aqueous dispersion ranged from 0.1 to 1 mg/mL GO at the air–water interface. However, no surface pressure was detected even when the area was compressed to the minimum (data not shown). Therefore, GO used in this study is not surface active. In Figure 4.1, the black curve (PF127/GO=0:1, w/w) shows the surface pressure−area isotherm of 35 uL of 0.05 mg/mL GO deposited at the air−water interface. One needs to notice that the molecular weight of GO was assumed to be as the same as PF127 for the area/molecule calculation in this study due to the unknown molecular weight of GO. This curve serves as a control experiment, just showing that no surface pressure was detected.

4.3.3 Surface Pressure−Area Isotherm of PF127/GO Mixture on the Pure Water Subphase

Family of Pluronics have been used as surfactants to efficiently disperse carbon black particles,[121] carbon nanotubes,[122,123] and graphene[62,109,124] in aqueous solution and graphene oxide[21] in electrolyte solution before. The suggested scenario for dispersion is that the hydrophobic PPO of Pluronic copolymer covers the hydrophobic part of dispersed nanomaterials with hydrophobic interaction, while the hydrophilic PEO extends to the aqueous solution, increasing the water solubility and blocking self−aggregation. When PF127 is mixed with GO, the conformation of PF127 should be changed due to the interaction between PF127 and GO. One will expect to observe different behaviors at the air−water interface of the mixture PF127/GO when compared with PF127 alone. Due to the unknown molecular weight of GO, as mentioned in the paragraph above, the molecular weight of PF127 is used for the surface pressure−area isotherm instead of mean molecular weight of the PF127/GO mixture. This approximation results in an inaccurate area; however, it does not affect the qualitative analysis of the results in this case. Usually, when a binary system of amphiphilic mixture is deposited at the air−water interface, the features of surface pressure−area isotherm curve (lifting area, limiting molecular area and phase transition) should shift to larger areas if the molecular weight of a single component is used. This is because the mixture has more molecules occupying the area at the air−water interface compared with a single component. Therefore, one would expect all the isotherms shift to a larger area/molecule in the case of PF127/GO mixture (PF127/GO=1:1, 1:2, 1:3 and 1:5, w/w, PF=0.05 mg/mL) compared with PF127 alone. However, all features of lifting area, limiting molecular area and phase transition shrink to a smaller area in the experiment, as shown in Figure 4.1. This effect of shrinking is more obvious with higher weight ratio of GO present in the mixture. In the case of PF127/GO=1:5, no surface pressure is even detected.

These results unambiguously indicate that there exists an interaction between PF127 and GO, which changes the properties and behavior of Langmuir monolayer of PF127 at the air−water interface. Therefore, when deposited at the air−water interface, the Langmuir monolayer of the mixture is very different from that of PF127 alone. The pancake conformation in the Langmuir monolayer of PF127 is not expected to exist in the monolayer of the mixture of PF127/GO. The hydrophobic PPO moiety of PF127 has interacted with the hydrophobic part of GO surface, leaving the two hydrophilic PEO chains as two "tails" extended to the water subphase, as shown in Figure 4.2B (top). Due to the fact that GO is a two dimensional sheet with a height around 1 nm, both sides of GO sheets can interact with PF127. Since the hydrophobic PPO serves as an anchor at the air−water interface of the Langmuir monolayer of PF127, our assumption for the observation of isotherms in Figure 4.1 is that the hydrophobic interaction between PPO and GO results in the loss of the anchor, dragging PF127 molecules to the bulk subphase when compressed, as shown in Figure 4.2B (bottom).

4.3.4 Adsorption Study of GO to the Langmuir Monolayer of PF127 at the Air−GO Aqueous Interface

To further support our hypothesis that GO drags PF127 molecules to the subphase, adsorption study of GO to PF127 was performed at the air−GO aqueous interface. Pure PF127 was first deposited at the air−aqueous interface of subphase with different concentrations of GO aqueous dispersion in the subphase (0, 0.02 and 0.04 mg/mL). After 15 min elapsed to reach equilibrium, the monolayer was compressed under the same conditions as in the previous experiment. The surface pressure−area isotherms obtained are shown in Figure 4.3. Clearly, when there is GO present in the subphase, the surface pressure−area isotherms shift to a smaller area/molecule compared with pure water subphase. Also, the shrinking of the isotherm curve is more obvious when higher concentration of GO is present in the subphase (Figure 4.3). This observation supports that a strong interaction exists between GO and PF127, changing the conformation of PF127 monolayer at the interface.

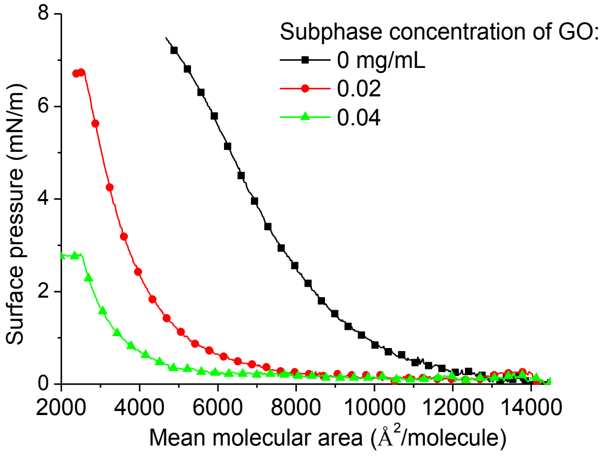

Figure 4.3 The surface pressure−area isotherm of Langmuir monolayer of PF127 at the air−GO aqueous dispersion interface. 35 μL of 0.05 mg/mL PF127 aqueous solution is deposited dropwise to the interface.

Different concentrations of GO (0, 0.02 and 0.04 mg/mL) aqueous dispersion are used as subphase. Please notice that the barriers could not compress further when the area/molecule went below 2300 Å^2.

4.3.5 Stability Study at the Air−Water Interface

To further support the hypothesis that GO drags PF127 from the air−water interface to bulk subphase solution, a stability study of Langmuir monolayer was performed at a surface pressure of 7 mN/m. As shown in Figure 4.4, the Langmuir monolayer of PF127 (blue curve, PF127/GO=1:0) is very stable. Even after 10000 seconds, the surface pressure is still around 7 mN/m (~4500 Å^2/molecule). However, for the Langmuir monolayer of PF127/GO=1:1, the surface pressure is not stable at all and keeps dropping to a final surface pressure around 1 mN/m after 10 000 seconds. The decreasing surface pressure suggests that the presence of GO in the mixture destroys the stability of the PF127 Langmuir monolayer by possibly dragging PF127 molecules into the subphase. This assumption will be discussed in the following section.

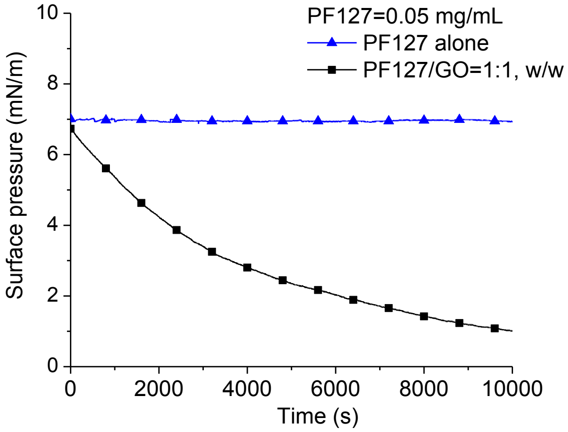

Figure 4.4 The stability of the Langmuir monolayer at the air−water interface: PF127 alone (blue curve); PF127/GO (1:1, w/w, black curve).

4.3.6 AFM Imaging

If GO can truly drag PF127 from the interface to the subphase, one will expect to find GO and PF127 in the subphase, especially when the monolayer is compressed to a small area by the movable barriers. Due to the stability of the PF127 Langmuir monolayer at a surface pressure of 7 mN/m at the air−water interface (Figure 4.4), the molecules of PF127 should stay at the air−water interface without loss of PF127 molecules to the subphase. When the surface pressure−area isotherm of PF127 Langmuir monolayer was compressed to 4500 $Å^2$/molecule (with surface pressure around 6 mN/m), 6 μL of the subphase solution was taken outside the barrier and cast on a freshly cleaved mica surface. After evaporation of solvent, a clean surface of mica was observed by AFM, indicating that PF127 was not dissolved or transferred from the interface to the subphase solution (Figure 4.5A). When the mixture of PF127/GO =1:1(w/w) was deposited at the air−water interface and compressed to the same area/molecule (4500 $Å^2$/molecule) under the same compression speed, GO was observed from the subphase solution by AFM, as shown in Figure 4.5B. The profile of the topography demonstrates that the height of GO is around 0.8 nm, which is consistent with reported results.[45,47,84] Figure 4.5B also shows the attached PF127 on GO surface, which can be seen clearly from the profile height and the 3D AFM image. The height of PF127/GO assembly is around 1.3 nm. Similar AFM image of surfactant dispersed reduced GO has also been observed in another study, which shows surfactant exists as dot on the surface of reduced GO.[110] When PF127/GO=1:5 (w/w) was deposited and compressed at the air−water interface under the same conditions, AFM images of GO were also obtained. It is worth noting that more pieces of

GO were observed on the surface of mica due to the higher ratio of GO in the mixture (Figure 4.5C).

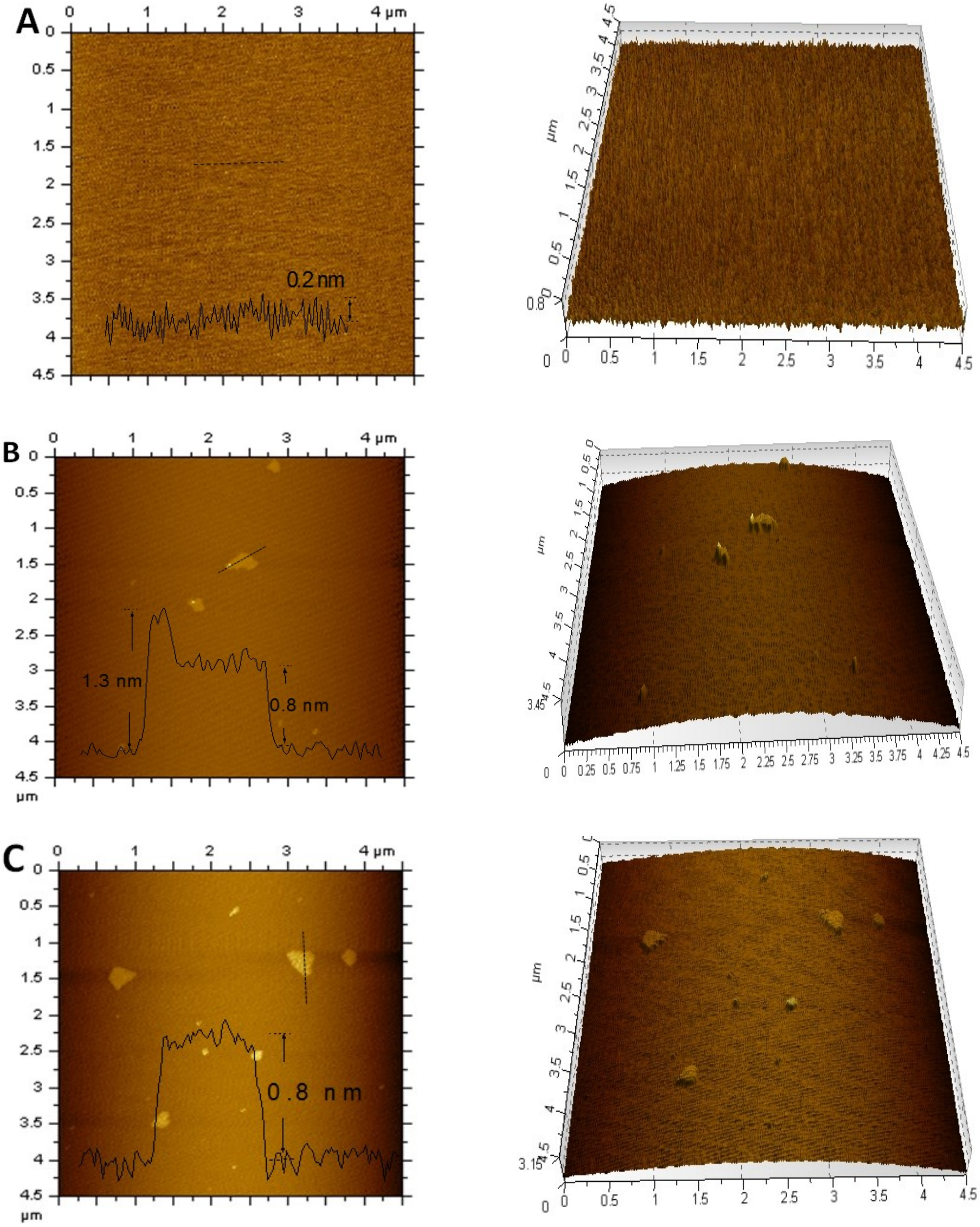

Figure 4.5 Topography (left) and 3D (right) AFM images of 6 μL subphase solution outside the compressing barriers spread on a freshly cleaved mica surface: (A) PF127 alone; (B) PF127/GO=1:1; and (C) PF127/GO=1:5. The black curve in the topography shows the profile of the dash line in the image.

4.4 Summary

In this study, Langmuir monolayer as a 2D surface chemistry approach is applied to investigate the interaction between graphene oxide and triblock copolymer PF127 at the air−water interface. Due to the hydrophobic PPO groups as anchors, PF127 Langmuir monolayer is very stable at the air−water interface. When PF127/GO mixture is deposited at the air−water interface, the PPO groups interact with the hydrophobic parts of GO surface, resulting in loss of the anchors at the air−water interface. Therefore, the Langmuir monolayer of PF127/GO is very unstable and tends to be dragged into the bulk subphase. Moreover, when PF127 is deposited at the interface of GO aqueous dispersion, the pancake conformation in the Langmuir monolayer of PF127 facilitates the availability of hydrophobic interaction between PF127 and GO, which drags PF127 molecules to the bulk subphase solution. AFM images support this assumption, as GO and PF127 can be observed from imaging the subphase solution outside the compressing barriers.

Chapter 5 Head Groups of Lipids Govern the Interaction and Orientation between Graphene Oxide and Lipids

5.1 Background

Graphene, a one−atom−thick planar sheet of sp^2 hybridized carbon atoms, has recently attracted tremendous attention in various studies and applications due to its novel optical, mechanical, electronic, thermal and biological properties.[1,2] Graphene oxide (GO) holds a similar atomically thin structure to graphene, but possesses plenty of oxygen−containing functional groups, such as carboxyls on the edges and hydroxyls and epoxies on the basal plane.[1] GO has demonstrated advantageous applications in biosensing and biomedical field owing to its special physical and chemical properties, such as low−cost manufacturing process, rich colloidal property, high adsorbility and universal fluorescence quenching.[4-6,84] Last few years has witnessed great progress of GO or functionalized GO as an efficient way to deliver therapeutic molecules from bioactive peptides, proteins, nucleic acids to anticancer drugs.[5,7,23] GO is also exploited for biosensing,[4,69] imaging,[22,24,71] real−time monitoring of protease activity,[43,44] and near−infrared photothermal treatment for cancers and Alzheimer's disease.[13,14,42]

Application of GO in biological system needs to address possible interaction between GO and cellular components, such as membranes. Membranes are natural two−dimensional (2−D) barriers, physically separating the interior environment of cells from the exterior environment. As main structural components of cell membranes, phospholipids are involved in various biological reactions, such as cell adhesion, ion conductivity, disease related reactions and transportation of signals and materials.[125] Previous studies have reported that GO could be applied for cellular imaging, drug and gene delivery, indicating it could possibly enter cells.[22-24] But studies on how GO interacts with cell membrane or model system are still extremely limited.[126] Inconsistent results are also obtained on the cytotoxicity of GO and how it enters cell membranes.[25,26] Moreover, compared with spherical or tubular nanomaterials, GO is an extremely thin layer (~1 nm) with large surface area and irregular shape.[1] It is still unknown how GO orientates itself when interacting with the cell membrane. Therefore, it is fundamentally important to understand the nature of the interaction between GO and various lipid models. Such knowledge could provide further information for future applications of GO in biological and biomedical field.

Besides application of GO in biosensing and biomedical studies, building and organization of mesoscopic or macroscopic well−defined composite using GO and some other components have been demonstrated as simple and useful methods to prepare electronic devices, such as supercapacitor electrodes, conducting polymers, field effect devices.[9,127,128] Therefore, understanding and manipulating the interaction, orientation, and structural control between GO and other components in the composite is of great importance for potential manufacturing and application.

Langmuir monolayer and Langmuir−Blodgett (LB) film at the air−water/aqueous interface are typical two−dimensional (2−D) surface chemistry approaches, widely applied for the structure and property study of amphiphilic molecules at the air−water/aqueous interface, such as proteins and lipids.[111,129,130] One striking feature of these methods is the intrinsic and precise control of the layer architecture down to molecular level. Due to the deprotonation of carboxyl groups at the edges of GO sheets,[9,131] electrostatic interaction is expected between negatively charged GO and charged lipids. The air−water/aqueous interface is expected to serve as a perfect playground for the study of interaction between lipids and GO, as the amphiphilic lipids have readily orientated themselves at the interface with polar/charged groups merged in the hydrophilic aqueous phase while nonpolar moiety facing toward the air phase.

In this study, in order to understand and define the nature and orientation of interaction between GO and lipid model with different head groups, Langmuir monolayer technique was applied at the air−water/aqueous interface to characterize the properties, such as molecule packing, adsorption and dipole moment. Five lipids with the same alkyl chain length (18 carbons) but different electric charges and head groups were chosen to rationalize the possible interactions. All alkyl groups of lipids used in this study were purposely chosen to have 18−carbon chains to eliminate the possible influence of terminal alkyl groups, as shown in Scheme 5.1. Langmuir−Blodgett films were transferred onto substrates to further characterize the morphology of monolayer using atomic force microscopy (AFM).

5.2 Experimental Section

5.2.1 Materials

Positively charged lipids dioctadecyldimethylammonium bromide (DODAB) and 1,2−distearoyl−*sn*−glycero−3−ethylphosphocholine chloride salt (DSEPC), neutrally charged zwitterionic lipid 1,2−distearoyl−*sn*−glycero−3−phosphocholine (DSPC), and negatively charged lipid 1,2−distearoyl−*sn*−glycero−3−phosphate sodium salt (DSPA) were purchased from Avanti Polar Lipids (Alabaster, AL). Stearic acid (SA) was bought from Sigma−Aldrich (St. Louis, MO). The chemical structures of these chemicals are shown in Scheme 5.1.

Scheme 5.1 Chemical structures of lipids and graphene oxide

a. Dioctadecyldimethylammonium bromide (DODAB)

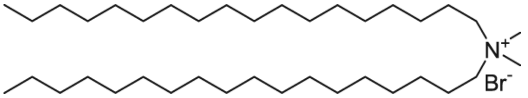

b. 1,2-Distearoyl-*sn*-glycero-3-ethylphosphocholine chloride salt (DSEPC)

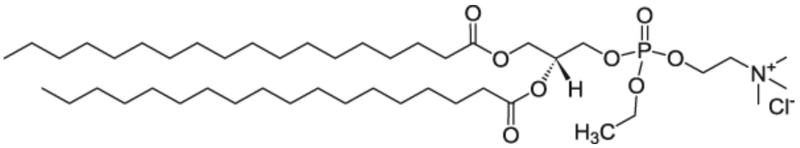

c. 1,2-Distearoyl-*sn*-glycero-3-phosphocholine (DSPC)

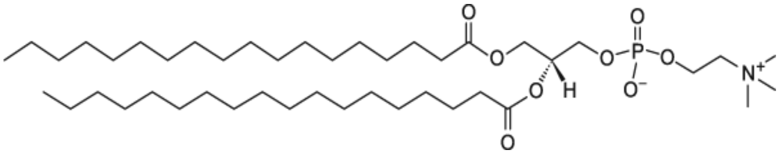

d. 1,2-Distearoyl-*sn*-glycero-3-phosphate sodium salt (DSPA)

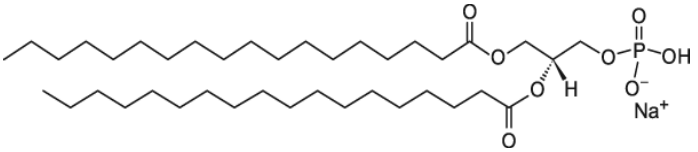

e. Stearic acid (SA)

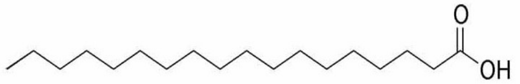

f. Schematic structure of graphene oxide (GO)

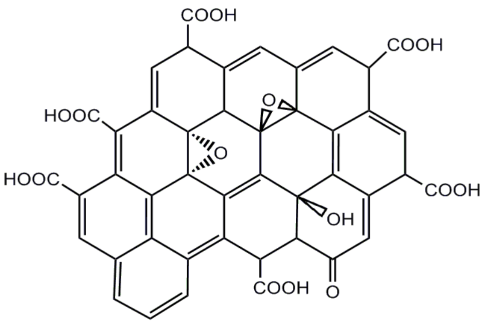

DSPC is neutrally charged due to the presence of the anionic phosphate and cationic quaternary ammonium centers in the head group, as shown in Scheme 5.1 c. SA was considered as negatively charged molecules due to the deprotonation of carboxyl group. All these lipids had 18−carbon chain alkyl group in the nonpolar tail. Spectroscopic grade chloroform and methanol were obtained from MP Biomedicals (Solon, OH). Single layer GO was purchased from ACS Material LLC (Medford, MA). All these chemicals were used without any further purification. The chemical structures were shown in Scheme 5.1. The deionized water used in the experiments was obtained from a Modulab 2020 Water purification system (San Antonio, TX). The resistivity, surface tension and pH of the deionized water were 18 MΩ·cm, 72.6 mN/m and 5.6 at 20.0 ± 0.5 °C, respectively. All experiments were performed in a clean room (class 1000) with constant temperature of 20.0 ± 0.5 ºC and humidity of 50 ± 1%.

5.2.2 Methods

1 mg/mL of GO aqueous dispersion was obtained by adding 10 mL deionized water to 10 mg GO, followed by sonication for 1 h in a cold water bath (Branson, model 1510, Danbury, CT). 0.01, 0.02 and 0.04 mg/mL GO dispersions were prepared by diluting with deionized water. We have previously shown that single layer GO was obtained using the same material and procedure by UV−vis spectroscopy and atomic force microscopy (AFM).[84] AFM images show that the height of exfoliated GO is around 1 nm while the lateral size is up to a few hundred nm. Each lipid except DSPA was dissolved in chloroform to obtain concentration around 0.3 mg/mL. A small amount of lipid: chloroform solution (from 25 to 45 uL) was deposited dropwise at the air−water or air−GO dispersion (0.01, 0.02 and 0.04 mg/mL) interface using a 100 uL syringe (Hamilton Co., Reno, NV). As DSPA was not totally soluble in chloroform, a mixture solvent of chloroform:methanol:water = 65:35:8 (volume ratio) was used to dissolve

DSPA. A Kibron μ−trough S (Kibron Inc., Helsinki, Finland) with an area of 5.9 cm × 21.1 cm was used throughout all surface chemistry measurement. The surface pressure was monitored with an alloy wire probe while surface potential by a Kelvin probe. When DSEPC was involved in the experiment, it is worth noticing that a piece of thin clean glass sheet was used to cover the inside surface of both Teflon barriers to prevent any interaction between DSEPC and Teflon barriers. A waiting time period of 15 min was taken to evaporate volatile solvent and allow the Langmuir monolayer to reach equilibrium. For adsorption of GO to lipid Langmuir monolayer, after the monolayer was compressed to certain surface pressure, 0.6 mL of 1 mg/mL GO dispersion was injected underneath the monolayer to reach 0.02 mg/mL of GO and followed by monitoring the change of surface pressure and surface potential versus elapsed time at a constant area.

Langmuir−Blodgett (LB) films were obtained by vertically pulling a piece of freshly cleaved V−1 grade mica sheet (Electron Microscopy Sciences, Hatfield, PA) from subphase at a constant speed of 1 mm/min. The transferred films were dried in the air for a few hours before imaging. Atomic force microscopy (AFM) images were taken with tapping mode using an Agilent 5420 AFM instrument (Santa Clara, CA) with a resolution of 512 × 512 pixels. The cantilever had a resonance frequency of ~170 kHz with typical force constant of 7.5 N/m and an uncoated silicon probe.

5.3 Results and Discussion

5.3.1 Surface Pressure−Area Isotherm of Lipids at the Air−GO Aqueous Dispersion Interface

Surface pressure is defined as the surface tension depression between a pure water surface and a monolayer−covered surface. It describes the molecular packing density at the air−water or air−aqueous interface. The surface pressure−area isotherm is obtained by monitoring the surface pressure change against mean molecular area during compression at a constant temperature. When molecules are closely packed before collapse, the area by extrapolation of the linear part of the surface pressure−area isotherm (solid phase or liquid condensed phase) to zero surface pressure (as shown by the dash lines in Figure 5.1 a) is termed as the limiting molecular area.[132] This important characteristic represents the mean molecular area occupied when the molecules are closely packed in a monolayer. The limiting molecular area is usually determined by the intermolecular interactions of the head groups and the packing of the alkyl chains.[133]

Figure 5.1 shows the surface pressure−area isotherms of positively charged DODAB (a) and DSEPC (b), neutrally charged DSPC (c), negatively charged DSPA (d) and SA (e) on pure water and GO aqueous dispersion subphase (0.01, 0.02 and 0.04 mg/mL GO). It is worth noticing that no surface pressure was detected at the interface using 0.01, 0.02, and 0.04 mg/mL GO aqueous dispersions as the subphase without spreading lipids (data not shown), indicating that GO itself used in this study is not surface active enough to affect the surface tension of water. The limiting molecular areas for positively charged DODAB and DSEPC on the pure water subphase are determined as 73 and 61 Å^2/molecule, respectively, as shown by the dash lines on the black curves in Figure 5.1 a and b. These numbers are consistent with previous studies.[133-135] When these two lipids are deposited at the air–GO dispersion interface, rise of limiting molecule area is unambiguously observed with increase of GO concentration in the subphase from 0.01, 0.02 to 0.04 mg/mL. Furthermore, the liquid condensed phase starts at higher mean molecular area as the GO concentration increases. This observation indicates that GO can incorporate or be adsorbed into the monolayer of DODAB and DSEPC, increasing the mean molecular area. However, when neutrally charged lipid DSPC, negatively charged lipid DSPA and fatty acid SA are deposited, the surface pressure–area isotherms on GO dispersion are almost exactly the same as isotherms obtained on pure water subphase, as shown in Figure 5.1 c–e. In each case of these three molecules, the surface pressures rise at almost the same mean molecular area and the limiting molecular areas are also very similar in spite of different concentrations of GO in the subphase. These observations suggest that GO cannot incorporate or be adsorbed into the monolayer of DSPC, DSPA or SA. Neither the presence of GO at the interface and subphase has any effect on the monolayer formation of these molecules. As phospholipids in cellular membranes are negatively or neutrally charged, the possible cellular uptake of GO into the membrane should not be due to the direct chemical interaction between GO and phospholipids but through biological processes such as endocytosis.[23,136]

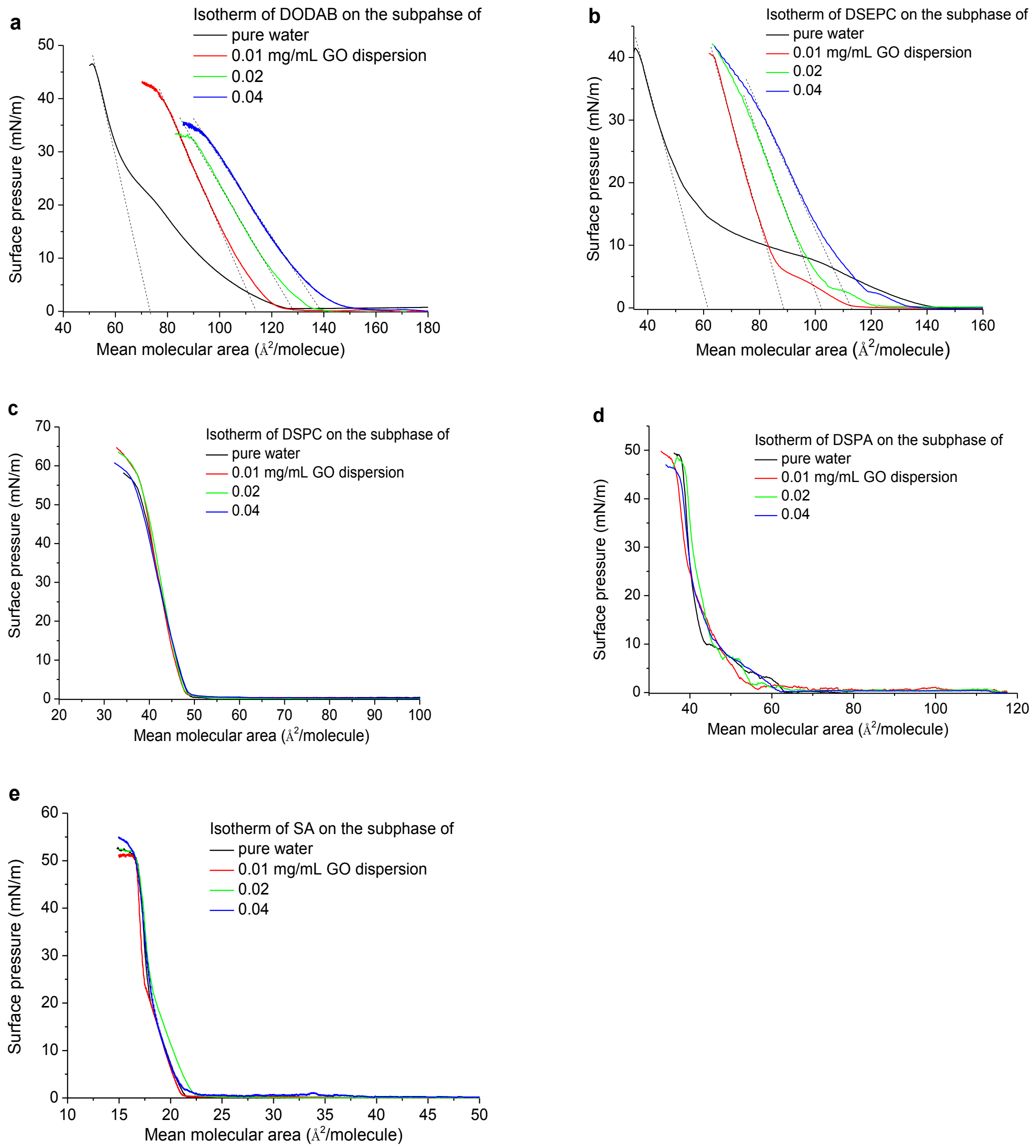

Figure 5.1 Surface pressure−area isotherms of lipids at the air–water or GO dispersion interface. (a) Positively charged DODAB; (b) Positively charged DSEPC; (c) Neutrally charged DSPC; (d) Negatively charged DSPA; and (e) negatively charged SA. Please notice that no surface pressure is detected at the air–GO dispersion interface without spreading lipids at the interface. The intercepts of dash lines with area per molecule axis indicate the limiting area per molecule.

Figure 5.1 clearly shows that the head groups with different charges have profound effect on the interaction between lipids and GO. The hydrophobic tail groups are not believed to be involved in this interaction. This is because the 18–carbon hydrophobic tail should be orientated towards the hydrophobic air phase. Even if the tail can be contacted with GO at the air–aqueous interface just after deposition, no effects on the lifting area or limiting molecular area are observed during the compression on the isotherms of DSPC, DSPA and SA. Especially, it is worth noticing that DSEPC, DSPC and DSPA have exactly the same 1,2–distearoyl–*sn*–glycero groups in common with the only difference from the head group, as shown in Scheme 5.1 b−d. Therefore, the factor governing the interaction between GO and lipid is the head groups. Positively charged head groups (ammonium and ethylphosphocholine) have strong electrostatic attraction with the negatively charged carboxyl groups of GO, resulting in the incorporation of GO into the monolayer. Neutrally charged head group (phosphocholine) or negatively charged head groups (phosphate and carboxyl) do not adsorb GO because of no favoring electrostatic interaction. Moreover, it seems that these neutrally charged and negatively charged head groups can repel GO sheets from the air−GO dispersion interface. This explains why these lipids have almost exactly the same isotherms on the dispersion of GO as on the pure water subphase. Therefore, we will focus on the interaction between GO and DODAB and DSEPC in the following discussions.

5.3.2 Adsorption of GO to the Monolayer of DODAB and DSEPC

Although both head groups of DODAB and DSEPC have the same amount of positive charge, the chemical structures are quite different. To further characterize the interaction between the positively charged head groups of DODAB and DSEPC and GO, adsorption studies of GO to the lipid monolayer are studied at surface pressure 20 mN/m, as shown in Figure 5.2. As control experiment, monolayer of DODAB or DSEPC is first compressed to 20 mN/m on pure water subphase, and then the surface pressure (black curves in Figure 5.2 a–b) and surface potential (black curve in Figure 5.2 c–d) are monitored against elapsed time. As expected, DODAB and DSEPC monolayers initially compressed to 20 mN/m are very stable on pure water subphase. In both cases, surface pressure is still around 18 mN/m after 6000 seconds (black curves in Figure 5.2 a–b). The quick decrease of surface pressure in the first 1000 seconds is probably due to the relaxation of monolayers after compression. Similar stable phenomenon of surface potential versus time is also observed, as shown in Figure 5.2 c and d. For adsorption of GO, after the monolayer of DODAB or DSEPC is initially compressed to 20 mN/m on pure water, 600 μL of 1 mg/mL GO dispersion is carefully and slowly injected into the water subphase to reach 0.02 mg/mL GO underneath the monolayer. And then monitor the surface pressure (red curves in Figure 5.2 a–b) or surface potential (red curves in Figure 5.2 c–d) changes versus time. It is worth noticing that the injection of GO to reach 0.02 mg/mL in the subphase does not result in surface pressure increase at the air–water interface in 6000 seconds. As shown in Figure 5.2 a and c, surface pressure of DODAB monolayer increases to 21.3 mN/m while surface potential drops to almost 0 mV in the first 500 seconds. It is worth noticing that the surface potential curve of DODAB (red) in Figure 5.2 c was initially around 300 mV before GO was carefully and slowly injected to the subphase. The changes of surface pressure and surface potential clearly indicate there exists electrostatic interaction between positive ammonium group of DODAB and negative carboxyl group of GO.

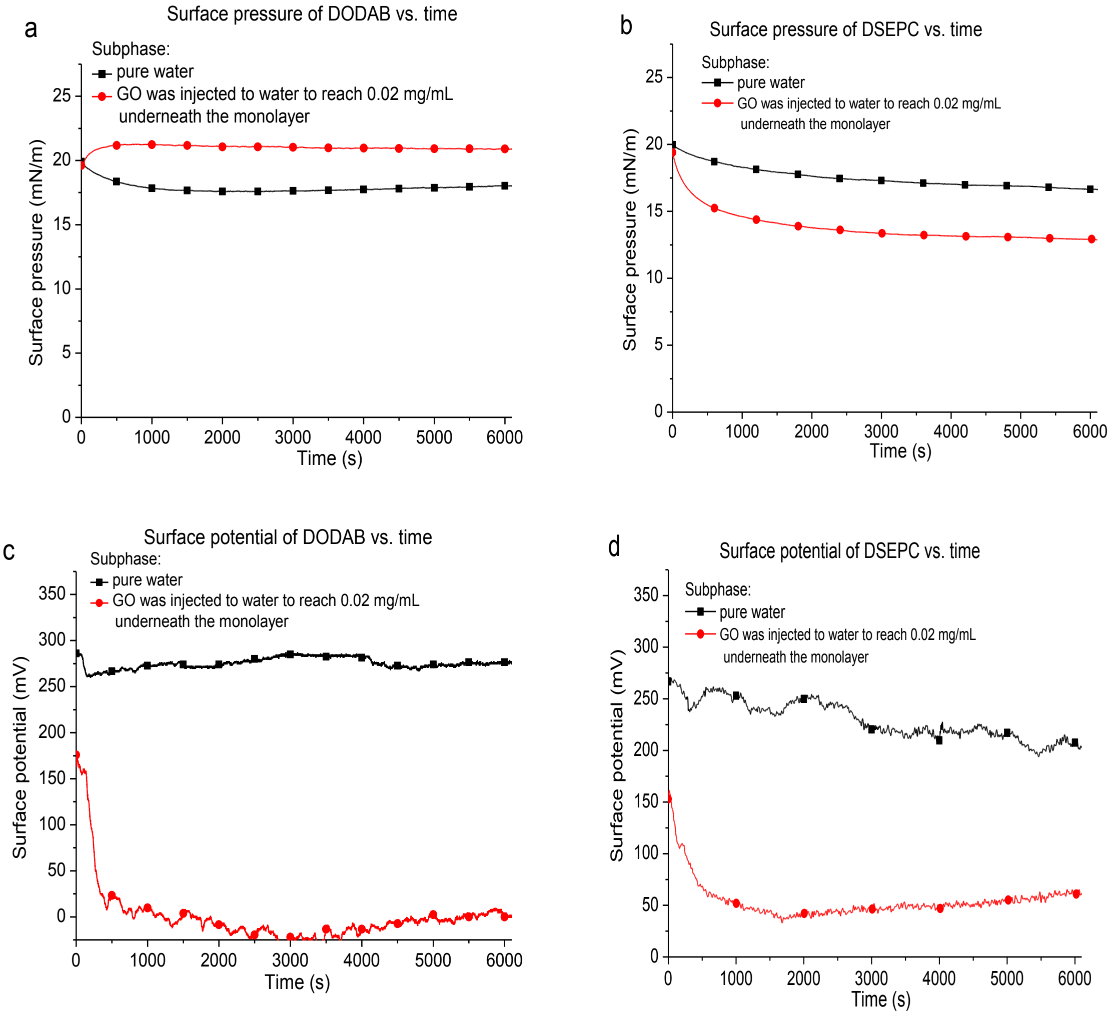

Figure 5.2 Adsorption of GO to positively charged lipid Langmuir monolayer. Surface pressure versus elapsed time of monolayer of (a) DODAB and (b) DSEPC; Surface potential versus elapsed time of monolayer of (c) DODAB and (d) DSEPC. Black curve: the monolayer was compressed to a surface pressure of 20 mN/m on pure water subphase. Red curve: after the monolayer was compressed to 20 mN/m, 600 μL of 1 mg/mL GO dispersion was carefully and slowly injected underneath the monolayer into the water subphase to reach 0.02 mg/mL of GO.

As GO is an extremely thin layer (~1 nm) with large surface area, it is very interesting to study its orientation when it interacts with lipid. Two possible orientations are involved here, “edge–in” and “face–in”. “Edge–in” means the surface of GO sheet is vertical, while “face–in” describes horizontal orientation. The observations at the air–

water/aqueous interface can provide some insights. We propose that GO sheets enter the ordered DODAB monolayer by insertion of carboxylic groups with an “edge–in” orientation due to the electrostatic interaction between ammonium groups and carboxylic groups, as shown in Figure 5.3 a. It is also possible that some GO sheets interact with positively charged head groups using a “face–in” orientation underneath the monolayer. GO nanosheets are less likely to incorporate into the monolayer with a “face–in” orientation (Figure 5.3 b). First, DODAB monolayer at 20 mN/m is closely packed enough that it is much easier for GO to squeeze in by edge (around 1 nm size) than lateral face (up to several hundred nm size). Second, negatively charged carboxyl groups mainly exist at the edges, not on the lateral surface of GO. The decrease of surface potential is also due to this electrostatic interaction, as the binding of negatively charged GO to the ordered DODAB monolayer neutralizes the charges of DODAB, lowering the dipole moment at the interface.

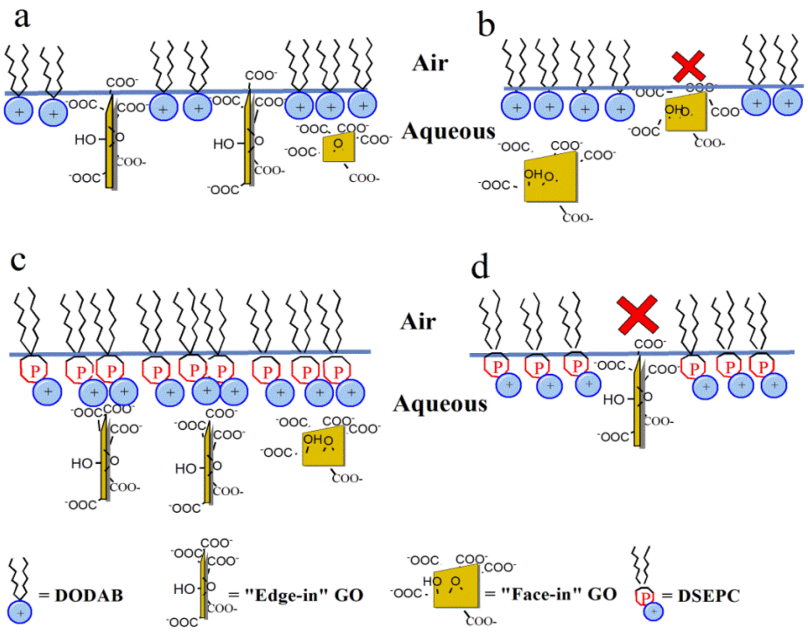

Figure 5.3 Schematic diagrams of the possible orientations of GO when it incorporates into the monolayer of DODAB (a–b) and DSEPC (c–d) at the air–water interface.

One would expect to observe similar phenomenon of surface pressure and surface potential if GO binds to DSEPC monolayer via the same way as DODAB. One does find that surface potential of DSEPC monolayer drops to around 50 mV when GO is introduced to the subphase (Figure 5.2 d, red curve), indicating that there exists dipole moment change of DSEPC monolayer. However, instead of increase, decrease of surface pressure is observed in experiment for DSEPC, as shown in Figure 5.2 b. As DSEPC has such big moiety of hydrophobic tails anchoring at the air–aqueous interface, it is not likely to lose DSEPC molecule to the subphase. It is worth noticing that at the air−aqueous interface the head group of DSEPC is bulk *sn*−glycero−3−ethylphosphocholine, with positively charged choline group and strong polar group of *sn*−glycero−3-ethylphospho. When GO is diffused from the subphase to DSEPC monolayer at the interface, it is possible that the negatively charged GO interacts with the positively charged choline moiety of DSEPC but without penetration into the monolayer due to shielding from *sn*−glycero−3−ethylphospho, as shown in Figure 5.3 c−d. It is also possible that GO interacts with DSEPC monolayer with both "edge−in" and "face−in" orientations underneath the monolayer, as shown in Figure 5.3 c. The electrostatic interaction of GO not only neutralizes the positive charge density of the head group in DSEPC, but also results in closer packing of DSEPC molecules at the interface. This assumption explains the drops of both surface pressure and surface potential when GO is diffused from the subphase to the DSEPC monolayer.

If our assumption regarding to the different binding behaviors of GO to monolayer of DODAB and DSEPC is right, one would expect to observe a larger increase of surface pressure of DODAB when the initial surface pressure is lower. Indeed, around 2.5 mN/m increase of surface pressure is found in experiment when GO binds to the DODAB monolayer initially compressed to 15 mN/m, as shown in Figure 5.4 a (pink curve). On the other hand, when the surface pressure of DODAB monolayer is high enough, no edges of GO can squeeze into the closely packed monolayer. As shown in Figure 5.4 a (black curve), GO in the subphase does not result in surface pressure increase when DODAB monolayer is compressed to 25 mN/m. In the case of DSEPC, surface pressure decreases of monolayer when GO is injected to the subphase. In summary, these observations verify our model proposed in Figure 5.3 of binding of GO to the monolayer of DODAB and DSEPC at the interface.

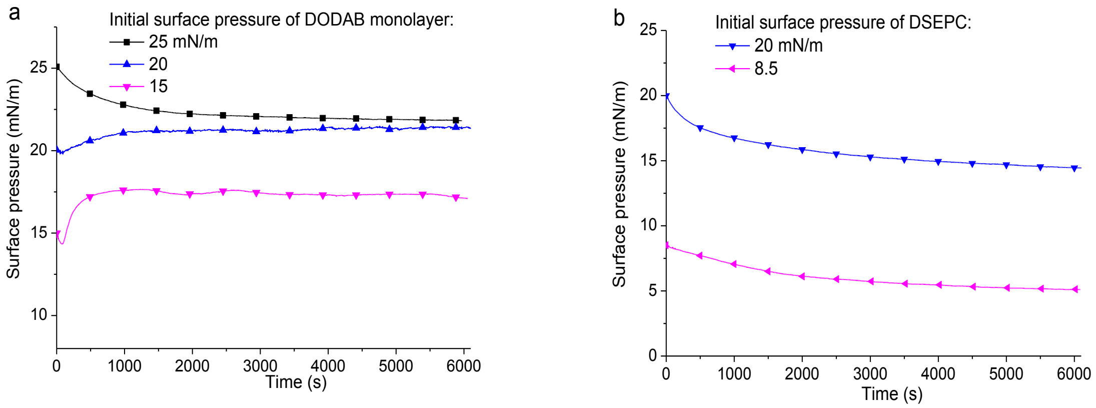

Figure 5.4 Adsorption study (surface pressure versus elapsed time) of GO to the Langmuir monolayer of (a) DODAB and (b) DSEPC at various surface pressure. The monolayer was first compressed to a certain surface pressure on pure water subphase, and then 600 μL of 1 mg/mL GO dispersion was carefully and slowly injected into the water subphase underneath the monolayer.

5.3.3 AFM images of Langmuir–Blodgett (LB) films

Atomic force microscopy (AFM) is a powerful, nondestructive method to visualize the morphology of LB films at high resolution. The surface of the LB films transferred on a substrate can be repeatedly imaged without damaging the sample. In this study, Langmuir monolayer of DODAB or DSEPC at surface pressure of 20 mN/m is first transferred from the air–pure water or air–GO aqueous dispersion interface to freshly cleaved mica substrate, followed by drying in the air and AFM imaging. Figure 5.5 a shows the morphology of GO nanosheets after 5 μL of 0.02 mg/mL GO dispersion was spread on mica and dried. The white curve in the figure shows the extracted profile for the cross–section trace of the white dashed line. The GO nanosheets are found to be uniformly about 1 nm in height with large length distributions. This confirms that GO is truly single layered.[42,48,137] Figure 5.5 c and e show the AFM images of LB films of DODAB and DSEPC transferred at 20 mN/m from the air–pure water interface, respectively. The films are quite uniform in both cases, demonstrating the formation of homogeneous monolayer.[138] There are some tiny holes with depth of 0.4–0.5 nm, which could be assumed as the height of a single molecular layer of DODAB or DSEPC. In order to study the morphology of LB films of DODAB and DSEPC formed at the air–GO dispersion interface, control experiment of LB film under the same condition (area, compression speed, and lifting rate) is performed without spreading DODAB or DSEPC at the air–GO dispersion interface. As shown in Figure 5.5 b, almost bare mica surface is observed, indicating that GO nanosheets from the GO dispersion subphase could not likely be transferred to the mica surface. This is probably due to the unfavorable interaction between the negatively charged GO nanosheets and negatively charged mica surface. When DODAB or DSEPC LB film is transferred at 20 mN/m from the air–GO dispersion interface, GO nanosheets are clearly found in the LB film of DODAB or DSEPC, as shown in Figure 5.5 d and f. The height of GO in the LB film is also around 1 nm. The presence of

GO confirms that GO nanosheets do adsorb or incorporate into the monolayer of DODAB or DSEPC.

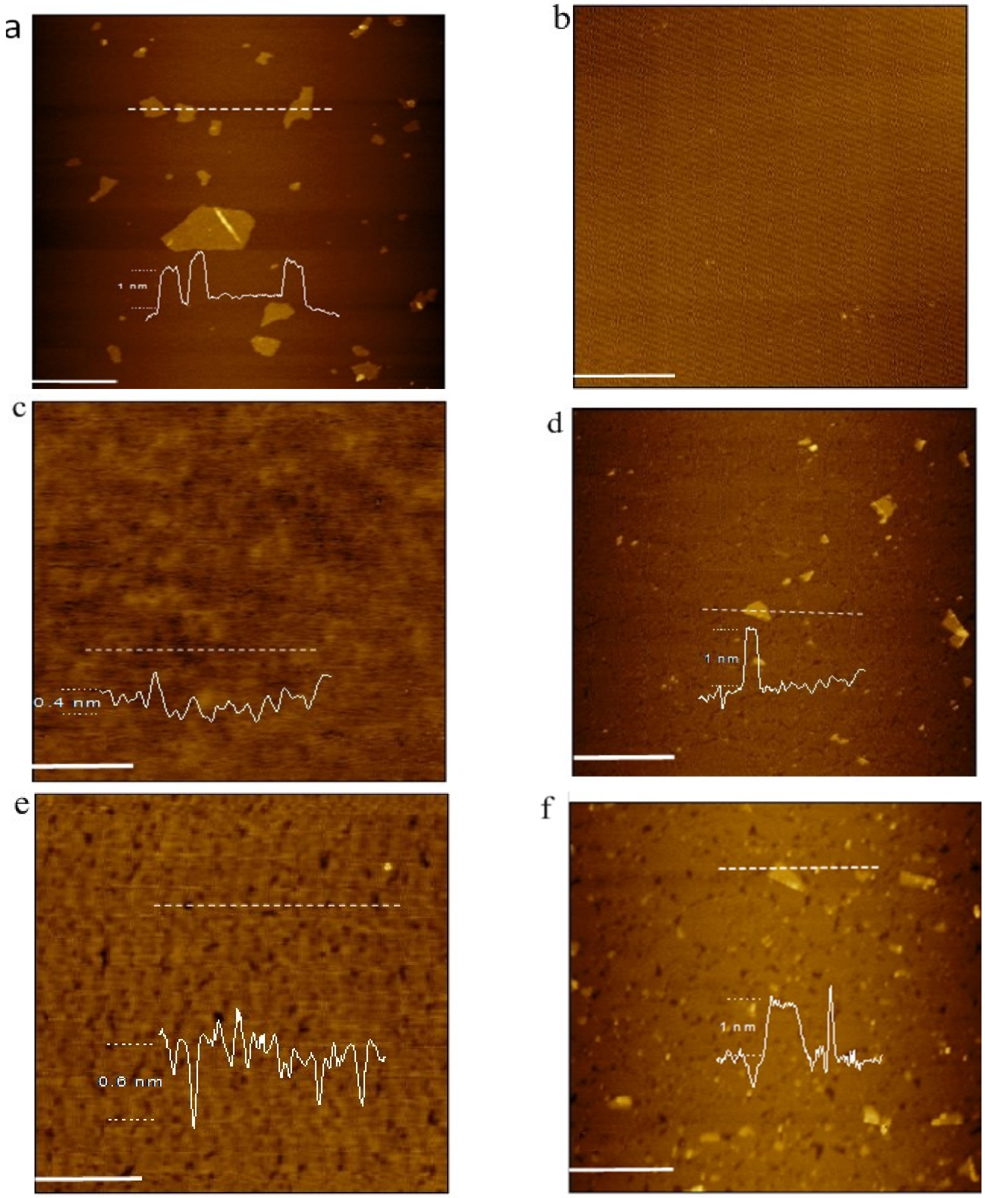

Figure 5.5 AFM images on freshly cleaved mica surfaces. (a) A drop of GO dispersion after drying; (b) A control experiment of LB film without deposition of lipids at the air–GO aqueous interface; (c) LB film of DODAB transferred from the air–pure water interface; (d) LB film of DODAB transferred from the air–GO aqueous interface; (e) LB film of DSEPC transferred from the air–pure water interface; (f) LB film of

DSEPC transferred from the air–GO aqueous interface. All lipid LB films are transferred at a constant surface pressure of 20 mN/m. Scale bar = 1 µm.

It is worth noticing that the lipids DODAB and DSEPC are directly deposited on the subphase of GO dispersion to obtain LB film for AFM imaging. Regarding to the orientation of GO when binding to lipid monolayer (Figure 5.5 d and f), only "face−in" orientation of GO is observed on the LB film by AFM imaging. Even if one can imagine there should exist some "edge−in" orientation of GO when DODAB or DSEPC is deposited at the air−GO aqueous dispersion interface, it is impossible to visualize this orientation by AFM. This is because the orientation of GO can be easily changed during the process of transferring. It is most unlikely that "edge−in" orientation could still "stand" on its edge with a dimension of 1 nm without "lying down" on its large flat surface when transferred on the surface of mica. Therefore, "face−in" orientation of GO is observed to incorporate or be adsorbed in the monolayer structure in the AFM images.

5.4 Summary

In this study, Langmuir monolayer technique as 2−dimensional method is applied at the air−water/aqueous interface to understand the nature and orientation of interaction between GO and lipid models. Five lipids with the same 18−carbon alkyl chain but different head groups of charges are purposely chosen to rationalize the possible interactions. Experimental results show that the interaction between these lipids and GO is clearly governed by electrostatic interaction. When these lipids are spread at the air−GO dispersion interface, GO can incorporate or be adsorbed into the monolayer of positively charged lipids DODAB and DSEPC, increasing the mean molecular areas.

However, the monolayers of neutrally charged head group (phosphocholine) or negatively charged head groups (phosphate and carboxyl) do not adsorb GO as there is no favoring electrostatic interaction. Due to the fact that phospholipids in biological systems are negatively or neutrally charged, the possible cellular uptake of GO into the membrane should not be due to the direct electrostatic interaction between GO and phospholipids but through the bioactivity of the membrane.

When GO is injected to the subphase underneath the positively charged monolayer of DODAB and DSEPC, different observations of surface pressure are found. GO can insert into the monolayer of DODAB at 20 mN/m increasing the surface pressure. However, GO cannot diffuse to incorporate with DSEPC monolayer even at much lower surface pressure probably due to the shielding from the ethylphospho groups. An orientation model of GO when it binds to DODAB and DSEPC monolayer is proposed to explain the different behaviors of adsorption of GO at the air–aqueous interface. An "edge–in" orientation instead of "face–in" is proposed to describe the orientation of GO nanosheets when it inserts into the monolayer of DODAB.

Chapter 6 Aggregation of Protein at the Interface: Insulin as An Example

6.1 Background

It has been known for several decades that failure to adopt or remain native conformations of some specific peptides or proteins can result in a wide range of human diseases.[28] The pathological conditions of these diseases are now known to be commonly associated with protein misfolding processes. More than 20 human peptides or proteins have been found to be able to misfold and develop aberrant self−assemblies *in vivo*, which are characterized by conformational conversion of soluble peptides or proteins into insoluble amyloid−like fibrils.[139] The misfolding peptides or proteins associated with serious human amyloidogenic diseases include amyloid−β peptide (Aβ) in Alzheimer's disease (AD), islet amyloid polypeptide (IAPP) in type 2 diabetes, α−synuclein in Parkinson's disease (PD), and prion protein in the spongiform encephalopathies.[29,30] Although these amyloidogenic peptides or proteins are not found to share sequence homology or related native structures with each other, their self−assembled fibrils possess strikingly similar characteristics (e.g. cross−β diffraction pattern, nucleation−dependent fibrillation, elongated morphology, Congo Red birefringence, and thioflavin T fluorescence), suggesting that the fibrillation process of these biomolecules may share a common molecular mechanism.[28,30,140] However, the current understanding of the mechanism and the structure evolution during aggregation or fibrillation is still very limited.

Insulin is a small polypeptide hormone composed of 51 amino acids with a largely α−helical structure in its native conformation. This hormone is produced by pancreatic β cells and stored predominantly as zinc−coordinated hexamers in the secretory granules within pancreatic islets. When released into bloodstream, insulin binds to its receptor in a monomeric form to regulate glucose metabolism in biological systems.[141] The insulin monomer has some hydrophobic amino acid residues exposed outside and tends to associate into dimer. The dimer−forming surface of the insulin monomer is almost flat and mainly composed by aromatic and aliphatic residues from the B chain: B8 Gly, B9 Ser, B12 Val, B13 Glu, B16 Tyr, B24 Phe, B25 Phe, B26 Tyr, B27 Thr, and B28 Pro.[142-146] This information is deduced from X−ray crystal structures or NMR structures of insulin or mutant insulin (PDB ID: 4INS, 2A3G, 2JV1, 1MHJ, 1MHI, 1MSO). The driving forces leading to dimerization are predominantly non−polar, reinforced and given direction by the antiparallel β sheet of hydrogen bonds.[146] Under certain conditions, such as higher insulin concentration, basic pH, and presence of zinc ions, three dimers associate to form a stable torus−shaped hexamer, in which both polar and non−polar residues are buried between the dimers.[146]

In vitro studies have shown that fibrillation of insulin can be induced under various conditions such as acidic pH, elevated temperature, hydrophobic interface, ionic strength, and mechanical agitation.[147,148] As its fibrils share common structures with other amyloidogenic proteins, insulin has been widely used as a suitable model system to fundamentally understand the pathologies of protein conformational misfolding diseases.[140,149,150] More than a model protein for fibril formation *in vitro*, insulin has been observed to develop fibrils *in vivo* near the sites of repeated insulin injection in the pathogenesis of some diabetic patients.[151] Insulin is also found in clinical practice to form aggregates immediately after injection in the bloodstream, exhibiting a reduced biological activity and an increased immunogenicity.[152] Therefore, it is necessary and crucial to fundamentally understand conformational changes that insulin undergoes in various conditions and the underlying mechanism involved in the reaction pathway.

Interfaces and surfaces are ubiquitous environments and play important roles in a multitude of physical and chemical processes, including biomedical engineering, catalysis, chemical sensors, and drug delivery.[31,32] As a large number of important physicochemical processes occur at the place of interfaces in biological systems, much attention has been drawn to the properties of biomolecules at interfaces, such as liquid−solid interface,[153,154] liquid−liquid interface,[155-159] and gas−liquid interface.[160,161] Adsorption of proteins at the interface often results in conformational changes, reducing the biological activity and physical/chemical stability of proteins.[162,163] This process has been shown to be very complex and can be influenced by many factors, such as electrostatic interactions, surface roughness and curvature, and hydrophilicity/hydrophobicity, to name a few.[163-168] In the case of insulin, the great interest for studies at various interfaces started from the early observation that insulin was vulnerable to change conformation and develop aggregates in storage vials, infusion pumps, controlled release devices, etc.[33-36] Since then, studies of adsorption, aggregation and fibril formation of insulin have been performed at various interfaces, such as aqueous−solid interface,[164,169-174] water−oil interface,[155,156,158,159] and air−water interface.[175-181] Although much progress has been achieved in the past few years, a molecule−level understanding of the detailed structure and property of insulin at the interfaces remains a great challenge.

The objective of this article is to provide an overview on the current state of our understanding of insulin aggregation at interfaces. We will first briefly summarize the recent understanding of the insulin fibrillation mechanism at a molecular level. Then, we will switch to the aggregation of insulin at the interfaces, with particular attention to the Langmuir monolayer technique at the air−water interface. Factors that may contribute to the aggregation or fibrillation of insulin at the air−water interface will be discussed, such as pH of subphase solution, zinc concentration, and presence of lipid. Finally, a summary of aggregation of insulin at the interfaces and outlook on the challenges and future studies will be given.

It is worth noticing that we summarize in this article the recent progress of insulin at the interfaces without distinction of the source of insulin used in experiments (human, bovine, or porcine). Due to the fact that the amino acid sequence of insulin is highly conserved within mammals, properties and functions of insulin from diverse species and even insulin mutants are very similar.[182,183] All of these insulin molecules undergo a similar chemical mechanism during the process of fibril formation in spite of the difference in speed of fibrillation.[183]

6.2 Mechanism of Insulin Aggregation or Fibrillation

A number of efforts have been devoted to elucidate the molecular mechanism of insulin aggregation or fibrillation by kinetic and structural studies.[140,148,170,174,183-189] Various kinetic studies have demonstrated that insulin fibril binds with dyes such as thioflavin T and Congo Red with characteristic enhancement of fluorescence emission.[148,170,183,187] Spectroscopic methods, such as Fourier transform infrared (FTIR) and circular dichroism (CD), have been widely used to monitor the protein conformation changes during fibrillation in aqueous solutions.[183,187,190] However, FTIR and CD provide limited information in structural studies, as the results from these spectroscopies only indicate the secondary structure changes, i.e., the components of α−helix, β−sheet, and random coil. Electron microscopy (EM) and atomic force microscopy (AFM) have been applied to directly visualize the morphologies in the pathway of insulin fibrillation.[189,191,192] Although the microscopic images are able to clearly reveal the morphology of insulin fibril architectures as unbranched, long, straight structures with periodic twists, neither EM nor AFM approaches atomic level resolution. More sophisticated and precise techniques such as small−angle X−ray scattering, X−ray microcrystallography, and solid−state nuclear magnetic resonance (NMR) spectroscopy have recently been emerging as new attempts to elucidate the atomic level structures of proteins in three dimensions.[184,188,192] However, the insoluble uncrystallizable nature of insulin fibrils is still severely challenging the applications of these structure determination methods.

Similar to other amyloidogenic proteins, fibrillation of insulin is proposed to occur under various conditions via the aggregation of partially folded intermediates through a nucleation mechanism.[149,185,186,193] The kinetic process of fibril formation in experiments is commonly characterized as an apparent lag period followed by an exponential growth regime, and a final plateau regime, as shown in Figure 6.1. The apparent lag period is mainly due to a reversible nucleation process, in which the amount and size of insulin aggregates (oligomers) are not significant enough to be detectable by current methods. Previous studies suggest that nucleation of insulin results from the simultaneous assembly of a few misfolded insulin monomers into oligomers via their hydrophobic surfaces.[148,186] Once the concentration of nucleation reaches its critical state, the exponential growth regime occurs, in which the subsequent addition of insulin monomers or oligomers to the nuclei elongates into long unbranched fibrils.[148] This eventually leads to the irreversible formation of large fibrils. When the concentration of insulin in solution falls below the threshold, a final stable plateau regime is achieved, aborting further fibril extension.

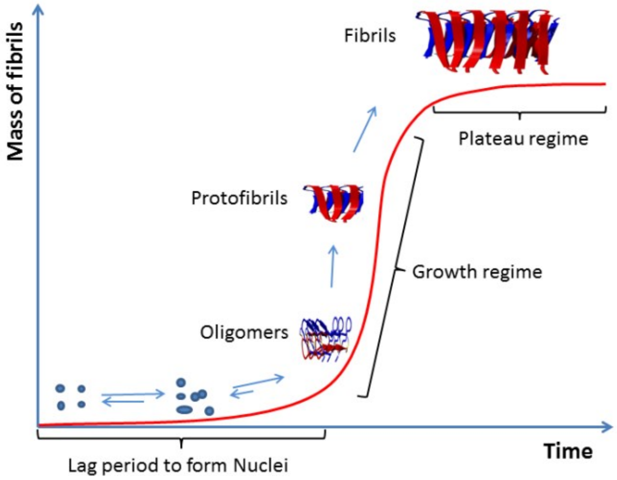

Figure 6.1 A typical kinetic graph of the insulin aggregation model.

The driving forces transforming native monomeric insulins to oligomers and eventual mature fibrils in the process of insulin fibrillation are assumed to: (1) minimize the exposure of the hydrophobic residues to aqueous environment, (2) saturate hydrogen bonding, and (3) reach an alternative non−native global free energy minimum.[189,193] It has been suggested that the initial step is probably to form a partially folded intermediate by a misfolding monomer (Figure 6.2), in which the hydrophobic residues, normally buried in the dimer and hexamer, become exposed to solvent.[148,184] When two conformationally changed monomers assemble together, a shared antiparallel β−sheet structure is formed with the structure different from that of the normal insulin dimer. This shared structure in the assembly makes the monomer−monomer binding even stronger than the interaction involved in the dimer and hexamer.[194] The assembly evolves into an oligomer and forms a nucleus (Figure 6.2). The subsequent step of assembling insulin molecules to the nuclei may result from an effort to minimize the exposure of hydrophobic residues. This process eventually promotes fibril formation with rich cross−β structures, which are energetically favored through forming intermolecular and intramolecular hydrogen bonding.[189]

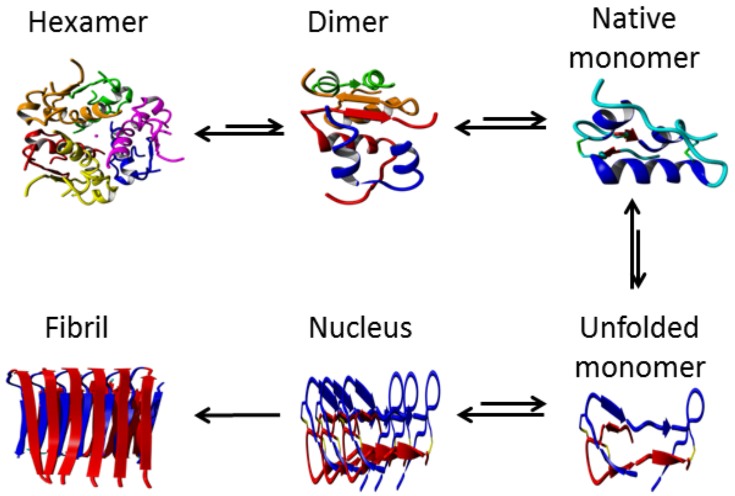

Figure 6.2 Schematic mechanism of the proposed pathway of insulin fibrillation.

6.3 Insulin Aggregation at the Aqueous−Solid and Water−Oil Interface

Like many other protein drugs, insulin is inevitably exposed to a diversity of interfaces, such as the aqueous−solid interface, water−oil interface, and air−water interface during production, purification, storage, delivery, and *in vivo* utilization. Particular interest of insulin at these interfaces is mostly based on observations that its adsorption and aggregation have long been recognized at the surfaces of syringes, infusion pumps, storage vials, and drug delivery materials, significantly decreasing the biological activity and stability of insulin.[33-36] Understanding the dynamics, properties, and structures of insulin exposed at the interfaces will be of great benefit to future development of insulin product. In the following part, we will briefly summarize the progress of insulin fibrillation studies at the aqueous−solid and water−oil interfaces. After that, we will focus on the air−water interface with Langmuir monolayer approach.

6.3.1 Insulin Aggregation at the Aqueous−Solid Interface

It has long been suggested that aggregation of dissolved proteins can occur at hydrophobic interfaces in a general process.[170,173,195] This process is initiated by diffusion and adsorption of protein molecules to the interface. It is widely accepted that the adsorbed protein changes its conformation upon adsorption, and thus, some hydrophobic regions are exposed to contact with the hydrophobic interface.[173] Subsequently, the protein molecules in the boundary layer associate over these exposed hydrophobic regions, forming aggregates. The aggregates eventually desorb from the surface to aqueous solution and may serve as nuclei for further fibrillation.

In the case of insulin at the aqueous−solid interface, Sluzky et al. verified the above model that insulin aggregation initiates with conformational changes of the monomer at hydrophobic interfaces by UV−vis absorption spectroscopy, quasi−elastic light scattering, and mathematical calculations.[174,186] The driving force is mainly hydrophobic interaction between the monomer and the hydrophobic interface. Recent investigations with new techniques provide more evidence. For example, using Fourier transform infrared spectroscopy, attenuated total reflection spectroscopy, thioflavin T fluorescence measurement, dynamic light scattering, and atomic force microscopy, Smith et al. found that the nucleation and fibril growth of insulin at the hydrophobic polystyrene surfaces follow the model pattern.[170] More than insulin itself, fluorescein isothiocyanate labeled insulin,[196] mutated insulin,[196] and acylated insulin[197] also show high affinity with hydrophobic surfaces.

Compared to hydrophobic surfaces, a much longer lag time of aggregation of insulin has been observed in the presence of a highly hydrophilic surface. This phenomenon may be attributed to the less conformational change of insulin induced by the hydrophilic surface.[198]

Besides the hydrophobicity of a surface, other parameters also contribute to the aggregation rate of insulin at the aqueous−solid interfaces, such as surface roughness[164,169] and additive in the aqueous solution.[174,186,199] Pandey et al. recently demonstrated that a larger initial surface roughness results in a faster rate of insulin adsorption and aggregation.[164] Stabilizing additives such as zinc and non−ionic surfactants are able to inhibit conformational changes of insulin. Therefore, they can prevent insulin fibril formation at the hydrophobic interfaces.[174,186]

6.3.2 Insulin Aggregation at the Water−Oil Interface

Similar to the aggregation process of insulin at the aqueous−solid interface discussed above, one will expect that the aggregation can also happen at the boundary between water and non−miscible liquid, i.e., a water−oil interface. As both solvent molecules are able to move freely in their own phase and penetrate from one phase to the other to a certain degree, the water−oil interface is considered to be much more continuous than the aqueous−solid interface.[156] Therefore, insulin molecules dissolved in aqueous solution can easily reach the hydrophobic interface, promoting unfolding and eventually fibril formation. Indeed, the rate of insulin aggregation induced by the water−methylene chloride interface was found by Kwon et al. to be an order of magnitude higher than that at the aqueous−solid interface.[156] Some factors contributing to the rate of aggregation at the water−oil interface are determined as associated states of insulin (such as monomer, dimer, and hexamer), charge of surfactant (non−ionic and anionic), agitation, and presence of another polymer component in the organic phase.[156]

6.3.3 Insulin Aggregation at the Air−Water Interface by the Langmuir Monolayer Approach

The air−water interface possesses hydrophilicity from the aqueous solution and hydrophobicity from the air phase, sharing some features of both the aqueous−hydrophobic solid interface and water−oil interface. Thanks to the Langmuir monolayer technique established and developed by Irving Langmuir, characterization of physical/chemical properties of various molecules at the air−water interface was made possible. This technique is a typical two−dimensional (2−D) surface chemistry approach, widely applied to investigate structures and properties of amphiphilic molecules at the interface, such as surfactants, proteins, lipids, and other materials.[85,137,176,177,179,200,201] A Langmuir monolayer is formed at the air−water interface when a one−molecule thick layer of amphiphilic organic or inorganic matter is spread onto an aqueous subphase. Advantages of the Langmuir monolayer technique lie in the possibility of controlling both the intermolecular structure and ordering of the amphiphilic molecules via controllable variables, such as the surface pressure, surface potential, monolayer and subphase component, temperature, pH and packing status.[202] Characterizations can be directly applied with ease at the air−water interface due to the accessibility from the air phase, such as UV−vis absorption, fluorescence, epi−fluorescence, infrared reflection−absorption spectroscopy (IRRAS), vibrational sum frequency generation spectroscopy (SFG), Brewster angle microscopy (BAM), and grazing incidence X−ray diffraction. However, direct characterization at the aqueous−solid interface and especially water−oil interface is more difficult and challenging, and even impossible in some cases due to the shielding from the solid or organic phase. Furthermore, Langmuir monolayer of lipid is a well−accepted *in vitro* model to mimic biological membranes, which can be considered as two weakly assembled Langmuir monolayers, as illustrated in Figure 6.3. In the following, we will focus on the aggregation of insulin using the Langmuir monolayer technique at the air−water interface in the absence and presence of lipid monolayer, respectively.

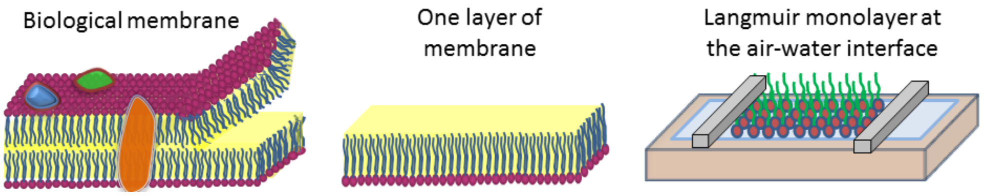

Figure 6.3 Cartoons of a biological membrane (left), one layer of membrane (middle), and Langmuir monolayer at the air−water interface to mimic the biological membrane (right).

6.3.4 Aggregation of Insulin at the Air−Water Interface in the Absence of Lipid Monolayer

Several studies of insulin aggregation have been investigated at the air−water interface under various conditions using the Langmuir monolayer technique combined with spectroscopy and microscopy.[178,179,181] When deposited at the air−water interface, molecules of insulin can stay at the air−water interface and form a uniform Langmuir monolayer due to the amphiphilicity of insulin. Before the monolayer is compressed, the distance between insulin molecules is so large that insulin molecules are extremely loosely packed. When compressed gradually, insulin molecules in the monolayer become closer and interact with each other. Therefore, the Langmuir monolayer is a good method to study intermolecular interactions induced by surface pressure.

Johnson et al. found that insulin spread from acidic insulin solution (pH 2) forms a homogeneous Langmuir monolayer at 20 ℃ at the air−water interface.[179] The conformational changes of the insulin Langmuir monolayer are monitored by infrared reflection−absorption spectroscopy (IRRAS), which is a good and sensitive technique to check secondary structure changes of protein molecules at the air−water interface. Results of IRRAS show that insulin adopts mainly α−helix and slightly β−sheet structures under different surface pressures at the air−water interface, but the spectra of amide I (1700−1600 cm^{-1}) and amide II (1600−1500 cm^{-1}) bands at the air−water interface are quite different from those obtained in aqueous solution. The spectra differences indicate that the air−water interface does change the conformation of insulin. Hydrophobic residues from insulin monomer probably misfold and are exposed to the hydrophobic air phase, while the hydrophilic residues are mainly submerged in the subphase of water. Furthermore, the air−water interface can anchor the misfolded insulin monomers from moving freely under a certain surface pressure (i.e. less freedom degree at the air−water interface than in aqueous solution).[112] As a result, it is probably more difficult or takes more time for insulin monomers to aggregate or form fibrils at the air−water interface.

Actually, no insulin aggregates are examined in experiments during compression by fluorescein isothiocyanate labeled insulin epi−fluorescence or Brewster angle microscopy (BAM).[179] A similar homogenous Langmuir monolayer without fibril formation is also observed by Pérez−López et al. using BAM at the air−water interface.[177]

Zinc is found to have a concentration as high as 11 mM in secretory granules in human pancreatic β−cells.[203] It has been known for many years that there exists a physical chemical relationship between insulin and zinc. Insulin is found to be stored predominantly as zinc−coordinated hexamers in the secretory granules of pancreas.[204] Therefore, it is necessary to study effects of zinc in the subphase on the aggregation of insulin at the air−water interface.[178,181,205] It has been previously known that zinc can induce the formation of dimers and hexamers in solutions.[174,206,207] Nieto−Suárez et al. observed using surface pressure−area isotherms that the presence of zinc ions has a profound effect on the lifting up molecular area and transition state at the air−water interface.[181] Liu et al. recently studied systematically the effects of zinc ions of the subphase on the aggregation of insulin at the air−water interface.[178] In this study, the insulin sample was first dissolved in either pH 2 HCl or pH 9 NaOH solution, and then was spread at the air−water interface with different concentrations of zinc ions in the subphase. In both cases (pH 2 and 9), insulin molecules in the Langmuir monolayer are found to form aggregates (oligomers) at the air−water interface in the presence of zinc in the subphase. The aggregation process is confirmed by the secondary structure changes during compression, with a decreased component of α−helical conformation and increased component of β−sheet and β−strand structures.[178] When the insulin Langmuir monolayer is compressed to reach collapse in the presence of zinc in the subphase, long insulin fibers are observed at the air−water interface using BAM.[177]

Besides zinc concentration, other factors such as pH, ionic strength, and proteins in the subphase also contribute to the aggregation of insulin at the air−water interface.[181] Compared to the surface pressure−area isotherm of the insulin Langmuir monolayer at pH 5.7, lowering the pH to 1 results in more expanded conformation of insulin with larger limiting molecular area, indicating more monomeric insulin present. Increasing the pH to 10 leads to the association of insulin molecules to form a more compact and rigid monolayer, shrinking the mean molecular area to a smaller number.[181] The larger ionic strength increases the molecular area occupied at a given surface pressure. This is probably due to the salting out effect: the presence of ions weakens the hydration of the polar residues of proteins, increasing intermolecular repulsion.[181,208] The presence of islet amyloid polypeptide (hIAPP) also contributes to the aggregation process of insulin due to the interaction and copolymerization between insulin and hIAPP.[112]

6.3.5 Aggregation of Insulin at the Air−Water Interface in the Presence of Lipid Monolayer

Amyloid fibers isolated from patients are determined to have some lipid content.[147,209] Therefore, it is necessary to study how the formation of amyloid fibril is affected by the presence of lipid interface and surface. As the Langmuir monolayer of lipid is analogous to half of a bio−membrane bilayer, it has been verified to be an excellent model to mimic *in vivo* conditions. Compared with a living cell, constituents in the Langmuir monolayer and subphase are known and can be controlled at ease, facilitating our understanding of the chemical/physical process at the interface of the lipid.

The property and aggregation of insulin have been investigated at the air−water interface in the presence of the lipid Langmuir monolayer, such as phospholipid and sphingomyelin.[175-177] Phospholipids containing phosphatidylcholine terminations are the main content of cellular membranes. Although sphingomyelin has a much lower content in mammals ranging from 2 to 15% in most tissues, it contributes significantly to the structural and functional roles in cellular membranes.[210] Pérez−López et al. investigated the behavior of the binary mixed Langmuir monolayer of phosphatidylcholine and bovine insulin spread at the air−water interface under various conditions.[177] They suggested that domain separation of phosphatidylcholine and insulin will probably promote insulin aggregation at the air−water interface. This assumption is supported by the observation that insulin aggregates are found on the monolayer edges and fractures using BAM.[177] In contrast with phosphatidylcholine, when sphingomyelin is present at the air−water interface, insulin does not form fibrils with various pH's and zinc concentrations in the subphase.[175] It is possible due to the miscibility and the strong intermolecular interaction between sphingomyelin and insulin associated states (such as dimer and hexamer), stabilizing insulin molecules from further fibrillation.

However, until now, there has been no investigation on the secondary structure and orientation changes of insulin when it interacts with lipid at the air−water interface, which will benefit our understanding of insulin aggregation in a biological environment. Methods such as polarization modulation infrared reflection−absorption spectroscopy (PM−IRRAS) and vibrational sum frequency generation (SFG) spectroscopy, have recently been successfully applied to study the secondary structure changes of proteins at the air−water interface.[160,211,212] PM−IRRAS is a highly surface specific Fourier transform infrared method that is able to detect chemical compositions and orientations down to one molecule thick films at the interface. Compared with regular IRRAS, the polarization modulation at high frequency of PM−IRRAS can almost completely eliminate the background interferences from environmental factors such as atmospheric water vapor, carbon dioxide, and instrumental noise.[160,213] The elimination of water background absorption of IR is extremely important, as it overlaps with the IR absorption of proteins in amide I and amide II regions. SFG has recently emerged as a novel second−order non−linear optical technique, which allows us to obtain vibrational spectra at surfaces and interfaces with high surface selectivity and resolution.[214,215] SFG is generated by one visible beam at a fixed frequency ω_{vis} and another beam at a scanning frequency ω_{ir} in the infrared region with an observation of a sum frequency $\omega_{SFG} = \omega_{vis} + \omega_{ir}$. When ω_{ir} is equal to a vibrational level of the molecule, the SFG signal is resonantly enhanced. Due to properties of non−centrosymmetry at the air−water interface, SFG is sensitive only to molecules at the interface but not in bulk solutions. It is therefore capable to provide direct information about the structure and orientation of proteins at the interface.[211,212] Most recently, Yan’s group at Yale University established vibrational SFG spectroscopy for the characterization of protein secondary structures. By probing the vibrational chirality of protein backbones at the interfaces, they found that the SFG signals of proteins are unique and sensitive to the secondary structures in amide I and N−H stretch spectra.[211,216] It is expected that PM−IRRAS and SFG will soon be used to characterize the structure and orientation changes of insulin aggregation in the presence of lipid at the air−water interface.

6.4 Summary and Outlook

In this article, the recent progress of insulin aggregation is briefly summarized at the aqueous−solid, water−oil, and air−water interfaces. The aggregation of insulin initiates with diffusion and adsorption of insulin at the hydrophobic solid or oil interfaces, resulting in conformational changes of the monomeric insulin to expose the hydrophobic residues.[170,174,186] The driving force is mainly hydrophobic interaction between the unfolded monomer and the hydrophobic interface.[173] Subsequently, the dissolved insulin molecules associate over the exposed hydrophobic regions, eventually forming aggregates. Compared to hydrophobic solid or oil surfaces, the hydrophilic surface induces less conformational change of insulin.[198] As a result, a much longer lag time of aggregation of insulin has been observed at the hydrophilic interfaces. To mimic a cellular environment, the Langmuir monolayer technique has been utilized to study the aggregation of insulin through intermolecular interaction in the absence and presence of lipid monolayer at the air−water interface. In the absence of lipid, insulin forms a homogeneous Langmuir monolayer on the pure water subphase without fibril formation at the air−water interface.[178,179,181] In the presence of a lipid Langmuir monolayer at the air−water interface, the component of lipid has a profound effect on the insulin aggregation: phosphatidylcholine promotes insulin aggregation while sphingomyelin stabilizes insulin at the air−water interface.[175-177] Other factors in the subphase, such as pH, zinc concentration, ionic strength, and presence of other proteins, also contribute to the aggregation of insulin at the air−water interface.[178,181] Higher pH and concentration of zinc promote the aggregation of insulin.

Although some progress has been recently made on the aggregation of insulin at the interfaces, a large number of open questions still exist about the structural changes and pathways during the process of insulin aggregation. These questions include: (1) a molecular level of understanding of the aggregation pathway from native insulin to insulin oligomers and mature fibers is still lacking; (2) once monomeric insulin molecules are adsorbed at various interface, it is still unclear to what extent these molecules can unfold, and what will be the conformation of the molecules after desorption from the interface; (3) the structure and misfolding pathway of transiently populated oligomeric insulin species remain to be detected and elucidated; (4) particularly at the air−water interface, the secondary structure and orientation changes of insulin are still lacking when insulin interacts with lipids and other proteins under various conditions of subphase. Although the first three questions are still challenging for the current techniques, the last one is expected to be answered in the near future by spectroscopic studies, such as polarization modulation infrared reflection−absorption spectroscopy (PM−IRRAS), and vibrational sum frequency generation spectroscopy (SFG).

Chapter 7 Human Islet Amyloid Polypeptide at the Air−Aqueous Interface: A Langmuir Monolayer Approach

7.1 Background

One of the major diseases of modern humanity, which can be effectively managed, but for which there is no permanent cure is diabetes mellitus. Due to increases in the quality of human life, associated with decreases in physical activity and increases in obesity, diabetes mellitus has reached epidemic proportions.[217] For example, in 2010 it was estimated that 285 million people were affected by diabetes compared with 30 million in 1985.[217] Type 2 diabetes mellitus, which is also known as non insulin−dependent diabetes mellitus (NIDDM), is determined by having a high blood glucose level associated with cellular insulin resistance, and relative insulin deficiency. It is the most common type of diabetes, and accounts for more than 90% of all diabetes cases. The age of onset of type 2 diabetes mellitus is also falling and it has become increasingly common amongst those under 30.[218,219] The two major hormones of the endocrine pancreas involved in diabetes are human insulin and human islet amyloid polypeptide (hIAPP, also known as human amylin). While the insulin has been probably the most studied hormone, the body of knowledge on the roles of hIAPP is much less.

hIAPP is a 37 amino acid residues peptide with a disulfide bridge and an amidated C−terminus. This hormone is co−synthesized and co−secreted to blood circulation together with insulin in an approximately 1:100 molar ratio (hIAPP:insulin) from secretory granules of pancreatic β−cells.[38] The monomeric hIAPP is involved in the glycemic down−regulation in a way that it slows gastric emptying, and thereby prevents sudden spikes in blood glucose levels.[220,221] It is responsible for the satiation signal, and is hypothesized as one of the preventers of obesity.[222,223] Similar to the Alzheimer−related beta amyloid, this hormone also is a highly amyloidogenic peptide, and its amyloid deposits are observed in the islets of Langerhans of around 95% type 2 diabetic patients,[39,40] as well as in pancreatic cancer.[41] The interaction of hIAPP with β−cell membrane is thought to play a crucial role in the dysfunction and death of β−cells.[224] Studies on both model membranes and cells show that this cytotoxicity is linked to peptide aggregation on the membrane surface by growing hIAPP fibrils or by toxic oligomers.[225-227] However, there is increasing evidence that hIAPP oligomers formed early during aggregation may be the most cytotoxic species, not the mature hIAPP amyloid fibrils.[227-230]

The molecular mechanism for the cytotoxicity of hIAPP is still unclear, although several mechanisms have been proposed, such as membrane disruption, the formation of reactive oxygen species, endoplasmic reticulum stress, and inflammatory response induced by amyloid formation.[231,232] Recent progress in the study between hIAPP and the phospholipid membrane model shows that the electrostatic interaction between the positively charged hIAPP and negatively charged phospholipid model accelerates the aggregation of hIAPP.[111,129,225,228,233-236] In the presence of such lipids, hIAPP fibrils form within a few minutes, while no fibrils are observed on a neutral phospholipid [111]. Besides membranes, it has been known that other factors can play important roles in the aggregation process of hIAPP, such as pH, metal ions, ionic strength and other protein components (for instance, insulin, C−peptide, pro−insulin and pro−amylin).[42,237-240] In the physiological range, acidic pH has been shown to inhibit fibrillation of hIAPP *in vitro* while basic pH promotes the fibril formation.[42,237,241,242] Zinc, which naturally occurs in the secretory granules at millimolar concentrations and can bind to the histidine residue at position 18 of hIAPP, has been found to have a dual effect on the aggregation: lower concentration inhibits aggregation while having the opposite effect at higher concentration.[243] The role of insulin in the fibrillation of hIAPP is more complicated, as there are variations for the fibril formation in the reported effects.[42,244-246]

The hIAPP is monomeric in its physiological state in healthy pancreas, but undergoes a multistep process of aggregation in the disease state. Detailed structural information could facilitate the understanding of the mechanism and therapeutic intervention. However, the three−dimensional structure of hIAPP in different aggregation states remains elusive, although much progress upon the structure has been made.[247] Several studies have shown that the structural changes of hIAPP accompany the changes from unstructured monomer to β−sheet amyloid aggregate in solution.[248-250] When bound to the negatively charged lipid membrane, hIAPP is found to adopt an α−helix conformation first before conversion to the β−sheet structure during aggregation.[235] In a micelle prepared from sodium dodecyl sulfate, hIAPP adopts an overall kinked helix motif, with residues 7−17 and 21−28 in a helical conformation.[242]

Langmuir monolayer technique is a two−dimensional (2D) method, well accepted for the structure and property study of the amphiphilic biomacromolecules at the interface, such as proteins and membrane components.[111,202,251-253] The advantages of this method for protein study lie in the possibility of controlling both the intramolecular structure and intermolecular ordering of the amphiphilic biomacromolecules via controllable variables, such as the surface pressure, monolayer and subphase composition, temperature, pH and phase transition.[202,254] Furthermore, the structures and properties of proteins in Langmuir monolayer could be quite different from those in bulk aqueous solution, as the degree of freedom of proteins in organized Langmuir monolayer is largely decreased. Among these variables, surface pressure is the dominant factor for the intramolecular and intermolecular interactions of protein in the Langmuir monolayer, as it represents how closely packed the protein molecules are between each other in 2D. When the Langmuir monolayer of protein is compressed, the increasing surface pressure promotes the intramolecular and intermolecular interactions, and thus helps to form self−assembly of protein.[255] Furthermore, the protein−protein and protein−interface interactions become the main forces to determine the conformation, orientation and activity of proteins.

Investigation on the conformation, orientation, and self−assembly of hIAPP at time zero could be beneficial for our understanding of its stability and aggregation process. To obtain these insights, the hIAPP in the present study was studied at the air−aqueous interface using the Langmuir monolayer technique with different experimental conditions, such as pH and ionic strength of the subphase. The compression−decompression cycles and stability measurements were employed to study the stability of the Langmuir monolayer, followed by the spectroscopic studies of UV−vis absorption and fluorescence emission. The conformational and orientational specifics of the hIAPP Langmuir monolayer induced by surface pressure was characterized by p−polarized infrared−reflection absorption spectroscopy (IRRAS). The morphology of the hIAPP domains, if formed by self−assembly at the air−aqueous interface, was observed by Brewster angle microscopy (BAM).

7.2 Experimental Section

7.2.1 Materials

hIAPP was obtained from MP Biomedicals (Solon, OH) with molecular weight of 3903 Da. The isoelectric point (pI) of hIAPP derived from its amino acid sequence is 8.9 [256]. Sodium chloride was purchased from Sigma Aldrich (St. Louis, MO) with purity higher than 99.5%. Hydrogen chloride and sodium hydroxide used for adjusting pH were from Pharmco (Brookfield, CT) and MP Biomedicals (Solon, OH), respectively. The solvents 1,1,1,3,3,3−hexafluoroisopropanol (HFIP), methanol and chloroform were obtained from MP Biomedicals (Solon, OH). All chemicals were used without any further purification. The pure water used in the experiments was obtained from a Modulab 2020 Water purification system (Continental Water System Corp. San Antonio, TX) with resistivity of 18 MΩ·cm, surface tension of 72.6 mN/m, and pH 5.6 at 20.0 ± 0.5 ^{o}C.

7.2.2 Methods

All the isotherm measurements and UV−vis absorption, fluorescence and IRRAS spectroscopy were measured in a clean room (class 1000) with constant temperature of 20.0 ± 0.5 ^{o}C and humidity of 50 ± 1 %. A Kibron μ−trough S (Kibron Inc., Helsinki, Finland) with an area of 5.9 cm × 21.1 cm was utilized for the studies of surface pressure− and surface potential−area isotherms, compression−decompression cycles, stability, IRRAS and BAM. Surface pressure was monitored by the Wilhelmy method using an alloy wire probe with a sensitivity of ± 0.01 mN/m. Surface potential was measured with a Kelvin probe to an accuracy of 10 mV.

The UV−vis absorption and fluorescence spectra of the hIAPP Langmuir monolayer were collected on the top of a KSV trough (KSV Instrument Ltd., Helsinki, Finland). The trough had an area of 7.5 cm × 30 cm and a quartz window in the middle. The UV−vis absorption spectra of the hIAPP Langmuir monolayer were measured with a Hewlett−Packard (HP) 8452A spectrophotometer, while the fluorescence spectra were measured by an optical fiber detector connected to a Fluorolog−3 spectrofluorimeter (Horiba Scientific, Edison, NJ). The slit widths in spectrofluorimeter were set at 5 nm. UV−vis and fluorescence spectra for the aqueous solutions of hIAPP were measured using a Lambda 900 UV/Vis/NIR spectrophotometer (Perkin−Elmer, Norwalk, CT) and a Fluorolog−3 spectrofluorimeter, respectively.

The IRRAS measurements of the hIAPP Langmuir monolayer at the air−aqueous interface were recorded with an EQUINOX 55 Fourier transform infrared (FTIR) spectrometer (Bruker Optics, Billerica, MA), connected to an XA−511 external reflection accessory with a mercury−cadmium−telluride (MCT) detector cooled by liquid nitrogen. The measurements were performed using p−polarized light on a Kibron μ−trough S. Each spectrum was acquired by the co−addition of 1200 scans with a resolution of 8 cm^{-1}. The IRRAS spectra were used without any processing or base line correction.

Brewster angle microscopy (BAM) was performed at the air−aqueous interface using an IElli−2000 imaging ellipsometer (Accurion, Menlo Park, CA) with BAM2plus software. The standard laser of the BAM2plus was a frequency−doubled Nd:YAG laser with a wavelength of 532 nm. The laser had a power of 50 mW in a collimated beam. The angle of incidence was set at 53.65° as the Brewster angle of 1.0 M NaCl with pH 5.6.

hIAPP was rendered in monomeric form by first dissolving in 1, 1, 1, 3, 3, 3−hexafluoroisopropanol (HFIP) and stored under room temperature for 2 h.[249,257] Then the solution was evaporated in a vacuum desiccator for 2 h to remove the solvent HFIP, followed by re−dissolving in deionized water (pH 5.6) at a concentration of 0.40 mg/mL (1.0×10^{-4} M). Different concentrations of NaCl solutions (0.1, 0.5, 1.0 and 2.0 M) were used as subphase at pH 2.0, 5.6 and 9.0, respectively. The volume of the spreading hIAPP solution was 30 and 60 μL for Kibron and KSV troughs, respectively. The freshly prepared hIAPP solution was spread at the air−aqueous interface using a 100 μL syringe (Hamilton Co., Reno, NV) by uniform droplet deposition over the subphase surface. A waiting time period of 20 min was taken for the hIAPP Langmuir monolayer to reach equilibrium. The monolayer was compressed at a rate of 50 $Å^2$/molecule. Triplicate experiments confirmed the reproducibility of the data.

7.3 Results and Discussion

7.3.1 Surface Pressure− and Surface Potential−area Isotherms

Pure water was first utilized as the subphase to form the hIAPP Langmuir monolayer. As shown in Figure 7.1, the surface pressure had a lifting point of around 350 $Å^2$/molecule on the pure water subphase. The extrapolation of the linear part of the plot to zero surface pressure gives a limiting molecular area of around 205 $Å^2$/molecule. During compression from 300 to 200 $Å^2$/molecule, the surface pressure increased steadily. The film was characterized by the liquid expanded phase at around 250 $Å^2$/molecule and the coexistence of a liquid expanded−liquid condensed phase between 250 and 150 $Å^2$/molecule. The monolayer collapsed at a surface pressure of around 20 mN/m.

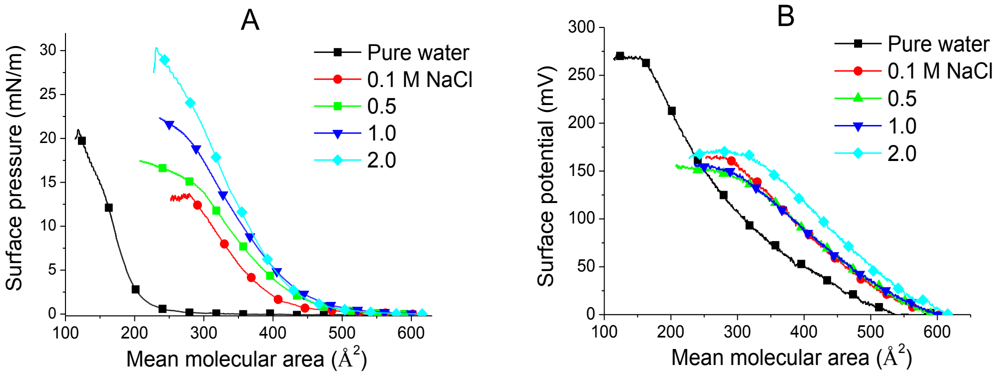

Figure 7.1 Surface pressure−area isotherm (A) and surface potential−area isotherm (B) of the hIAPP Langmuir monolayer on different subphase solutions.

Due to the possible dissolution of protein molecules into the pure water subphase, the surface pressure and limiting molecular area of the obtained protein Langmuir monolayer may be smaller than its actual number.[258] Addition of sodium chloride in the subphase could be used to decrease the quantity of hIAPP molecules that dissolve or sink into the bulk subphase solution, resulting in the formation of a more closely−packed hIAPP Langmuir monolayer. Different concentrations of NaCl (0.1, 0.5, 1.0 and 2.0 M) were introduced to the subphase solution in order to maximize the number of hIAPP molecules at the air−aqueous interface. As shown in Figure 7.1 (A), all the four concentrations of NaCl present in the subphase show a higher lifting area at about 550 Å^2/molecule, indicating that more molecules are present at the air−aqueous interface. The limiting molecular area increases to around 400, 430, 445, and 440 Å^2/molecule for 0.1, 0.5, 1.0 and 2.0 M NaCl subphase, respectively. An increase of collapse surface pressure was also observed as the NaCl concentration in the subphase increased. Therefore, the dissolution of hIAPP in the subphase solution decreases in the presence of the electrolyte, which is similar to other proteins, such as alcohol dehydrogenease[258] and acetylcholinesterase[259].

The decreasing solubility of hIAPP is due to the salting−out effects, which comes from dehydration of the protein by the added sodium chloride. The salt ions would have stronger attraction with the highly polar water molecules than the less polar protein molecules.[260] Also, ion−protein dispersion potentials originating from the polarizabilities of ions and hIAPP could be involved in the salting−out effect.[258]

The surface potential–area isotherm was also correlated with the surface pressure–area isotherm as shown in Figure 7.1 (B). Because the surface potential measures the dipole−dipole interactions at much longer distances than the interactions measured by surface pressure (usually due to van der Waals interactions), the surface potential−area isotherm shows an increase in the surface potential as soon as the compression of the monolayer was started [261]. The collapse surface potential on pure water was observed at about 270 mV, much higher than that on the subphase that contained NaCl. The reason might be that the presence of NaCl neutralized the charge of the protein, thus reducing the net surface potential.

Based on the salt effect on the surface pressure− and surface potential−area isotherms, an ionic concentration of NaCl at 1.0 M in the subphase was selected for the pH effect.

7.3.2 The pH Effect on the hIAPP Langmuir Monolayer

hIAPP contains a single histidine residue at position 18 (His−18) of its amino acid sequence with a pK_a near 6.5 in the monomer state.[42] In healthy pancreas, the hIAPP is safely stored in the β−cell granules with pH around 5.5 and released into the extracellular environment with pH about 7.4. It is feasible to think that the pH has an effect on the aggregation of hIAPP. Indeed, studies have shown that the aggregation of hIAPP in solution at pH 4.0 is much slower than that at pH of 8.8.[237,241] In order to study the pH effect on the self−assembly of hIAPP as Langmuir monolayer, 1.0 M NaCl subphase solution with pHs 2.0, 5.6 and 9.0 was investigated, as shown in Figure 7.2. Under these three pH values, the lifting areas were similar, around 550 Å^2/molecule. The limiting molecular areas for both pH 2.0 and 9.0 were smaller, around 410 Å^2/molecule, compared with 445 Å^2/molecule at pH 5.6.

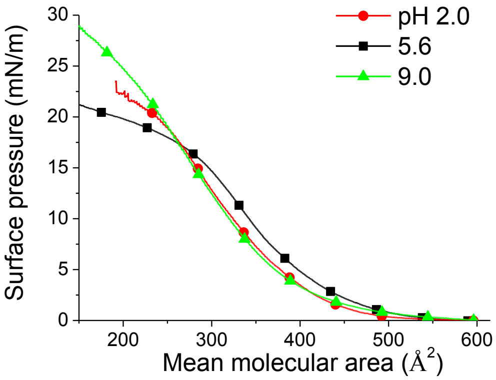

Figure 7.2 Surface pressure−area isotherms of the hIAPP Langmuir monolayer. The subphase was 1.0 M NaCl solution with pH 2.0, 5.6 and 9.0, respectively.

Different surface pressure−area isotherm with a smaller limiting molecular area was expected for higher pH at 9.0, as it had been shown to promote aggregation of the hIAPP in solution. However, the pH did not seem to have pronounced effect on the hIAPP Langmuir monolayer during the time of experiment. One possible reason for this observation could be that it might take a longer time for the hIAPP molecules to form aggregates than the time needed for Langmuir monolayer experiment. It typically took a few hours to detect the fibril formation by thioflavin T fluorescence in solution,[237,241,243] but one set of Langmuir monolayer experiment needed only 30−40 min. Another possibility could be that some amount of aggregation did form, but the surface pressure−area isotherm could not detect it. However, it could be excluded as the compression−decompression cycles, UV−vis absorption, IRRAS and BAM in the following sections did not detect large aggregation or domain formation, although the existence of some oligomers could not be ruled out.

Based on the effects of salt and pH, 1.0 M NaCl aqueous solution with pH 5.6 was chosen as the subphase for compression−decompresssion cycles and stability studies of the hIAPP Langmuir monolayer at the air−aqueous interface.

7.3.3 The Compression−Decompression Cycles and Stability Measurements of the hIAPP Langmuir Monolayer

Three compression−decompression cycles of the hIAPP Langmuir monolayers were examined for the stability of hIAPP Langmuir monolayer at surface pressures of 15 and 5 mN/m on a 1.0 M NaCl subphase, as shown in Figure 7.3. From the surface pressure−area isotherm shown in Figure 7.1, the hIAPP Langmuir monolayer at both 15 and 5 mN/m was in liquid−condensed phase. A hysteresis was observed at both surface pressures but the difference between the first compression and the last compression was relatively small, i.e. 8 and 12 %, respectively. Also, the surface pressure could return 0 mN/m when the barriers moved to the maximum area position. These facts showed that the formation of the hIAPP Langmuir monolayer was reversible, suggesting the self−assembly or domain formation of the hIAPP at time zero did not happen.

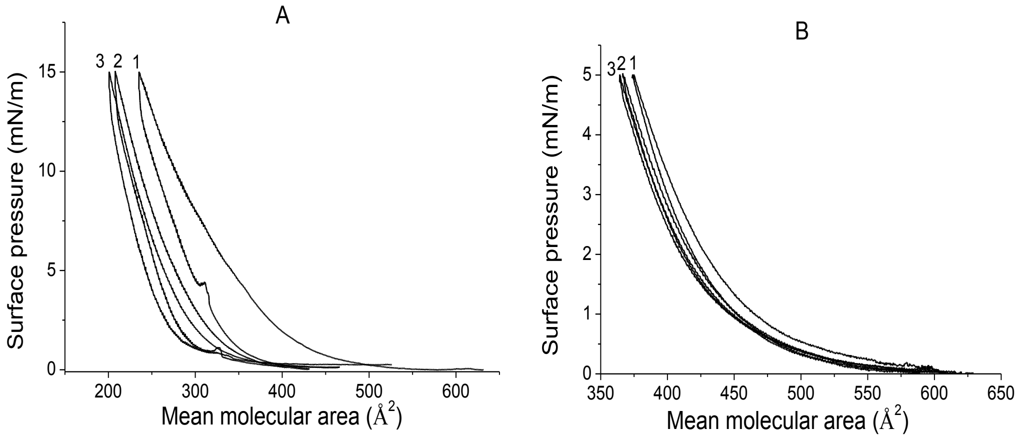

Figure 7.3 Compression−decompression cycles of the hIAPP Langmuir monolayer on 1.0 M NaCl subphase with pH 5.6 at surface pressure 15 (A) and 5 mN/m (B).

The stability measurements of the Langmuir monolayer were also obtained over a period of time at a constant surface pressure of 10 mN/m, as shown in Figure 7.4. Over 250 min, the approximate mean molecular area change was about 20%. The reason could be the relaxation of the Langmuir monolayer, dissolution of hIAPP into the subphase, or a change of conformation of the protein over time. The hypothesis of the dissolution of hIAPP into the subphase would be ruled out based on the UV−vis spectra discussed below.

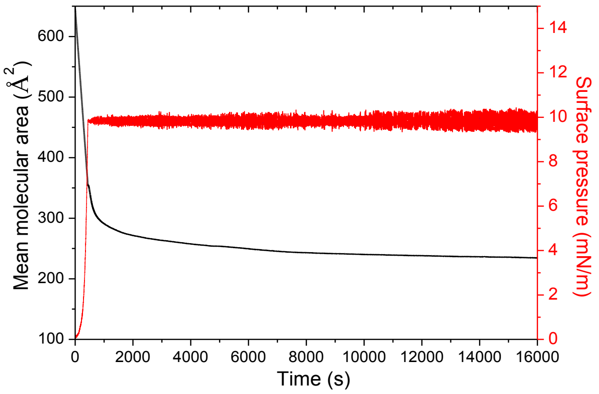

Figure 7.4 Stability measurement of the hIAPP Langmuir monolayer at surface pressure 10 mN/m. The subphase was 1.0 M NaCl with pH 5.6 (surface pressure: red; mean molecular area: black).

7.3.4 UV−vis Absorption of hIAPP at the Air−Aqueous Interface

The UV−vis absorption of the hIAPP Langmuir monolayer on 1.0 M NaCl with pH 2.0, 5.6 and 9.0 was investigated under different surface pressures. As shown in Figure 7.5, it did not have any significant absorbance except at 202 nm with pH 5.6, which corresponded to n−π^* transition of C=O chromophore of the amide bonds in hIAPP. The inset shows the linear relationship between the absorbance at 202 nm and the surface pressure. The hIAPP Langmuir monolayer had the same absorption and linearity at 202 nm with pH 2.0. The linearity of absorption at pH 2.0 and 5.6 is proof that during compression, the number of hIAPP molecules per unit area were increasing linearly, indicating that: aggregation most likely did not happen, nor was there an effect on the solubility of the protein.

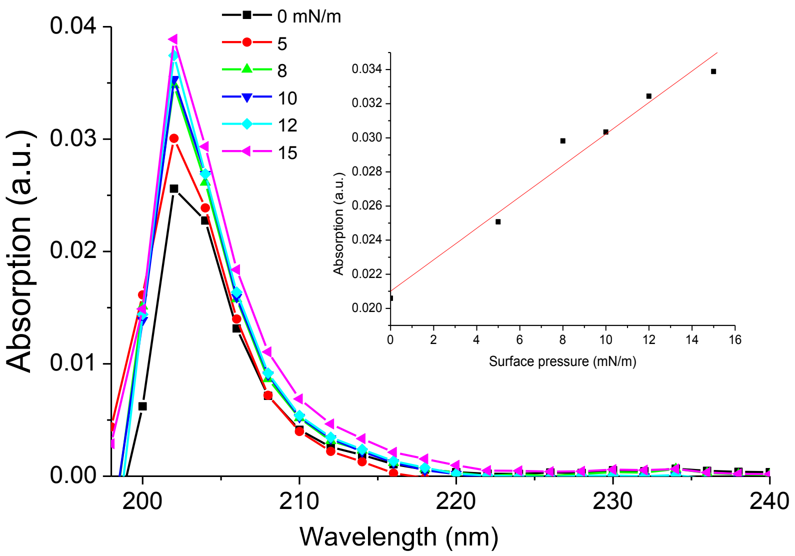

Figure 7.5 UV−vis absorption spectra of the hIAPP Langmuir monolayer. The subphase was 1.0 M NaCl at pH 5.6. Inset: absorbance at 202 nm vs. surface pressure.

Compared with the absorption of hIAPP in the Langmuir monolayer, the aqueous solution of hIAPP had a weak broad band around 275 nm due to the $\pi-\pi^*$ transition of the tyrosine residue in hIAPP. The absence of this band for the hIAPP Langmuir monolayer can be explained by the fact that the amount of tyrosine residue per unit area was too low to be detected. Due to the extremely strong absorption of peptide bond in aqueous solution, the UV−vis absorption bands of hIAPP below 225 nm could not be observed.

7.3.5 Fluorescence of the hIAPP Langmuir Monolayer at the Air−Aqueous Interface

The molecule of hIAPP contains one fluorescent tyrosine residue. The fluorescence emission wavelength of hIAPP in aqueous solution is 309 nm at the excitation wavelength 270 nm. However, no fluorescence of tyrosine in the hIAPP Langmuir monolayer was observed on 1.0 M NaCl subphase with pH 2.0, 5.6 or 9.0 due to the small amount of hIAPP molecules per unit area and low quantum yield of fluorescence of tyrosine.

7.3.6 IRRAS of the hIAPP Langmuir Monolayer at the Air−Aqueous Interface

The hIAPP can appear in various aggregation states, i.e. monomer, oligomer or fibril, all with variations in secondary, tertiary and quaternary structure. The synthetically produced hIAPP monomer in aqueous solution exhibits typically a random coil structure from circular dichroism (CD) spectra.[262] In contrast, hIAPP treated with helix promoting solvent, such as trifluoroethanol (TFE) and 1, 1, 1, 3, 3, 3−hexafluoroisopropanol (HFIP), predominantly adopts α−helical conformation.[242,243,249,257,263] Besides the structure information in solution, the interaction study between hIAPP and negatively charged lipid membrane suggests that the hIAPP adopts α−helix conformation first before conversion to β−sheet structure during aggregation.[111,235,264]

Since Dluhy's research group in the mid 1980's first acquired molecular structure information from Langmuir lipid monolayers *in situ* at the air−aqueous interface using infrared spectroscopy,[265] this technique has been widely expanded to investigate the conformational and orientational studies of lipid, peptide, or protein monolayer at the air−aqueous interface.[266-269] As one of the leading structural methods for the in situ characterization of the secondary structures of protein at the air−aqueous interface, IRRAS facilitates the spectroscopic analysis of the amide bands of proteins caused by possible conformational or orientational changes. For most proteins, α−helix predominated structures exhibit amide I (mainly the C=O stretching vibration of the peptide bond) and amide II (the N−H bending vibration and the C−N stretching vibration of the peptide bond) absorptions in the spectral range from 1650 to 1660 cm^{-1} and 1540 to 1550 cm^{-1}, respectively. β−sheets exhibit similar absorptions at 1620 to 1640 and 1520 to 1535 cm^{-1}.[270-272]

p−Polarized IRRAS has been intensively applied to the investigation of secondary structure and orientation changes of protein Langmuir monolayer at air−aqueous interface. It is due to the fact that p−polarized light probes the dipole moments parallel and perpendicular to the interface, while the s−polarized light probes only the dipole moment components parallel to the interface.[273] For the p−polarized IRRAS, the measured signal can contain positive and negative bands, depending on the angles of incidence and orientation of the transition dipole moment with respect to the air−aqueous interface.[235,274] If the transition dipole moments preferentially parallel to the air−aqueous interface, the absorbance bands are initially negative and increase in intensity with an increase in the incident angle until the Brewster angle (*e.g.*, 54.2 ° for the IR light at 2850 cm^{-1}) is reached.[275] Above the Brewster angle, there is an inversion of the bands to positive values and the intensity decreases with a further increase in the incident angle. If the transition dipole moment is preferentially perpendicular to the interface, the opposite should be observed for both the sign and intensity of the bands when the angle of the incident light is varied.[273,274,276]

The p−polarized IRRAS of the hIAPP Langmuir monolayer on 1.0 M NaCl subphase with pH 2.0, 5.6 and 9.0 were investigated for the information about the molecular orientation and conformation of the protein in the Langmuir monolayer. Figure 7.6 shows the p−polarized IRRAS spectra of the hAPP Langmuir monolayer at incident angle 65 ° (this angle was chosen based on its good signal−to−noise ratio[254]) on 1.0 M NaCl subphase with pH 5.6 (IRRAS spectra with pH 2.0 and 9.0 are very similar to those with pH 5.6, data not shown). The bands of ~1650 and ~1545 cm^{-1} were assigned to the α−helix conformation, corresponding to the vibrations of the amide I and II absorptions, respectively, whereas the band at ~1525 cm^{-1} was the β−sheet conformation.[271]

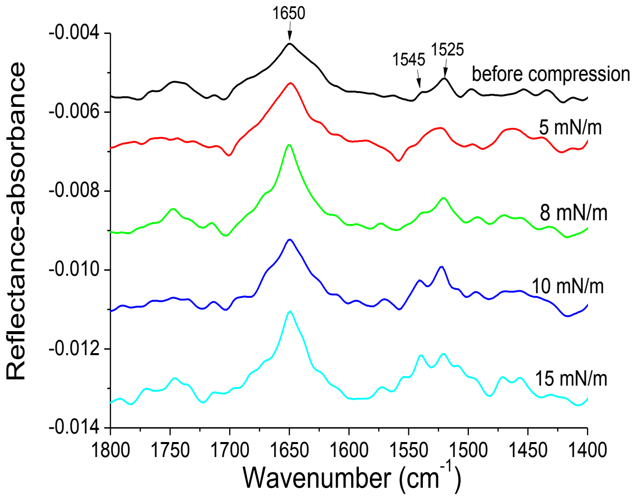

Figure 7.6 p-Polarized IRRAS at 65° of the hIAPP Langmuir monolayer at different surface pressures. The subphase was 1.0 M NaCl with pH 5.6. The spectra were shifted vertically for better visibility.

The possibility of conformational or orientational changes induced by increasing surface pressure at the air−aqueous interface was examined by analyzing band position and intensity of amide I and amide II of IRRAS.[277] As shown in Figure 7.6, the band positions of the hIAPP Langmuir monolayer on 1.0 M NaCl subphase with pH 2.0, 5.6 and 9.0 remained almost the same as the surface pressure increased, indicating that the hIAPP Langmuir monolayer did not undergo conformational changes upon compression during the time of experiment and retained mainly α−helical structure. This is probably due to the electrostatic repulsion of the positively charged hIAPP molecules. However, as previous studies shown, the conformation of hIAPP changed from α−helix to β−sheet with the presence of negatively charged phospholipid, while no obvious structural changes were observed with the presence of neutral phospholipid.[129,227,235] This suggested that the attraction between the negatively charged phospholipid and positively charged hIAPP might play a critical role to accelerate or catalyze the aggregation of hIAPP. No notable intensity of amide I and amide II was observed on the subphase with each pH, indicating that the orientations of hIAPP molecules at air−aqueous interface were almost parallel to the interface even before compression and remained the same orientation during the time of compression.[278]

The secondary structure information gained here was consistent with the previous theoretical and experimental results. It has been shown using molecular simulation that hIAPP monomer could adopt an **α**−helical conformation with a short β−sheet near the C−terminus.[249] The adsorption study of the hIAPP at the air−aqueous interface also found that it adopted an α−helix structure before conversion to β−sheet−rich fibril.[235] A recent NMR study in solution found that the structure of hIAPP was defined by a kinked helix from residue 11 to residue 30. Significantly, this finding was a relatively close match to the crystalline structure of the hIAPP dimer fused to maltose−binding protein, indicating that the helix−kink−helix motif was likely an early on−pathway intermediate to aggregation.[243] Therefore, it was also very likely that the *α*−helical conformation obtained here at the air−aqueous interface was a relatively stable intermediate before conversion to aggregates.

7.3.7 Brewster Angle Microscopy (BAM) of the hIAPP Langmuir Monolayer

Brewster angle microscopy (BAM) was employed to see visually the changes of phase domain and morphology of hIAPP in Langmuir monolayer at air−aqueous interface. As a reference, BAM of phase domains of arachidic acid monolayer were obtained in the two−phase coexistence region of the isotherm at pH 12 under 25°C,[279] as shown in Figure 7.7 (A). Unfortunately, we could not see the BAM image of the hIAPP Langmuir monolayer on 1.0 M NaCl subphase with pH 2.0, 5.6 and 9.0 under different surface pressures. Figure 7.7 (B) and (C) only show the BAM images of hIAPP Langmuir monolayer on 1.0 M NaCl subphase with pH 5.6 before compression (B) and at 10 mN/m (C). The microscopy ruled out the formation of domains from self−assembly of the protein at any surface pressure during the time of experiment.

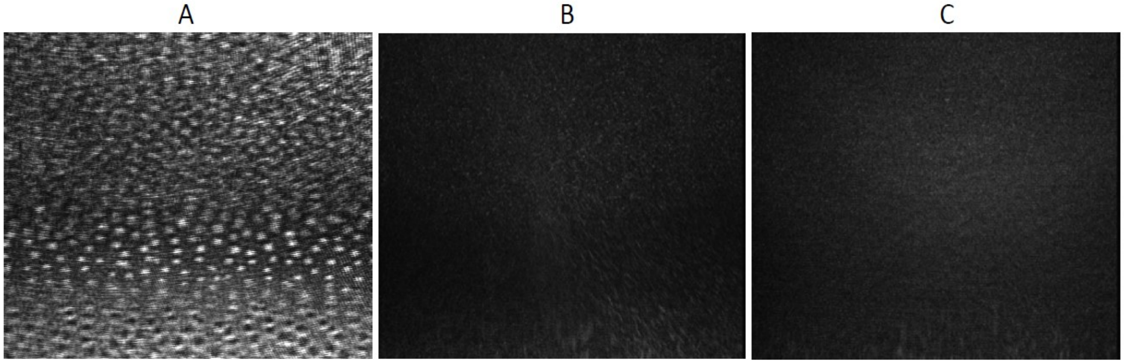

Figure 7.7 BAM images of phase domains of Langmuir monolayer. (A) Arachidic acid monolayer with pH 12 at 25 °C; (B) hIAPP Langmuir monolayer at 0 mN/m; and (C) hIAPP Langmuir monolayer at 10 mN/m. Size: 768 × 572 μm^2.

7.4 Summary

The conformation, orientation, and self−assembly of the hIAPP at time zero were studied at the air−aqueous interface using the Langmuir monolayer technique. The limiting molecular area of hIAPP on 1.0 M NaCl subphase as the optimal condition was found to be around 445 $Å^2$/molecule. The pH of the subphase solution (2.0, 5.6 and 9.0) did not seem to have much effect on the isotherms. The compression−decompression cycles and stability studies of the hIAPP Langmuir monolayer showed that it was relatively stable and did not form aggregates or domains during the time of experiment. UV−vis absorption of hIAPP Langmuir monolayer on 1.0 M NaCl with pH 2.0 and 5.6 showed the linearity of absorbance of peptide bonds at 202 nm, confirming that no aggregate or domain was formed. p−Polarized IRRAS was employed to study the conformational and orientational changes of the hIAPP Langmuir monolayer on 1.0 M NaCl subphase with pH 2.0, 5.6 and 9.0. The spectra showed that the predominant secondary structures of the hIAPP Langmuir monolayer were α−helix conformation, independent with the pH of subphase and the induced surface pressure. It was also very likely that this ***α***−helical conformation was a relatively stable intermediate before the conversion to aggregates. The orientation of hIAPP Langmuir monolayer at air−aqueous interface was parallel to the air−aqueous interface during compression. No BAM image of domains of the hIAPP Langmuir monolayer was observed on 1.0 M NaCl subphase with pH 2.0, 5.6 or 9.0, further confirming its stability during the time of Langmuir monolayer experiment. However, on−going study did show that the process of aggregation of hIAPP could be promoted by human insulin.

Chapter 8 Interaction between Human Insulin and Human Islet Amyloid Polypeptide at the Air−Aqueous Interface

8.1 Background

Diabetes mellitus is a major disease in the modern society, for which there is no permanent cure. Unbalanced diets and the lack of physical exercises can lead to obesity, which in turn contributes to the onset of diabetes to a great extent.[217] In 2010, it was estimated that 285 million people suffered from diabetes compared with 30 million in 1985.[217] In the United States alone, people with diabetes constitute 8.3% of the whole population and 26.9% of the diabetes patients were 65 years or older. Diabetes is also a major cause of heart attack and stroke. Type 2 diabetes mellitus, also known as non−insulin−dependent diabetes mellitus (NIDDM), accounts for more than 90% of all diabetes cases. Patients of NIDDM typically have a high level of blood glucose associated with cellular insulin resistance, and a relatively low level of insulin. There is a tendency for the early onset of type 2 diabetes mellitus, and it has become increasingly common to find NIDDM patients under the age of 30.[218,219]

Human insulin and human islet amyloid polypeptide (hIAPP, also known as amylin) are two major hormones involved in diabetes, which are co−secreted by the endocrine pancreas. Human insulin is a protein hormone that regulates physiological glucose levels, enhancing glucose uptake in muscle while inhibiting hepatic glucose production.[280] Although insulin exists as an equilibrating mixture of several oligomeric forms in solutions, it is important to note that insulin is mainly biologically active as a monomer.[281] Human insulin monomer consists of the A chain with 21 amino acid residues and the B chain with 30 residues, with two disulfide bridges linking the two chains and one disulfide bridge joining two sections of A chain together. As a monomer, the majority of human insulin exists in α−helical structure. Human insulin is known to form β−sheet rich fibrils under certain condition *in vitro*, such as incubation at high concentrations, low pH, and high temperatures.[192]

hIAPP is a 37 amino−acid−residue peptide produced by pancreatic β−cells with a disulfide bridge and an amidated C−terminus. Although the physiological functions of hIAPP are not well understood, the monomeric hIAPP is believed to be involved in the glycemic down−regulation that slows down gastric emptying and prevents sudden spikes in blood glucose levels.[220,221] It is responsible for the satiation signal, and is hypothesized as one of the preventers of obesity.[222,223] Similar to Alzheimer−related amyloid beta peptides, this hormone is also highly amyloidogenic. It can easily misfold and aggregate into dense, insoluble β−sheet rich amyloid plaques. These deposits are found in the islets of Langerhans among around 95% type 2 diabetic patients.[39,40] A similar phenomenon is also observed in pancreatic cancer.[41] The association of hIAPP with type 2 diabetes has been further supported and verified by transgenic rats engineered to express hIAPP, which develop diabetes in a progressive pathology similar to human patients with type 2 diabetes.[282] The interaction of hIAPP with β−cell membrane is thought to play a crucial role in the dysfunction and death of β−cells.[224] Studies on both model membranes and cells show that the cytotoxicity originates from the growth of hIAPP fibrils or the toxic oligomers on the membrane surface.[225-227] However, increasing evidence shows that hIAPP oligomers formed during the early−stage aggregation are the most cytotoxic species, not the mature hIAPP amyloid fibrils.[227-230]

Similar to other amyloidogenic proteins (e.g. amyloid β−40 and α−synuclein), fibrillation of hIAPP is proposed to occur under various conditions via the aggregation of partially folded intermediates through a nucleation mechanism.[149,185] The kinetic process of fibril formation in experiments is commonly characterized as an apparent lag period followed by an exponential growth regime, and a final plateau regime. *In vitro*, hIAPP can aggregate into fibrils within a timescale of around 30 h at much lower concentrations (< 1 μM) than *in vivo* (0.8−4 mM).[245] This fibrillization process of hIAPP can be further accelerated to less than 100 min in the presence of negatively−charged phospholipid molecules.[236] However, hIAPP fibrils are rarely observed in healthy people, even if they have higher hIAPP production and secretion level than normal. Moreover, progression of the type 2 diabetes usually takes many years. The plausible conflict between the *in vivo* and *in vitro* observations suggests the existence of a natural mechanism to inhibit the fibril formation of hIAPP *in vivo*. Factors that might play an inhibitive role include components of the granule like insulin, pH, and zinc concentration.[237,240,243,245]

hIAPP and insulin are innately related, as both hormones possess common promoter sequences. They are synthesized by pro−peptides in an approximately 1:100 molar ratio (hIAPP: insulin) from secretory granules of pancreatic β−cells.[38] Therefore, a potential interaction exists between hIAPP and human insulin throughout the secretory pathway. Insulin has been suggested as a possible natural regulator for hIAPP fibrillization. The first observation of inhibition to hIAPP fibril formation was noted using Congo Red.[220] Later, hIAPP fibrillogenesis experiments *in vitro* showed that insulin was probably a potent inhibitor for the hIAPP fibrillization due to the heterocomplexes formed between insulin and hIAPP.[244,283,284] Nevertheless, several other investigations found that insulin could promote amyloid formation of hIAPP by enhancing the binding of hIAPP to preformed fibrils.[285] A recent study showed that insulin is a kinetic inhibitor for the aggregation of hIAPP, only keeping its inhibitive effect for a limited period of time.[246] After long time incubation, insulin was found to promote hIAPP aggregation on the hypothesis of copolymerization of insulin and hIAPP.[246] One recent study revealed that insulin has biphasic effects on the membrane disruption caused by hIAPP aggregation.[245] Insulin is effective for preventing fibril−dependent membrane disruption, but not effective in stopping the initial phase of membrane disruption before fibrillogenesis, and does not prevent the formation of small IAPP oligomers on the membrane.[245] Another recent morphology study using atomic force microscopy (AFM) showed that insulin and hIAPP formed co−assembled aggregates on negatively charged tantalum oxide (Ta_2O_5) surfaces. The two peptides could form co−assembly fibrils.[238] These results suggest the interaction between hIAPP and insulin is still poorly understood.[112]

Zinc is an important trace element required in almost every living system and plays an essential role in the functions and structures of many proteins and metalloenzymes.[286] Zinc is found to have a concentration as high as 11 mM in secretory granules of human pancreatic β−cells.[203] It has been known for many years that there exists a close relationship between insulin and zinc. The tendency for insulin to form self−assembly in solution is strongly enhanced in the presence of zinc ion, which is normally present in the secretory granules at millimolar concentrations.[287-289] Furthermore, zinc can bind to the histidine residue at position 18 of hIAPP and has been found to have a dual effect on the aggregation: lower concentration inhibits aggregation, while higher concentration has the opposite effect.[243] However, very limited information is available about the roles of zinc when both hIAPP and insulin are present.

Recent studies on hIAPP and phospholipid membrane model show that the electrostatic interaction between the positively charged hIAPP and negatively charged phospholipid accelerates the aggregation of hIAPP.[111,129,225,228,233-235] In the presence of such charged lipids, hIAPP fibril forms within a few minutes in *in vitro* studies, while a neutral phospholipid has no such effect.[111] Rather than using homogeneous model membrane systems, a recent study focuses on the principles of aggregation and amyloid formation of hIAPP by applying lipid raft membranes, suggesting that lipid raft model is also involved in the aggregation of hIAPP.[290] Lipid raft models, composed of phospholipids with rich cholesterol and sphingolipids, are more appropriate systems for mimicking the cellular membrane of pancreatic β−cells than homogeneous lipid model. Therefore, to further characterize the interaction and fibrillation process between hIAPP and insulin *in vivo*, it is necessary to investigate with the presence of lipid raft.

Investigation of amyloid aggregation process opens the gateway for new drug discovery. Hence, it is very important to scrutinize the physical process behind amyloid aggregation like human insulin and hIAPP. We hereby propose a new approach to systematically investigate the nature of interaction and fibril formation between hIAPP and insulin. Each step of the amyloid aggregation will be probed by selectively suitable techniques, including 2−D Langmuir technique, surface−selective spectroscopies, and microscopic imaging. Furthermore, various factors such as zinc concentrations, pH value and the effect of lipid raft, will be studied in detail for the understanding of interaction and co−assembly or fibril formation between hIAPP and insulin.

8.2 Experimental Design

We are proposing a new approach to understand the nature of hIAPP−insulin interactions using Langmuir technique in conjunction with surface chemistry, spectroscopic and microscopic studies as a 2−Dimension (2−D) method. Prof. Elsa Yan from Yale University has recently discovered that chiral sum frequency generation (SFG) spectroscopy is able to provide vibrational signatures of peptide backbones, which can distinguish protein secondary structures at the interfaces. Therefore, we expect to apply this new technique to investigate the interaction and early stage of fibrillation between hIAPP and human insulin. Factors possibly affecting the interaction and fibrillation between hIAPP and insulin will be systematically examined, such as different ratios of hIAPP: insulin, zinc concentrations, pH of solution and the effect of lipid raft. Compared with other methodologies, this approach has the following advantages. First, Langmuir technique is a good *in vitro* model for modeling *in vivo* conditions because it can mimic the common surface pressure environment of bio−membranes, bridging the gap between *in vitro* model studies and *in vivo* conditions. Surface pressures ranging between 30 and 35 mN/m are commonly found in the natural cellular membrane, and can be simulated on the Langmuir monolayer as a model for bio−membranes.[291] Therefore, Langmuir technique has been commonly and intensively used for the interaction study between peptides and lipid as a biomembrane model.[111,233,235,292-294] Second, compared with peptides in bulk aqueous solution, the structures and properties of peptides in Langmuir monolayer as a 2−D system could be quite different, as the degree of freedom of peptides in organized Langmuir monolayer is largely decreased. Third, spectroscopic methods can be used to directly monitor at the interface the interaction and fibrillation in real time without perturbation. Particularly, sum frequency generation (SFG) spectroscopy has advantages in its ability to be surface sensitive, which means it is only sensitive to molecules at the interface.[211,295-297] The fourth advantage of Langmuir monolayer lies in the possibility of controlling both the intramolecular structure and intermolecular ordering of hIAPP and insulin via controllable variables, such as the surface pressure, pH, monolayer composition (different components of lipid, various ratio between hIAPP and insulin), subphase composition (ionic concentrations, especially zinc), and temperature.[254]

8.3 Preliminary Results

Our recent research shows the stability of hIAPP Langmuir monolayer at air−water interface without detection of aggregates or domains formation at time zero. Due to the fact that hIAPP and insulin have intrinsic connections in secretory granules of pancreatic β−cells,[38] insulin has been suggested as a possible natural regulator of hIAPP fibrillization. However, some studies do show that hIAPP and insulin can also form co−assembly fibrils.[238] It is necessary to study the interaction between hIAPP and insulin. We have recently observed an important fibrillation process for the mixed hIAPP:insulin (1:1, molar ratio). The mixture was incubated at 37 ^{0}C at different time period intervals and their surface pressure−area isotherm was measured at these time intervals. At any surface pressure, the corresponding area per molecule diminishes with the time of incubation, as shown in Figure 8.1 (A). However, incubation of one protein alone (such as insulin, human serum albumin, bovine serum albumin and lysozyme) under 37 ^{0}C at different time period intervals does not result in diminished area per molecule of the corresponding protein (results not shown). Surprisingly, at chosen surface pressure, such as 12.5 mN/m, the mean area per hIAPP molecule is linearly decreasing with increasing incubation times, as shown in Figure 8.1 (B). This observation clearly indicates that there is an interaction between hIAPP and insulin to favor the fibrillation process. However, more work needs to be done to understand the nature of the interaction between human insulin and hIAPP.

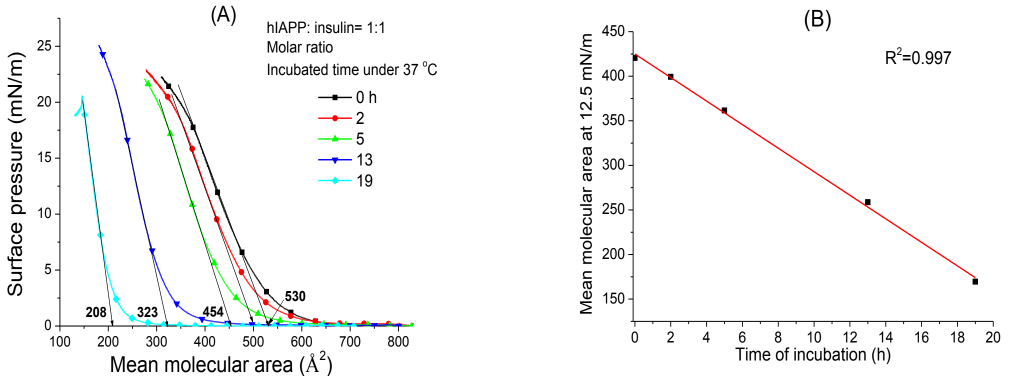

Figure 8.1 (A) Surface pressure−area isotherms of hIAPP:insulin (molar ratio=1:1) mixture; (B) the mean molecular area of mixture at surface pressure 12.5 mN/m vs. incubation time. It was incubated under 37 °C for different hours.

8.4 Future Plan

The future plans for this study will be focused on the following topics using 2−D surface chemistry methodologies combined with spectroscopic and microscopic measurements: (1) the nature of the interaction between hIAPP and human insulin; (2) characterization of the fibril formation between hIAPP and insulin; (3) understanding the factors contributing to the fibrillation, such as zinc concentration and pH value in solution; (4) the interaction and fibrillation between hIAPP and insulin in the presence of lipid raft model. Understanding these topics could facilitate the knowledge of the role of insulin and factors contributing to the fibrillation of hIAPP in type 2 diabetes.

Chapter 9 Conclusion

Part I: Interaction between Graphene Oxide and Biomolecules

Great progress has been recently achieved to apply a novel 2−dimensional nanomaterial graphene oxide (GO) in biomedical and biological field, including drug and gene delivery, biological sensing, and bio−imaging. Although it has shown potential applications in these studies, one critical question needs to be addressed before any actual application: How does GO interact with biological molecules, such as amino acids, peptides, and proteins? Particularly, GO has been explored for analyte detection and quantification from biological fluid sample. Due to the fact that these samples contain fairly high amount of positively charged lysozyme, it is therefore necessary to investigate the interaction between lysozyme and negatively charged GO. Another research challenge associated with GO is about how GO interacts with biomembrane components. Inconsistent results are obtained on the cytotoxicity of GO and how it enters membranes. Also, there is no study on how GO orientates itself when it interacts with the membrane. Therefore, it is fundamentally important to understand the interaction between GO and biomolecules, such as amino acids, peptides, proteins, and lipids. Such knowledge will provide further information for applications of GO in biological and biomedical field.

In this study, GO was found to interact with amino acids, peptides, and proteins by fluorescence quenching. Based on the Stern−Volmer plot and fluorescence lifetime study between Trp or Tyr and GO, the main quenching mechanism was determined as static quenching, slightly combined with dynamic quenching (Förster resonance energy transfer). Both electrostatic interaction and hydrophobic interaction contribute to the interactions between Trp or Tyr and GO. Due to the quenching effect on peptides and proteins, it is possible that GO could be a universal fluorescent quencher for tryptophan or tyrosine containing peptides and proteins.

Strong electrostatic interaction between GO and lysozyme is demonstrated and confirmed using fluorescence quenching, zeta potential, dynamic light scattering, and atomic force microscopy. This interaction is so strong that one is able to subsequently eliminate and separate lysozyme from aqueous solution using GO. The adsorbed lysozyme can be released from the surface of GO by adding NaOH and then precipitating GO with $CaCl_2$. More importantly, the strong electrostatic interaction also renders the selective adsorption of lysozyme on GO from a mixture of proteins, which was confirmed by fluorescence, UV−vis absorption, and sodium dodecyl sulfate polyacrylamide gel electrophoresis (SDS−PAGE).

As Pluronic F127 (PF127) was used to disperse GO and screen the interaction between GO and Trp or Tyr, it is necessary to study the behaviors between GO and PF127. Langmuir monolayer as a 2−D surface chemistry approach was applied to investigate the interaction at the air−water interface. Due to the hydrophobic poly propylene oxide (PPO) groups as anchors, PF127 Langmuir monolayer is very stable at the air−water interface. When PF127/GO mixture is deposited at the air−water interface, the PPO groups interact with the hydrophobic parts of GO surface, resulting in loss of the anchors at the air−water interface. Therefore, the Langmuir monolayer of PF127/GO is very unstable and tends to be dragged into the bulk subphase. Moreover, when PF127 is deposited at the interface of GO aqueous dispersion, the pancake conformation in the

Langmuir monolayer of PF127 facilitates the availability of hydrophobic interaction between PF127 and GO, which drags PF127 molecules to the bulk subphase solution.

To understand the nature and orientation of interaction between GO and lipid models, Langmuir monolayer technique was applied at the air−water/aqueous interface. Five lipids with the same 18−carbon alkyl chain but different head groups of charges are purposely chosen to rationalize the possible interactions. Experimental results show that the interaction between these lipids and GO is clearly governed by electrostatic interaction. When these lipids are spread at the air−GO dispersion interface, GO can incorporate or be adsorbed into the monolayer of positively charged lipids DODAB and DSEPC, increasing the mean molecular areas. However, the monolayers of neutrally charged head group (phosphocholine) or negatively charged head groups (phosphate and carboxyl) do not adsorb GO as there is no favoring electrostatic interaction. Due to the fact that phospholipids in biological systems are negatively or neutrally charged, the possible cellular uptake of GO into the membrane should not be due to the direct electrostatic interaction between GO and phospholipids but through the bioactivity of the membrane.

When GO is injected to the subphase underneath the positively charged monolayer of DODAB and DSEPC, different observations of surface pressure are found. GO can insert into the monolayer of DODAB at 20 mN/m increasing the surface pressure. However, GO cannot diffuse to incorporate with DSEPC monolayer even at much lower surface pressure probably due to the shielding from the ethylphospho groups. An orientation model of GO when it binds to DODAB and DSEPC monolayer is proposed to explain the different behaviors of adsorption of GO at the air–aqueous interface. An “edge–in” orientation instead of “face–in” is proposed to describe the orientation of GO nanosheets when it inserts into the monolayer of DODAB.

Part II. Protein Fibrillation at the Interface and Interaction between Human Insulin and Human Islet Amyloid Polypeptide

It has been known for several decades that failure to adopt or remain native conformations of some peptides or proteins can result in a wide range of human diseases. The pathological conditions of these diseases are now known to be commonly associated with protein misfolding processes. In this part, the recent progress of insulin aggregation was briefly summarized at the aqueous–solid, water–oil, and air–water interfaces. The aggregation of insulin initiates with diffusion and adsorption of insulin at the hydrophobic solid or oil interfaces, resulting in conformational change of the monomeric insulin to expose the hydrophobic residues. The driving force is mainly hydrophobic interaction between the unfolded monomer and the hydrophobic interface. Subsequently, the dissolved insulin molecules associate over the exposed hydrophobic regions, eventually forming aggregates. Compared to hydrophobic solid or oil surfaces, the hydrophilic surface induces less conformational change of insulin. As a result, a much longer lag time of insulin fibrillation has been observed at the hydrophilic interfaces.

The conformation and self–assembly of the hIAPP (human islet amyloid polypeptide) at time zero were studied at the air–aqueous interface using the Langmuir monolayer technique. The limiting molecular area of hIAPP on 1.0 M NaCl subphase was found to be around 445 Å^2/molecule. The pH of the subphase solution (2.0, 5.6 and 9.0) did not seem to affect much on the isotherms and IRRAS spectra. The compression–decompression cycles, stability studies, and IRRAS spectra of the hIAPP Langmuir monolayer showed that it was relatively stable and did not form aggregates or domains during the period of experiment.

hIAPP and insulin are innately related, as both hormones possess common promoter sequences and are co−synthesized in an approximately 1:100 molar ratio (hIAPP:insulin) from secretory granules of pancreatic β−cells. It is necessary to study the interaction between hIAPP and insulin. We have recently observed an important fibrillation process for the mixed hIAPP:insulin (1:1, molar ratio). The mixture was incubated at 37 ^{o}C at different time period intervals and their surface pressure−area isotherm was measured at these time intervals. At any surface pressure, the corresponding area per molecule diminishes with the time of incubation. However, incubation of insulin alone under 37 ^{0}C at different time period intervals does not result in diminished area per molecule of insulin. Surprisingly, at chosen surface pressure, such as 12.5 mN/m, the mean area per hIAPP molecule is linearly decreasing with increasing incubation times. This observation clearly indicates that there is an interaction between hIAPP and insulin to favor the fibrillation process. However, various factors need to be examined in the future to understand the interaction between human insulin and hIAPP, such as the molar ratios, zinc concentrations, pH value and the presence of lipid raft.

References

(1) Dreyer, D. R.; Park, S.; Bielawski, C. W.; Ruoff, R. S. *Chem. Soc. Rev.* **2010**, *39*, 228.

(2) Geim, A. K.; Novoselov, K. S. *Nat. Mater.* **2007**, *6*, 183.

(3) Novoselov, K. S.; Geim, A. K.; Morozov, S. V.; Jiang, D.; Zhang, Y.; Dubonos, S. V.; Grigorieva, I. V.; Firsov, A. A. *Science* **2004**, *306*, 666.

(4) Morales-Narváez, E.; Merkoçi, A. *Adv. Mater.* **2012**, *24*, 3298.

(5) Yang, X.; Wang, Y.; Huang, X.; Ma, Y.; Huang, Y.; Yang, R.; Duan, H.; Chen, Y. *J. Mater. Chem.* **2011**, *21*, 3448.

(6) Nguyen, P.; Berry, V. *J. Phys. Chem. Lett.* **2012**, *3*, 1024.

(7) Liu, Z.; Robinson, J. T.; Sun, X.; Dai, H. *J. Am. Chem. Soc.* **2008**, *130*, 10876.

(8) Rana, V. K.; Choi, M.-C.; Kong, J.-Y.; Kim, G. Y.; Kim, M. J.; Kim, S.-H.; Mishra, S.; Singh, R. P.; Ha, C.-S. *Macromol. Mater. Eng.* **2011**, *296*, 131.

(9) Zhang, L. L.; Zhao, S.; Tian, X. N.; Zhao, X. S. *Langmuir* **2010**, *26*, 17624.

(10) Pan, Y.; Bao, H.; Sahoo, N. G.; Wu, T.; Li, L. *Adv. Funct. Mater.* **2011**, *21*, 2754.

(11) Kim, H.; Namgung, R.; Singha, K.; Oh, I.-K.; Kim, W. J. *Bioconjugate Chem.* **2011**, *22*, 2558.

(12) Lu, C.-H.; Yang, H.-H.; Zhu, C.-L.; Chen, X.; Chen, G.-N. *Angew. Chem. Int. Ed.* **2009**, *48*, 4785.

(13) Tian, B.; Wang, C.; Zhang, S.; Feng, L.; Liu, Z. *ACS Nano* **2011**, *5*, 7000.

(14) Robinson, J. T.; Tabakman, S. M.; Liang, Y.; Wang, H.; Sanchez Casalongue, H.; Vinh, D.; Dai, H. *J. Am. Chem. Soc.* **2011**, *133*, 6825.

(15) Liu, J.; Liu, Y.; Gao, M.; Zhang, X. *J. Am. Soc. Mass Spectrom.* **2012**, *23*, 1424.

(16) Sha, Y.; Huang, D.; Zheng, S.; Deng, C. *Anal. Methods* **2013**, *5*, 4585.

(17) Mannoor, M. S.; Tao, H.; Clayton, J. D.; Sengupta, A.; Kaplan, D. L.; Naik, R. R.; Verma, N.; Omenetto, F. G.; McAlpine, M. C. *Nat. Commun.* **2012**, *3*, 763.

(18) Braun, O.; Sandkühler, H. *J. Pediatr. Gastroenterol. Nutr.* **1985**, *4*, 583.

(19) Yeh, C.-K.; Dodds, M. W. J.; Zuo, P.; Johnson, D. A. *Arch. Oral Biol.* **1997**, *42*, 25.

(20) Li, S.; Mulloor, J. J.; Wang, L.; Ji, Y.; Mulloor, C. J.; Micic, M.; Orbulescu, J.; Leblanc, R. M. *ACS Appl. Mater. Interfaces.* **2014**, *6*, 5704.

(21) Hong, B. J.; Compton, O. C.; An, Z.; Eryazici, I.; Nguyen, S. T. *ACS Nano* **2012**, *6*, 63.

(22) Sun, X.; Liu, Z.; Welsher, K.; Robinson, J.; Goodwin, A.; Zaric, S.; Dai, H. *Nano Res.* **2008**, *1*, 203.

(23) Mu, Q.; Su, G.; Li, L.; Gilbertson, B. O.; Yu, L. H.; Zhang, Q.; Sun, Y.-P.; Yan, B. *ACS Appl. Mater. Interfaces.* **2012**, *4*, 2259.

(24) Peng, C.; Hu, W.; Zhou, Y.; Fan, C.; Huang, Q. *Small* **2010**, *6*, 1686.

(25) Chang, Y.; Yang, S.-T.; Liu, J.-H.; Dong, E.; Wang, Y.; Cao, A.; Liu, Y.; Wang, H. *Toxicol. Lett.* **2011**, *200*, 201.

(26) Liao, K.-H.; Lin, Y.-S.; Macosko, C. W.; Haynes, C. L. *ACS Appl. Mater. Interfaces.* **2011**, *3*, 2607.

(27) Gregersen, N.; Bross, P.; Vang, S.; Christensen, J. H. *Annu. Rev. Genomics Hum. Genet.* **2006**, *7*, 103.

(28) Chiti, F.; Dobson, C. M. *Annu. Rev. Biochem.* **2006**, *75*, 333.

(29) Eisenberg, D.; Jucker, M. *Cell* **2012**, *148*, 1188.

(30) Sunde, M.; Serpell, L. C.; Bartlam, M.; Fraser, P. E.; Pepys, M. B.; Blake, C. C. F. *J. Mol. Biol.* **1997**, *273*, 729.

(31) Moilanen, D. E.; Fenn, E. E.; Wong, D.; Fayer, M. D. *J. Phys. Chem. B* **2009**, *113*, 8560.

(32) McFearin, C. L.; Beaman, D. K.; Moore, F. G.; Richmond, G. L. *J. Phys. Chem. C* **2008**, *113*, 1171.

(33) Hill, J. B. *Endocrinology* **1959**, *65*, 515.

(34) Renard, E. *Curr. Opin. Pharmacol.* **2002**, *2*, 708.

(35) Harris, M. D.; Davidson, M. B.; Rosenberg, C. S. *Diabetes Care* **1986**, *9*, 356.

(36) Weisenfeld, S.; Podolsky, S.; Goldsmith, L.; Ziff, L. *Diabetes* **1968**, *17*, 766.

(37) Li, S.; Leblanc, R. M. *J. Phys. Chem. B* **2014**, *118*, 1181.

(38) Gedulin, B.; Cooper, G. J. S.; Young, A. A. *Biochem. Biophys. Res. Commun.* **1991**, *180*, 782.

(39) Westermark, P.; Wernstedt, C.; Wilander, E.; Hayden, D. W.; O'Brien, T. D.; Johnson, K. H. *Proc. Natl. Acad. Sci. U.S.A.* **1987**, *84*, 3881.

(40) Hull, R. L.; Westermark, G. T.; Westermark, P.; Kahn, S. E. *J. Clin. Endocrinol. Metab.* **2004**, *89*, 3629.

(41) Permert, J.; Larsson, J.; Westermark, G. T.; Herrington, M. K.; Christmanson, L.; Pour, P. M.; Westermark, P.; Adrian, T. E. *N. Engl. J. Med.* **1994**, *330*, 313.

(42) DeToma, A. S.; Salamekh, S.; Ramamoorthy, A.; Lim, M. H. *Chem. Soc. Rev.* **2012**, *41*, 608.

(43) Wang, Y.; Li, Z.; Hu, D.; Lin, C.-T.; Li, J.; Lin, Y. *J. Am. Chem. Soc.* **2010**, *132*, 9274.

(44) Zhang, M.; Yin, B.-C.; Wang, X.-F.; Ye, B.-C. *Chem. Commun.* **2011**, *47*, 2399.

(45) Wang, H.; Zhang, Q.; Chu, X.; Chen, T.; Ge, J.; Yu, R. *Angew. Chem. Int. Ed.* **2011**, *50*, 7065.

(46) Feng, D.; Zhang, Y.; Feng, T.; Shi, W.; Li, X.; Ma, H. *Chem. Commun.* **2011**, *47*, 10680.

(47) Li, D.; Muller, M. B.; Gilje, S.; Kaner, R. B.; Wallace, G. G. *Nat. Nano.* **2008**, *3*, 101.

(48) Dong, H.; Gao, W.; Yan, F.; Ji, H.; Ju, H. *Anal. Chem.* **2010**, *82*, 5511.

(49) Balapanuru, J.; Yang, J.; Xiao, S.; Bao, Q.; Jahan, M.; Polavarapu, L.; Wei, J.; Xu, Q.; Loh, K. P. *Angew. Chem. Int. Ed.* **2010**, *49*, 6549.

(50) Liu, Y.; Liu, C.; Liu, Y. *Appl. Surf. Sci.* **2011**, *257*, 5513.

(51) Kim, J.; Cote, L. J.; Kim, F.; Huang, J. *J. Am. Chem. Soc.* **2009**, *132*, 260.

(52) Wu, M.; Kempaiah, R.; Huang, P.-J. J.; Maheshwari, V.; Liu, J. *Langmuir* **2011**, *27*, 2731.

(53) Yoo, S. I.; Yang, M.; Brender, J. R.; Subramanian, V.; Sun, K.; Joo, N. E.; Jeong, S.-H.; Ramamoorthy, A.; Kotov, N. A. *Angew. Chem. Int. Ed.* **2011**, *50*, 5110.

(54) Sheng, L.; Ren, J.; Miao, Y.; Wang, J.; Wang, E. *Biosens. Bioelectron.* **2011**, *26*, 3494.

(55) Morales-Narváez, E.; Pérez-López, B.; Pires, L. B.; Merkoçi, A. *Carbon* **2012**, *50*, 2987.

(56) van de Weert, M.; Stella, L. *J. Mol. Struct.* **2011**, *998*, 144.

(57) Lakowicz, J. R. *Principles of Fluorescence Spectroscopy*; 2nd ed.; Kluwer Academic/Plenum Publishers: New York, 1999.

(58) Rajesh, C.; Majumder, C.; Mizuseki, H.; Kawazoe, Y. *J. Chem. Phys.* **2009**, *130*, 124911.

(59) Lerf, A.; He, H.; Forster, M.; Klinowski, J. *J. Phys. Chem. B* **1998**, *102*, 4477.

(60) Cai, W.; Piner, R. D.; Stadermann, F. J.; Park, S.; Shaibat, M. A.; Ishii, Y.; Yang, D.; Velamakanni, A.; An, S. J.; Stoller, M.; An, J.; Chen, D.; Ruoff, R. S. *Science* **2008**, *321*, 1815.

(61) Ahmad, A.; Kurkina, T.; Kern, K.; Balasubramanian, K. *ChemPhysChem* **2009**, *10*, 2251.

(62) Seo, J.-W. T.; Green, A. A.; Antaris, A. L.; Hersam, M. C. *J. Phys. Chem. Lett.* **2011**, *2*, 1004.

(63) He, X. M.; Carter, D. C. *Nature* **1992**, *358*, 209.

(64) Gelamo, E. L.; Tabak, M. *Spectrochim. Acta Mol. Biomol. Spectros.* **2000**, *56*, 2255.

(65) Wang, Y.; Li, Z.; Wang, J.; Li, J.; Lin, Y. *Trends Biotechnol.* **2011**, *29*, 205.

(66) Chung, C.; Kim, Y.-K.; Shin, D.; Ryoo, S.-R.; Hong, B. H.; Min, D.-H. *Acc. Chem. Res.* **2013**, *46*, 2211.

(67) Zhu, Y.; Murali, S.; Cai, W.; Li, X.; Suk, J. W.; Potts, J. R.; Ruoff, R. S. *Adv. Mater.* **2010**, *22*, 3906.

(68) Kasry, A.; Afzali, A. A.; Oida, S.; Han, S.-J.; Menges, B.; Tulevski, G. S. *Chem. Mater.* **2011**, *23*, 4879.

(69) Sharma, P.; Tuteja, S. K.; Bhalla, V.; Shekhawat, G.; Dravid, V. P.; Suri, C. R. *Biosens. Bioelectron.* **2013**, *39*, 99.

(70) Othman, A. M.; Li, S.; Leblanc, R. M. *Anal. Chim. Acta.* **2013**, *787*, 226.

(71) Wang, Y.; Zhen, S. J.; Zhang, Y.; Li, Y. F.; Huang, C. Z. *J. Phys. Chem. C* **2011**, *115*, 12815.

(72) Murugan, V.; Yeong-Tai, S.; Hyunkyung, S.; Kyusik, Y.; Min-Ho, L. *Int. J. Nanomedicine* **2012**, *7*, 6123.

(73) Aine, E.; Mörsky, P. *Acta Ophthalmol.* **1984**, *62*, 932.

(74) Venge, P.; Foucard, T.; Henriksen, J.; Håkansson, L.; Kreuger, A. *Clin. Chim. Acta.* **1984**, *136*, 121.

(75) Houser, M. T. *Clin. Chem.* **1983**, *29*, 1488.

(76) Prockop, D. J.; Davidson, W. D. *N. Engl. J. Med.* **1964**, *270*, 269.

(77) Osserman, E. F.; Lawlor, D. P. *J. Exp. Med.* **1966**, *124*, 921.

(78) Perillie, P. E.; Kaplan, S. S.; Lefkowitz, E.; Rogaway, W.; Finch, S. C. *J. Am. Med. Assoc.* **1968**, *203*, 317.

(79) Zhang, D.; Zhang, Y.; Zheng, L.; Zhan, Y.; He, L. *Biosens. Bioelectron.* **2013**, *42*, 112.

(80) Yan, L.; Wang, Y.; Xu, X.; Zeng, C.; Hou, J.; Lin, M.; Xu, J.; Sun, F.; Huang, X.; Dai, L.; Lu, F.; Liu, Y. *Chem. Res. Toxicol.* **2012**, *25*, 1265.

(81) Zhang, J.; Zhang, F.; Yang, H.; Huang, X.; Liu, H.; Zhang, J.; Guo, S. *Langmuir* **2010**, *26*, 6083.

(82) Zhang, Y.; Zhang, J.; Huang, X.; Zhou, X.; Wu, H.; Guo, S. *Small* **2012**, *8*, 154.

(83) Zhou, L.; Jiang, Y.; Gao, J.; Zhao, X.; Ma, L. *Appl Biochem Biotechnol* **2012**, *168*, 1635.

(84) Li, S.; Aphale, A. N.; Macwan, I. G.; Patra, P. K.; Gonzalez, W. G.; Miksovska, J.; Leblanc, R. M. *ACS Appl. Mater. Interfaces.* **2012**, *4*, 7069.

(85) Li, S.; Stein, A. J.; Kruger, A.; Leblanc, R. M. *J. Phys. Chem. C* **2013**, *117*, 16150.

(86) Wetter, L. R.; Deutsch, H. F. *J. Biol. Chem.* **1951**, *192*, 237.

(87) Shih, C.-J.; Lin, S.; Sharma, R.; Strano, M. S.; Blankschtein, D. *Langmuir* **2011**, *28*, 235.

(88) Hasan, S. A.; Rigueur, J. L.; Harl, R. R.; Krejci, A. J.; Gonzalo-Juan, I.; Rogers, B. R.; Dickerson, J. H. *ACS Nano* **2010**, *4*, 7367.

(89) Jans, H.; Liu, X.; Austin, L.; Maes, G.; Huo, Q. *Anal. Chem.* **2009**, *81*, 9425.

(90) Saterlie, M. S.; Sahin, H.; Kavlicoglu, B.; Liu, Y.; Graeve, O. A. *Chem. Mater.* **2012**, *24*, 3299.

(91) Chowdhury, I.; Duch, M. C.; Mansukhani, N. D.; Hersam, M. C.; Bouchard, D. *Environ. Sci. Technol.* **2013**, *47*, 6288.

(92) Cedervall, T.; Lynch, I.; Lindman, S.; Berggård, T.; Thulin, E.; Nilsson, H.; Dawson, K. A.; Linse, S. *Proc. Natl. Acad. Sci. U.S.A.* **2007**, *104*, 2050.

(93) Hamada, K.; Kaneko, T.; Chen, M. Q.; Akashi, M. *Chem. Mater.* **2007**, *19*, 1044.

(94) Stroh, C. M.; Ebner, A.; Geretschläger, M.; Freudenthaler, G.; Kienberger, F.; Kamruzzahan, A. S. M.; Smith-Gill, S. J.; Gruber, H. J.; Hinterdorfer, P. *Biophys. J.* **2004**, *87*, 1981.

(95) Kim, D. T.; Blanch, H. W.; Radke, C. J. *Langmuir* **2002**, *18*, 5841.

(96) Nicolas, J.; Mura, S.; Brambilla, D.; Mackiewicz, N.; Couvreur, P. *Chem. Soc. Rev.* **2013**, 1147.

(97) Ulery, B. D.; Nair, L. S.; Laurencin, C. T. *J. Polym. Sci., Part B: Polym. Phys.* **2011**, *49*, 832.

(98) Fox, M. E.; Szoka, F. C.; Fréchet, J. M. J. *Acc. Chem. Res.* **2009**, *42*, 1141.

(99) Romão, R. I. S.; Ferreira, Q.; Morgado, J.; Martinho, J. M. G.; Gonçalves da Silva, A. l. M. P. S. *Langmuir* **2010**, *26*, 17165.

(100) James, J.; Mandal, A. B. *Colloids Surf. B* **2011**, *84*, 172.

(101) Phani Kumar, B. V. N.; Umayal Priyadharsini, S.; Prameela, G. K. S.; Mandal, A. B. *J. Colloid. Interf. Sci.* **2011**, *360*, 154.

(102) James, J.; Mandal, A. B. *J. Colloid. Interf. Sci.* **2011**, *360*, 600.

(103) James, J.; Ramalechume, C.; Mandal, A. B. *Colloids Surf. B* **2011**, *82*, 345.

(104) Leiva, A.; Farias, A.; Gargallo, L.; Radic´, D. *Eur. Polym. J.* **2008**, *44*, 2589.

(105) Frey, S. L.; Lee, K. Y. C. *Langmuir* **2007**, *23*, 2631.

(106) Wu, G.; Lee, K. Y. C. *Langmuir* **2009**, *25*, 2133.

(107) Maskarinec, S. A.; Hannig, J.; Lee, R. C.; Lee, K. Y. C. *Biophys. J.* **2002**, *82*, 1453.

(108) Zhang, Y.; Nayak, T. R.; Hong, H.; Cai, W. *Nanoscale* **2012**, *4*, 3833.

(109) Hu, H.; Yu, J.; Li, Y.; Zhao, J.; Dong, H. *J. Biomed. Mater. Res. A.* **2012**, *100A*, 141.

(110) Fernández-Merino, M. J.; Paredes, J. I.; Villar-Rodil, S.; Guardia, L.; Solís-Fernández, P.; Salinas-Torres, D.; Cazorla-Amorós, D.; Morallón, E.; Martínez-Alonso, A.; Tascón, J. M. D. *Carbon* **2012**, *50*, 3184.

(111) Engel, M. F. M.; Yigittop, H.; Elgersma, R. C.; Rijkers, D. T. S.; Liskamp, R. M. J.; de Kruijff, B.; Höppener, J. W. M.; Killian, J. A. *J. Mol. Biol.* **2006**, *356*, 783.

(112) Li, S.; Micic, M.; Orbulescu, J.; Whyte, J. D.; Leblanc, R. M. *J. R. Soc. Interface* **2012**.

(113) Imperiali, L.; Liao, K.-H.; Clasen, C.; Fransaer, J.; Macosko, C. W.; Vermant, J. *Langmuir* **2012**, *28*, 7990.

(114) Cote, L. J.; Kim, F.; Huang, J. *J. Am. Chem. Soc.* **2009**, *131*, 1043.

(115) Bohorquez, M.; Koch, C.; Trygstad, T.; Pandit, N. *J. Colloid. Interf. Sci.* **1999**, *216*, 34.

(116) McNamee, C. E.; Graf, K.; Butt, H.-J.; Higashitani, K.; Kappl, M. *Colloids Surf. A* **2011**, *383*, 32.

(117) Blomqvist, B. R.; Wärnheim, T.; Claesson, P. M. *Langmuir* **2005**, *21*, 6373.

(118) Juárez, J.; Goy-López, S.; Cambón, A.; Valdez, M. A.; Taboada, P.; Mosquera, V. c. *J. Phys. Chem. C* **2010**, *114*, 15703.

(119) Joncheray, T. J.; Bernard, S. A.; Matmour, R.; Lepoittevin, B.; El-Khouri, R. J.; Taton, D.; Gnanou, Y.; Duran, R. S. *Langmuir* **2007**, *23*, 2531.

(120) Haefele, T.; Kita-Tokarczyk, K.; Meier, W. *Langmuir* **2005**, *22*, 1164.

(121) Lin, Y.; Alexandridis, P. *J. Phys. Chem. B* **2002**, *106*, 10834.

(122) Granite, M.; Radulescu, A.; Cohen, Y. *Langmuir* **2012**, *28*, 11025.

(123) Xin, X.; Xu, G.; Zhao, T.; Zhu, Y.; Shi, X.; Gong, H.; Zhang, Z. *J. Phys. Chem. C* **2008**, *112*, 16377.

(124) Zu, S.-Z.; Han, B.-H. *J. Phys. Chem. C* **2009**, *113*, 13651.

(125) Spector, A. A.; Yorek, M. A. *J. Lipid Res.* **1985**, *26*, 1015.

(126) Frost, R.; Jönsson, G. E.; Chakarov, D.; Svedhem, S.; Kasemo, B. *Nano Lett.* **2012**, *12*, 3356.

(127) Wang, Z.-M.; Wang, W.; Coombs, N.; Soheilnia, N.; Ozin, G. A. *ACS Nano* **2010**, *4*, 7437.

(128) Gao, Y.; Yip, H.-L.; Chen, K.-S.; O'Malley, K. M.; Acton, O.; Sun, Y.; Ting, G.; Chen, H.; Jen, A. K. Y. *Adv. Mater.* **2011**, *23*, 1903.

(129) Evers, F.; Jeworrek, C.; Tiemeyer, S.; Weise, K.; Sellin, D.; Paulus, M.; Struth, B.; Tolan, M.; Winter, R. *J. Am. Chem. Soc.* **2009**, *131*, 9516.

(130) Theumer, M. G.; Clop, P. D.; Rubinstein, H. R.; Perillo, M. A. *J. Phys. Chem. B* **2012**, *116*, 14216.

(131) Si, Y.; Samulski, E. T. *Nano Lett.* **2008**, *8*, 1679.

(132) Constantine, C. A. E., B. J.; Leblanc R. M. *Encyclopedia of Surface And Colloid Science*; Taylor & Francis Group, 2006.

(133) Engelking, J.; Menzel, H. *Eur. Phys. J. E* **2001**, *5*, 87.

(134) Bao, Y.-Y.; Bi, L.-H.; Wu, L.-X.; Mal, S. S.; Kortz, U. *Langmuir* **2009**, *25*, 13000.

(135) MacDonald, R. C.; Gorbonos, A.; Momsen, M. M.; Brockman, H. L. *Langmuir* **2006**, *22*, 2770.

(136) Zhang, H.; Peng, C.; Yang, J.; Lv, M.; Liu, R.; He, D.; Fan, C.; Huang, Q. *ACS Appl. Mater. Interfaces.* **2013**, *5*, 1761.

(137) Li, S.; Guo, J.; Patel, R. A.; Dadlani, A. L.; Leblanc, R. M. *Langmuir* **2013**, *29*, 5742.

(138) Gosvami, N. N.; Parsons, E.; Marcovich, C.; Berkowitz, M. L.; Hoogenboom, B. W.; Perkin, S. *RSC Adv.* **2012**, *2*, 4181.

(139) Nelson, R.; Eisenberg, D. *Curr. Opin. Struct. Biol.* **2006**, *16*, 260.

(140) Ahmad, A.; Uversky, V. N.; Hong, D.; Fink, A. L. *J. Biol. Chem.* **2005**, *280*, 42669.

(141) Orci, L.; Ravazzola, M.; Amherdt, M.; Madsen, O.; Vassalli, J.-D.; Perrelet, A. *Cell* **1985**, *42*, 671.

(142) Jørgensen, A. M. M.; Olsen, H. B.; Balschmidt, P.; Led, J. J. *J. Mol. Biol.* **1996**, *257*, 684.

(143) Smith, G. D.; Pangborn, W. A.; Blessing, R. H. *Acta Crystallogr., Sect. D: Biol. Crystallogr.* **2005**, *61*, 1476.

(144) Vinther, T. N.; Norrman, M.; Strauss, H. M.; Huus, K.; Schlein, M.; Pedersen, T. A.; Kjeldsen, T.; Jensen, K. J.; Hubálek, F. *PLoS ONE* **2012**, *7*, e30882.

(145) Blundell, T.; Dodson, G.; Hodgkin, D.; Mercola, D. In *Adv. Protein Chem.*; C.B. Anfinsen, J. T. E., Frederic, M. R., Eds.; Academic Press: 1972; Vol. 26, p 279.

(146) Baker, E. N.; Blundell, T. L.; Cutfield, J. F.; Cutfield, S. M.; Dodson, E. J.; Dodson, G. G.; Hodgkin, D. M. C.; Hubbard, R. E.; Isaacs, N. W.; Reynolds, C. D.; Sakabe, K.; Sakabe, N.; Vijayan, N. M. *Philos. Trans. R. Soc. London, B* **1988**, *319*, 369.

(147) Sharp, J. S.; Forrest, J. A.; Jones, R. A. L. *Biochemistry* **2002**, *41*, 15810.

(148) Nielsen, L.; Khurana, R.; Coats, A.; Frokjaer, S.; Brange, J.; Vyas, S.; Uversky, V. N.; Fink, A. L. *Biochemistry* **2001**, *40*, 6036.

(149) Kelly, J. W. *Curr. Opin. Struct. Biol.* **1998**, *8*, 101.

(150) Pasternack, R. F.; Gibbs, E. J.; Sibley, S.; Woodard, L.; Hutchinson, P.; Genereux, J.; Kristian, K. *Biophys. J.* **2006**, *90*, 1033.

(151) Dische, F. E.; Wernstedt, C.; Westermark, G. T.; Westermark, P.; Pepys, M. B.; Rennie, J. A.; Gilbey, S. G.; Watkins, P. J. *Diabetologia* **1988**, *31*, 158.

(152) Fineberg, S. E.; Kawabata, T. T.; Finco-Kent, D.; Fountaine, R. J.; Finch, G. L.; Krasner, A. S. *Endocr. Rev.* **2007**, *28*, 625.

(153) Chan, V.; Graves, D. J.; Fortina, P.; McKenzie, S. E. *Langmuir* **1997**, *13*, 320.

(154) Jena, K. C.; Hore, D. K. *Phys. Chem. Chem. Phys.* **2010**, *12*, 14383.

(155) Jørgensen, L.; Vermehren, C.; Bjerregaard, S.; Froekjaer, S. *Int. J. Pharm.* **2003**, *254*, 7.

(156) Kwon, Y.; Baudys, M.; Knutson, K.; Kim, S. *Pharm Res* **2001**, *18*, 1754.

(157) McConnell, H. M.; Vrljic, M. *Annu. Rev. Biophys. Biomol. Struct.* **2003**, *32*, 469.

(158) Donsmark, J.; Jorgensen, L.; Mollmann, S.; Frokjaer, S.; Rischel, C. *Pharm Res* **2006**, *23*, 148.

(159) Baldursdottir, S. G.; Fullerton, M. S.; Nielsen, S. H.; Jorgensen, L. *Colloids Surf. B* **2010**, *79*, 41.

(160) Wang, C.; Zheng, J.; Zhao, L.; Rastogi, V. K.; Shah, S. S.; DeFrank, J. J.; Leblanc, R. M. *J. Phys. Chem. B* **2008**, *112*, 5250.

(161) Sankaranarayanan, K.; Dhathathreyan, A.; Krägel, J.; Miller, R. *J. Phys. Chem. B*, 895.

(162) Yano, Y. F.; Uruga, T.; Tanida, H.; Toyokawa, H.; Terada, Y.; Takagaki, M.; Yamada, H. *Langmuir* **2008**, *25*, 32.

(163) Roach, P.; Farrar, D.; Perry, C. C. *J. Am. Chem. Soc.* **2005**, *127*, 8168.

(164) Pandey, L. M.; Le Denmat, S.; Delabouglise, D.; Bruckert, F.; Pattanayek, S. K.; Weidenhaupt, M. *Colloids Surf. B* **2012**, *100*, 69.

(165) Constantine, C. A.; Mello, S. V.; Dupont, A.; Cao, X.; Santos, D.; Oliveira, O. N.; Strixino, F. T.; Pereira, E. C.; Cheng, T.-C.; De Frank, J. J.; Leblanc, R. M. *J. Am. Chem. Soc.* **2003**, *125*, 1805.

(166) Steiner, G.; Tunc, S.; Maitz, M.; Salzer, R. *Anal. Chem.* **2007**, *79*, 1311.

(167) Giamblanco, N.; Martines, E.; Marletta, G. *Langmuir* **2013**, *29*, 8335.

(168) Sigal, G. B.; Mrksich, M.; Whitesides, G. M. *J. Am. Chem. Soc.* **1998**, *120*, 3464.

(169) Nayak, A.; Dutta, A. K.; Belfort, G. *Biochem. Biophys. Res. Commun.* **2008**, *369*, 303.

(170) Smith, M. I.; Sharp, J. S.; Roberts, C. J. *Biophys. J.* **2007**, *93*, 2143.

(171) Nault, L.; Guo, P.; Jain, B.; Bréchet, Y.; Bruckert, F.; Weidenhaupt, M. *Acta Biomater.* **2013**, *9*, 5070.

(172) Malik, R.; Roy, I. *Int. J. Pharm.* **2011**, *413*, 73.

(173) Thurow, H.; Geisen, K. *Diabetologia* **1984**, *27*, 212.

(174) Sluzky, V.; Tamada, J. A.; Klibanov, A. M.; Langer, R. *Proc. Natl. Acad. Sci. U.S.A.* **1991**, *88*, 9377.

(175) Nieto-Suárez, M.; Vila-Romeu, N.; Dynarowicz-Łątka, P. *Colloids Surf. A* **2008**, *321*, 189.

(176) Shigenobu, H.; McNamee, C. E. *J. Colloid. Interf. Sci.* **2012**, *388*, 274.

(177) Pérez-López, S.; Blanco-Vila, N. M.; Vila-Romeu, N. *J. Phys. Chem. B* **2011**, *115*, 9387.

(178) Liu, W.; Johnson, S.; Micic, M.; Orbulescu, J.; Whyte, J.; Garcia, A. R.; Leblanc, R. M. *Langmuir* **2012**, *28*, 3369.

(179) Johnson, S.; Liu, W.; Thakur, G.; Dadlani, A.; Patel, R.; Orbulescu, J.; Whyte, J. D.; Micic, M.; Leblanc, R. M. *J. Phys. Chem. B* **2012**, *116*, 10205.

(180) Balashev, K.; Ivanova, T.; Mircheva, K.; Panaiotov, I. *J. Colloid. Interf. Sci.* **2011**, *360*, 654.

(181) Nieto-Suárez, M.; Vila-Romeu, N.; Prieto, I. *Thin Solid Films* **2008**, *516*, 8873.

(182) Grodsky, G. M.; Forsham, P. H. *Annu. Rev. Physiol.* **1966**, *28*, 347.

(183) Nielsen, L.; Frokjaer, S.; Brange, J.; Uversky, V. N.; Fink, A. L. *Biochemistry* **2001**, *40*, 8397.

(184) Brange, J.; Dodson, G. G.; Edwards, D. J.; Holden, P. H.; Whittingham, J. L. *Proteins: Struct., Funct., Bioinf.* **1997**, *27*, 507.

(185) Hua, Q.; Weiss, M. A. *J. Biol. Chem.* **2004**, *279*, 21449.

(186) Sluzky, V.; Klibanov, A. M.; Langer, R. *Biotechnol. Bioeng.* **1992**, *40*, 895.

(187) Khurana, R.; Uversky, V. N.; Nielsen, L.; Fink, A. L. *J. Biol. Chem.* **2001**, *276*, 22715.

(188) Vestergaard, B.; Groenning, M.; Roessle, M.; Kastrup, J. S.; de Weert, M. v.; Flink, J. M.; Frokjaer, S.; Gajhede, M.; Svergun, D. I. *PLoS Biol.* **2007**, *5*, e134.

(189) Jansen, R.; Dzwolak, W.; Winter, R. *Biophys. J.* **2005**, *88*, 1344.

(190) Nielsen, L.; Frokjaer, S.; Carpenter, J. F.; Brange, J. *J. Pharm. Sci.* **2001**, *90*, 29.

(191) Manno, M.; Craparo, E. F.; Martorana, V.; Bulone, D.; San Biagio, P. L. *Biophys. J.* **2006**, *90*, 4585.

(192) Jiménez, J. L.; Nettleton, E. J.; Bouchard, M.; Robinson, C. V.; Dobson, C. M.; Saibil, H. R. *Proc. Natl. Acad. Sci. U.S.A.* **2002**, *99*, 9196.

(193) Gazit, E. *Angew. Chem. Int. Ed.* **2002**, *41*, 257.

(194) Mollmann, S. H.; Bukrinsky, J. T.; Frokjaer, S.; Elofsson, U. *J. Colloid. Interf. Sci.* **2005**, *286*, 28.

(195) Macritchie, F. *Adv. Protein Chem.* **1978**, 32, 283.

(196) Mollmann, S. H.; Jorgensen, L.; Bukrinsky, J. T.; Elofsson, U.; Norde, W.; Frokjaer, S. *Eur. J. Pharm. Sci.* **2006**, *27*, 194.

(197) Pinholt, C.; Hostrup, S.; Bukrinsky, J.; Frokjaer, S.; Jorgensen, L. *Pharm. Res.* **2011**, *28*, 1031.

(198) Nilsson, P.; Nylander, T.; Havelund, S. *J. Colloid. Interf. Sci.* **1991**, *144*, 145.

(199) Nault, L.; Vendrely, C.; Bréchet, Y.; Bruckert, F.; Weidenhaupt, M. *FEBS Lett.* **2013**, *587*, 1281.

(200) Lodi, A.; Momicchioli, F.; Caselli, M.; Giancane, G.; Ponterini, G. *RSC Adv.* **2013**, *3*, 1468.

(201) Sessions, K.; Sacks, S.; Li, S.; Leblanc, R. M. *Chem. Commun.* **2014**, *50*, 8955.

(202) Leblanc, R. M. *Curr. Opin. Chem. Biol.* **2006**, *10*, 529.

(203) Foster, M. C.; Leapman, R. D.; Li, M. X.; Atwater, I. *Biophys. J.* **1993**, *64*, 525.

(204) Brange, J.; Havelund, S.; Hommel, E.; Sørensen, E.; Kühl, C. *Diabetic Med.* **1986**, *3*, 532.

(205) Grasso, E. J.; Oliveira, R. G.; Oksdath, M.; Quiroga, S.; Maggio, B. *Colloids Surf. B* **2013**, *107*, 59.

(206) Attri, A. K.; Fernández, C.; Minton, A. P. *Biophys. Chem.* **2010**, *148*, 23.

(207) Dzwolak, W.; Ravindra, R.; Lendermann, J.; Winter, R. *Biochemistry* **2003**, *42*, 11347.

(208) Aston, M. S.; Herrington, T. M. *J. Colloid. Interf. Sci.* **1991**, *141*, 50.

(209) Sparr, E.; Engel, M. F. M.; Sakharov, D. V.; Sprong, M.; Jacobs, J.; de Kruijff, B.; Höppener, J. W. M.; Antoinette Killian, J. *FEBS Lett.* **2004**, *577*, 117.

(210) Ramstedt, B.; Slotte, J. P. *FEBS Lett.* **2002**, *531*, 33.

(211) Fu, L.; Liu, J.; Yan, E. C. Y. *J. Am. Chem. Soc.* **2011**, *133*, 8094.

(212) Weidner, T.; Castner, D. G. *Phys. Chem. Chem. Phys.* **2013**, *15*, 12516.

(213) Islam, M. N.; Ren, Y.; Kato, T. *Langmuir* **2002**, *18*, 9422.

(214) Eisenthal, K. B. *Chem. Rev.* **1996**, *96*, 1343.

(215) Richmond, G. L. *Chem. Rev.* **2002**, *102*, 2693.

(216) Fu, L.; Wang, Z.; Yan, E. C. Y. *Int. J. Mol. Sci.* **2011**, *12*, 9404.

(217) Shaw, J. E.; Sicree, R. A.; Zimmet, P. Z. *Diabetes Res. Clin. Pract.* **2010**, *87*, 4.

(218) Song, S. H. *Br. J. Diabetes Vasc. Dis.* **2008**, *8*, 61.

(219) Alberti, G.; Zimmet, P.; Shaw, J.; Bloomgarden, Z.; Kaufman, F.; Silink, M. *Diabetes Care* **2004**, *27*, 1798.

(220) Westermark, P.; Li, Z.-C.; Westermark, G. T.; Leckström, A.; Steiner, D. F. *FEBS Lett.* **1996**, *379*, 203.

(221) Gedulin, B. R.; Jodka, C. M.; Herrmann, K.; Young, A. A. *Regul. Pept.* **2006**, *137*, 121.

(222) Reda, T. K.; Geliebter, A.; Pi-Sunyer, F. X. *Obesity* **2002**, *10*, 1087.

(223) Wielinga, P. Y.; Löwenstein, C.; Muff, S.; Munz, M.; Woods, S. C.; Lutz, T. A. *Physiol. Behav.* **2010**, *101*, 45.

(224) Höppener, J. W. M.; Ahrén, B.; Lips, C. J. M. *N. Engl. J. Med.* **2000**, *343*, 411.

(225) Engel, M. F. M.; Khemtémourian, L.; Kleijer, C. C.; Meeldijk, H. J. D.; Jacobs, J.; Verkleij, A. J.; de Kruijff, B.; Killian, J. A.; Höppener, J. W. M. *Proc. Natl. Acad. Sci. U.S.A.* **2008**, *105*, 6033.

(226) Demuro, A.; Mina, E.; Kayed, R.; Milton, S. C.; Parker, I.; Glabe, C. G. *J. Biol. Chem.* **2005**, *280*, 17294.

(227) Jayasinghe, S. A.; Langen, R. *BBA-Biomembr.* **2007**, *1768*, 2002.

(228) Engel, M. F. M. *Chem. Phys. Lipids* **2009**, *160*, 1.

(229) Gurlo, T.; Ryazantsev, S.; Huang, C.; Yeh, M. W.; Reber, H. A.; Hines, O. J.; O'Brien, T. D.; Glabe, C. G.; Butler, P. C. *Am. J. Path.* **2010**, *176*, 861.

(230) Brender, J. R.; Hartman, K.; Reid, K. R.; Kennedy, R. T.; Ramamoorthy, A. *Biochemistry* **2008**, *47*, 12680.

(231) Westermark, P.; Andersson, A.; Westermark, G. T. *Physiol. Rev.* **2011**, *91*, 795.

(232) Brender, J. R.; Salamekh, S.; Ramamoorthy, A. *Acc. Chem. Res.* **2012**, *45*, 454.

(233) Jayasinghe, S. A.; Langen, R. *Biochemistry* **2005**, *44*, 12113.

(234) Khemtémourian, L.; Lahoz Casarramona, G.; Suylen, D. P. L.; Hackeng, T. M.; Meeldijk, J. D.; de Kruijff, B.; Höppener, J. W. M.; Killian, J. A. *Biochemistry* **2009**, *48*, 10918.

(235) Lopes, D. H. J.; Meister, A.; Gohlke, A.; Hauser, A.; Blume, A.; Winter, R. *Biophys. J.* **2007**, *93*, 3132.

(236) Knight, J. D.; Miranker, A. D. *J. Mol. Biol.* **2004**, *341*, 1175.

(237) Khemtémourian, L.; Doménech, E.; Doux, J. P. F.; Koorengevel, M. C.; Killian, J. A. *J. Am. Chem. Soc.* **2011**, *133*, 15598.

(238) Liu, P.; Zhang, S.; Chen, M.; Liu, Q.; Wang, C.; Wang, C.; Li, Y.; Besenbacher, F.; Dong, M. *Chem. Commun.* **2012**, *48*.

(239) Jha, S.; Sellin, D.; Seidel, R.; Winter, R. *J. Mol. Biol.* **2009**, *389*, 907.

(240) Salamekh, S.; Brender, J. R.; Hyung, S.-J.; Nanga, R. P. R.; Vivekanandan, S.; Ruotolo, B. T.; Ramamoorthy, A. *J. Mol. Biol.* **2011**, *410*, 294.

(241) Abedini, A.; Raleigh, D. P. *Biochemistry* **2005**, *44*, 16284.

(242) Nanga, R. P. R.; Brender, J. R.; Vivekanandan, S.; Ramamoorthy, A. *BBA-Biomembr.* **2011**, *1808*, 2337.

(243) Brender, J. R.; Hartman, K.; Nanga, R. P. R.; Popovych, N.; de la Salud Bea, R.; Vivekanandan, S.; Marsh, E. N. G.; Ramamoorthy, A. *J. Am. Chem. Soc.* **2010**, *132*, 8973.

(244) Larson, J. L.; Miranker, A. D. *J. Mol. Biol.* **2004**, *335*, 221.

(245) Brender, J. R.; Lee, E. L.; Hartman, K.; Wong, P. T.; Ramamoorthy, A.; Steel, D. G.; Gafni, A. *Biophys. J.* **2011**, *100*, 685.

(246) Cui, W.; Ma, J.; Lei, P.; Wu, W.; Yu, Y.; Xiang, Y.; Tong, A.; Zhao, Y.; Li, Y. *FEBS J.* **2009**, *276*, 3365.

(247) Bedrood, S.; Li, Y.; Isas, J. M.; Hegde, B. G.; Baxa, U.; Haworth, I. S.; Langen, R. *J. Biol. Chem.* **2012**, *287*, 5235.

(248) Mishra, R.; Geyer, M.; Winter, R. *ChemBioChem* **2009**, *10*, 1769.

(249) Reddy, A. S.; Wang, L.; Singh, S.; Ling, Y. L.; Buchanan, L.; Zanni, M. T.; Skinner, J. L.; de Pablo, J. J. *Biophys. J.* **2010**, *99*, 2208.

(250) Padrick, S. B.; Miranker, A. D. *J. Mol. Biol.* **2001**, *308*, 783.

(251) Pavinatto, F. J.; Caseli, L.; Pavinatto, A.; dos Santos, D. S.; Nobre, T. M.; Zaniquelli, M. E. D.; Silva, H. S.; Miranda, P. B.; de Oliveira, O. N. *Langmuir* **2007**, *23*, 7666.

(252) Dabkowska, A. P.; Barlow, D. J.; Hughes, A. V.; Campbell, R. A.; Quinn, P. J.; Lawrence, M. J. *J. R. Soc. Interface* **2011**, 548.

(253) Du, X.; Hlady, V.; Britt, D. *Biosens. Bioelectron.* **2005**, *20*, 2053.

(254) Mendelsohn, R.; Mao, G.; Flach, C. R. *BBA-Biomembr.* **2010**, *1798*, 788.

(255) Liao, Z.; Lampe, J. W.; Ayyaswamy, P. S.; Eckmann, D. M.; Dmochowski, I. J. *Langmuir* **2011**, *27*, 12775.

(256) Bjellqvist, B.; Hughes, G. J.; Pasquali, C.; Paquet, N.; Ravier, F.; Sanchez, J.-C.; Frutiger, S.; Hochstrasser, D. *Electrophoresis* **1993**, *14*, 1023.

(257) Cort, J.; Liu, Z. H.; Lee, G.; Harris, S. M.; Prickett, K. S.; Gaeta, L. S. L.; Andersen, N. H. *Biochem. Biophys. Res. Commun.* **1994**, *204*, 1088.

(258) Kamilya, T.; Pal, P.; Mahato, M.; Talapatra, G. B. *J. Phys. Chem. B* **2009**, *113*, 5128.

(259) Dziri, L.; Puppala, K.; Leblanc, R. M. *J. Colloid. Interf. Sci.* **1997**, *194*, 37.

(260) Zhou, H. *Proteins: Struct., Funct., Bioinf.* **2005**, *61*, 69.

(261) Orbulescu, J.; Micic, M.; Ensor, M.; Trajkovic, S.; Daunert, S.; Leblanc, R. M. *Langmuir* **2009**, *26*, 3268.

(262) Higham, C. E.; Jaikaran, E. T. A. S.; Fraser, P. E.; Gross, M.; Clark, A. *FEBS Lett.* **2000**, *470*, 55.

(263) McLean, L. R.; Balasubramaniam, A. *BBA-Protein Struct. Mol. Enzymol.* **1992**, *1122*, 317.

(264) Apostolidou, M.; Jayasinghe, S. A.; Langen, R. *J. Biol. Chem.* **2008**, *283*, 17205.

(265) Dluhy, R. A. *J. Phys. Chem.* **1986**, *90*, 1373.

(266) Thakur, G.; Wang, C.; Leblanc, R. M. *Langmuir* **2008**, *24*, 4888.

(267) Xu, Z.; Brauner, J. W.; Flach, C. R.; Mendelsohn, R. *Langmuir* **2004**, *20*, 3730.

(268) Hussain, H.; Kerth, A.; Blume, A.; Kressler, J. *J. Phys. Chem. B* **2004**, *108*, 9962.

(269) Baekmark, T. R.; Wiesenthal, T.; Kuhn, P.; Bayerl, T. M.; Nuyken, O.; Merkel, R. *Langmuir* **1997**, *13*, 5521.

(270) Surewicz, W. K.; Mantsch, H. H.; Chapman, D. *Biochemistry* **1993**, *32*, 389.

(271) Pelton, J. T.; McLean, L. R. *Anal. Biochem.* **2000**, *277*, 167.

(272) Li, S.; Potana, S.; Keith, D. J.; Wang, C.; Leblanc, R. M. *Chem. Commun.* **2014**, *50*, 3931.

(273) Meister, A.; Nicolini, C.; Waldmann, H.; Kuhlmann, J.; Kerth, A.; Winter, R.; Blume, A. *Biophys. J.* **2006**, *91*, 1388.

(274) Wang, C.; Zheng, J.; Oliveira, O. N.; Leblanc, R. M. *J. Phys. Chem. C* **2007**, *111*, 7826.

(275) Dluhy, R. A.; Cornell, D. G. *J. Phys. Chem.* **1985**, *89*, 3195.

(276) Ren, Y.; Kato, T. *Langmuir* **2002**, *18*, 6699.

(277) Golczak, M.; Kirilenko, A.; Bandorowicz-Pikula, J.; Desbat, B.; Pikula, S. *Biophys. J.* **2004**, *87*, 1215.

(278) Yassine, W.; Milochau, A.; Buchoux, S.; Lang, J.; Desbat, B.; Oda, R. *BBA-Biomembr.* **2010**, *1798*, 928.

(279) Fainerman, V. B.; Vollhardt, D.; Johann, R. *Langmuir* **2000**, *16*, 7731.

(280) Bouché, C.; Serdy, S.; Kahn, C. R.; Goldfine, A. B. *Endocr. Rev.* **2004**, *25*, 807.

(281) Melberg, S. G.; Johnson, W. C. *Proteins: Struct., Funct., Bioinf.* **1990**, *8*, 280.

(282) Matveyenko, A. V.; Butler, P. C. *Diabetes* **2006**, *55*, 2106.

(283) Wei, L.; Jiang, P.; Yau, Y. H.; Summer, H.; Shochat, S. G.; Mu, Y.; Pervushin, K. *Biochemistry* **2009**, *48*, 2368.

(284) Knight, J. D.; Williamson, J. A.; Miranker, A. D. *Protein Sci.* **2008**, *17*, 1850.

(285) Charge, S. B. P.; de Koning, E. J. P.; Clark, A. *Biochemistry* **1995**, *34*, 14588.

(286) Vallee, B. L.; Falchuk, K. H. *Physiol. Rev.* **1993**, *73*, 79.

(287) Xu, Y.; Yan, Y.; Seeman, D.; Sun, L.; Dubin, P. L. *Langmuir* **2011**, *28*, 579.

(288) Dunn, M. F. *BioMetals* **2005**, *18*, 295.

(289) Ciszak, E.; Smith, G. D. *Biochemistry* **1994**, *33*, 1512.

(290) Weise, K.; Radovan, D.; Gohlke, A.; Opitz, N.; Winter, R. *ChemBioChem* **2010**, *11*, 1280.

(291) Gaines, G. L., Jr. *Insoluble monolayers at liquid-gas interfaces*; Interscience Publishers: New York, 1966.

(292) Sánchez-Martín, M. J.; Haro, I.; Alsina, M. A.; Busquets, M. A.; Pujol, M. *J. Phys. Chem. B* **2009**, *114*, 448.

(293) Vollhardt, D.; Fainerman, V. B. *Adv. Colloid Interface Sci.* **2000**, *86*, 103.

(294) Khandelia, H.; Ipsen, J. H.; Mouritsen, O. G. *BBA-Biomembr.* **2008**, *1778*, 1528.

(295) Fu, L.; Ma, G.; Yan, E. C. Y. *J. Am. Chem. Soc.* **2010**, *132*, 5405.

(296) Fu, L.; Xiao, D. Q.; Wang, Z. G.; Batista, V. S.; Yan, E. C. Y. *J. Am. Chem. Soc.* **2013**, *135*, 3592.

(297) Wang, Z. G.; Fu, L.; Yan, E. C. Y. *Langmuir* **2013**, *29*, 4077.